Elasto-viscoplastic modelling of ground-improvements via vacuum-assisted prefabricated vertical drains with time-dependent boundary conditions

Poorna Kumarage

A thesis in fulfilment of the requirements for the degree of

Doctor of Philosophy

School of Engineering and Information Technology

The University of New South Wales, Canberra, Australia

October 2019

Thesis/Dissertation Sheet

Surname/Family Name	:	**Kumarage**
Given Name/s	:	**Poorna Isuranga**
Abbreviation for degree as give in the University calendar	:	**PhD**
Faculty	:	**UNSW Canberra**
School	:	**School of Engineering and Information Technology**
Thesis Title	:	**Elasto-viscoplastic modelling of ground-improvements via vacuum-assisted prefabricated vertical drains with time-dependent boundary conditions**

Abstract 350 words maximum: (PLEASE TYPE)

In this thesis, time-dependent boundary conditions are introduced to a creep based elasto-viscoplastic (EVP) model, which can be used to predict soft soil deformations with vacuum consolidation. Use of vacuum-assisted prefabricated vertical drains (PVDs) is a relatively new method and is getting popularity in ground-improvement projects due to its ability to consolidate deep-buried soft clay layers in a comparatively short period. Simple approximations have been reported to idealise vacuum consolidation equivalent to surcharge preloading in previous research. Conversely, in this thesis, it has been shown that considering vacuum consolidation as a time-dependent boundary condition unfolds a large number of possibilities to accurately represent ground improvements with vacuum-assisted PVDs. Combined with a creep based EVP model, it is illustrated that the accuracy of both short and long-term settlement and excess pore pressure (EPP) predictions can be improved.

Finite element analyses (FEA) of several case histories and laboratory experimental data have been used in this thesis to illustrate the improvements made in the predictability of the soft soil behaviour. Both axisymmetric and plane strain (PS) FEA are carried out for a period over three years for the Ballina test embankment vacuum applied section. Improvements made in the proposed method are highlighted against the field data and previous FEA attempts. In PS conditions, the implications of unit cell width on the FEA results such as settlements, EPP and lateral deformations are demonstrated which would serve as a guide for predicting the performance in similar scenarios.

Also, time-dependent boundary conditions are successfully used in this thesis to capture the removal and re-application of vacuum to model practical scenarios such as vacuum pump breakdowns and recoveries. Validations have been carried out against published laboratory results and with a case history from Singapore. Simple yet effective methods to avoid numerical instabilities in simulating vacuum removal and re-application are proposed and improvements achieved with these solutions are illustrated.

Later in the thesis, implications of vacuum distributions with depth of PVDs are discussed. Subsequently, a convenient method to model complex yet practically realistic vacuum distributions encountered in PVDs is presented and validated.

UNSW SYDNEY | Australia's Global University

Thesis/Dissertation Sheet

Declaration relating to disposition of project thesis/dissertation

I hereby grant to the University of New South Wales or its agents the right to archive and to make available my thesis or dissertation in whole or in part in the University libraries in all forms of media, now or here after known, subject to the provisions of the Copyright Act 1968. I retain all property rights, such as patent rights. I also retain the right to use in future works (such as articles or books) all or part of this thesis or dissertation.

I also authorise University Microfilms to use the 350 word abstract of my thesis in Dissertation Abstracts International (this is applicable to doctoral theses only).

.....	.....	.....
Signature	Witness Signature	Date

The University recognises that there may be exceptional circumstances requiring restrictions on copying or conditions on use. Requests for restriction for a period of up to 2 years must be made in writing. Requests for a longer period of restriction may be considered in exceptional circumstances and require the approval of the Dean of Graduate Research.

FOR OFFICE USE ONLY Date of completion of requirements for Award:

Originality Statement

'I hereby declare that this submission is my own work and to the best of my knowledge it contains no materials previously published or written by another person, or substantial proportions of material which have been accepted for the award of any other degree or diploma at UNSW or any other educational institution, except where due acknowledgement is made in the thesis. Any contribution made to the research by others, with whom I have worked at UNSW or elsewhere, is explicitly acknowledged in the thesis. I also declare that the intellectual content of this thesis is the product of my own work, except to the extent that assistance from others in the project's design and conception or in style, presentation and linguistic expression is acknowledged.'

Poorna Isuranga Kumarage

Signed .....

Date .....

INCLUSION OF PUBLICATIONS STATEMENT

UNSW is supportive of candidates publishing their research results during their candidature as detailed in the UNSW Thesis Examination Procedure.

Publications can be used in their thesis in lieu of a Chapter if:

- The student contributed greater than 50% of the content in the publication and is the "primary author", ie. the student was responsible primarily for the planning, execution and preparation of the work for publication
- The student has approval to include the publication in their thesis in lieu of a Chapter from their supervisor and Postgraduate Coordinator.
- The publication is not subject to any obligations or contractual agreements with a third party that would constrain its inclusion in the thesis

Please indicate whether this thesis contains published material or not.

☐ *This thesis contains no publications, either published or submitted for publication*

☒ *Some of the work described in this thesis has been published and it has been documented in the relevant Chapters with acknowledgement*

☐ *This thesis has publications (either published or submitted for publication) incorporated into it in lieu of a chapter and the details are presented below*

CANDIDATE'S DECLARATION

I declare that:

- I have complied with the Thesis Examination Procedure
- where I have used a publication in lieu of a Chapter, the listed publication(s) below meet(s) the requirements to be included in the thesis.

Name	Signature	Date (dd/mm/yy)
Poorna Kumarage		

Postgraduate Coordinator's Declaration (to be filled in where publications are used in lieu of Chapters)

I declare that:

- the information below is accurate
- where listed publication(s) have been used in lieu of Chapter(s), their use complies with the Thesis Examination Procedure
- the minimum requirements for the format of the thesis have been met.

PGC's Name	PGC's Signature	Date (dd/mm/yy)

COPYRIGHT STATEMENT

Signed …….....

Date …….....

AUTHENTICITY STATEMENT

‘I certify that the Library deposit digital copy is a direct equivalent of the final officially approved version of my thesis.’

Signed …….....

Date …….....

Dedicated to my family

Acknowledgement

First and foremost, the author would like to express the gratitude towards his supervisor Dr. C.T. (Rajah) Gnanendran for the close supervision of the research, continuous encouragement and being a friendly and supportive supervisor. Without his professional and experienced guidance this research project would not have been successful.

The author would also like to thank Dr. M.N. Islam (Post-doctoral researcher, US Department of Energy, Pittsburgh, USA) for the advices given in debugging FORTRAN codes and subsequent compiling.

The financial supports provided by the University of New South Wales (UNSW), Canberra throughout the PhD candidature including the conference travels are highly appreciated.

The high-performance computer resources and relevant trainings provided by the National Computer Infrastructure (NCI) at the Australian National University are gratefully acknowledged.

The copyediting and proofreading service for this thesis was provided by the Capstone Editing, Canberra and their timely service is acknowledged.

Appreciations go to all of my friends in the School of Engineering and Information Technology at UNSW Canberra for making the postgraduate life happy and vibrant.

Author wishes to thank his beloved parents, parents in-law, sister and brother in-law for their affection and encouragement throughout the course of this study.

Last but not least, heartiest gratefulness goes to my wife Sewwandi for her understanding, moral support, continuous love and affection throughout the PhD candidature period, which was a strong encouragement.

P.S.: The beloved father of the author passed away while this thesis was under examination. His guidance, love and affection throughout the life made this journey possible. May he attain supreme bliss of Nibbana !

Abstract

In this thesis, time-dependent boundary conditions are introduced to a creep based elasto-viscoplastic (EVP) model, which can be used to predict soft soil deformations with vacuum consolidation. Use of vacuum-assisted prefabricated vertical drains (PVDs) is a relatively new method and is getting popularity in ground-improvement projects due to its ability to consolidate deep-buried soft clay layers in a comparatively short period. In numerical modelling of this technology, simple approximations (such as treating vacuum as an equivalent surcharge preloading or altering the mass permeability of soil) have been used in the literature to idealise the phenomena that occur around a vacuum-assisted PVD, which do not accurately represent the soft soil behaviour. Most numerical analyses reported are limited to short periods and analysed either the settlement or excess pore pressure (EPP) behaviour only.

Conversely, in this thesis, vacuum-assisted PVD is modelled as a time-dependent boundary condition. It is shown that this method could be used to predict the ground deformational behaviour accurately. Especially after combining with an EVP model, the proposed method becomes a powerful tool to predict both short-term and long-term soft soil behaviours with vacuum-assisted PVDs. Time-dependent boundary conditions with the EVP model is implemented in the finite element code AFENA.

Finite element analyses (FEA) of several case histories and laboratory experimental data have been used in this thesis to illustrate the improvements made in the predictability of the soft soil behaviour in the presence of vacuum. Both axisymmetric and plane strain (PS) FEA are carried out for a period of over three years for the Ballina test embankment

vacuum applied section. A non-linear creep function was calibrated and used to improve the accuracy of long-term predictions. FEA results are validated against field data and the improvements achieved by the use of the proposed method are highlighted in comparison to previously published FEA attempts. In PS conditions, the implications of unit cell width on the FEA results such as settlements, EPP and lateral deformations are demonstrated which would serve as a guide for predicting the ground performance in similar scenarios.

Also, time-dependent boundary conditions are successfully used in this thesis to capture the stoppage, removal and re-application of vacuum to model practical scenarios such as construction control, vacuum pump breakdowns and recoveries. It is illustrated that numerical instabilities can occur when changing boundary conditions or else can converge misleadingly to a wrong solution. The term, vacuum surcharge ratio (VSR) is introduced and used as an indication of possible numerical instability. Furthermore, an effective algorithm is proposed and applied to obtain accurate solution when a numerical instability occurs. FEA and validations are carried out against published laboratory results to illustrate the improvements, both with and without the proposed algorithm. An interesting, case history from Singapore where vacuum is applied only to a sandwiched clay layer along with a vacuum pump breakdown and recovery is also analysed with the proposed methodology.

Later in the thesis, the implication of vacuum suction distribution along the depth in a PVD is discussed. It is shown that vacuum distribution can have complex shapes rather than a constant value or a linear reduction with depth. However, the linear reduction with depth has been the widespread assumption adopted in the literature due to its simplicity

in incorporating into closed-form solutions. Conversely, it is shown that vacuum distribution can have complex shapes (which are close to elliptical), especially when the PVDs are made with improved geosynthetic technology such as capped-PVDs (CPVDs). It is shown that linear or non-linear nodal constraining can be used as a convenient method to model such complex yet practically realistic vacuum distributions encountered in vacuum-assisted PVDs. The method is first validated against laboratory experimental data and subsequently a case history from Japan was also analysed and validated in which a non-linear vacuum reduction with depth was reported.

Table of Contents

List of Tables

List of Figures

List of Abbreviations

1-D	One dimensional
2-D	Two dimensional
3-D	Three dimensional
CPVD	Capped prefabricated vertical drains
CSL	Critical state line
EOP	End of primary (consolidation)
EPP	Excess pore pressure
EVP	Elasto-viscoplastic
FEA	Finite element analysis
FEM	Finite element method
HKMD	Hong-Kong Marine Deposit
MCC	Modified Cam-Clay
MNRM	Modified Newton-Raphson method
NCI	National computer infrastructure
NRM	Newton-Raphson method
NSW	New South Wales
OCR	Over-consolidation ratio
PVD	Prefabricated vertical drains
VSR	Vacuum surcharge ratio

List of Symbols

$\Delta a, \delta a$	Virtual nodal displacement vector
Δb	Nodal EPP vector
$2B$	Unit cell width
B	Half unit cell width
c	Cohesion
C_α	Secondary compression
$C_{\alpha 0}$	Secondary compression measured in 1-D
$C_{\alpha\text{-}max}$	Maximum value of C_α
C_c	Compression index
C_k	Coefficient for the variation of permeability with void ratio
C_s	Re-compression index
c_h	Coefficient of consolidation (vertical)
c_v	Coefficient of consolidation (horizontal)
D_e	Equivalent diameter of the PVD
E	Young's module
e	Void ratio
e_0	Initial void ratio
e_{cs}	Void Ratio at the CSL when $p' = 1$
e_N	Void Ratio at the normal consolidation line when $p' = 1$
e_r	Reference void ratio
$\bar{e}$	Void ratio at the reference time ($\bar{t}$)
F	Overstress function
f	Loading surface
$\bar{f}$	Reference surface
K	Hydraulic conductivity matrix
K_0	Coefficient of lateral earth pressure at rest
k, k_w	Permeability
k_v	Permeability in the vertical direction
k_h	Permeability in the horizontal direction
k_s	Permeability in the smear zone
k_{hs}	Horizontal permeability in the smear zone
k_{vs}	Vertical permeability in the smear zone
k_{ax}	Axisymmetric permeability
k_{ps}	PS permeability
k_{11}	Permeability in the x-direction
k_{33}	Permeability in the z-direction
M	Slope of the CSL

m	Slope of log C_α-log OCR plot
m^*	Slope of the log C_α-log e plot
N_s	Shape function
N	Constant for the creep function
n_1, n_2, n_3	Constants
p	Mean stress
p'	Effective mean stress
p_L	Intersection of the f surface with positive p' axis
p_c	Pre-consolidation pressure
$\bar{p}_0$	Intersection of the $\bar{f}$ surface with positive p' axis
p_v, p_{vac}	Vacuum suction
q	Deviatoric stress
q_w	Discharge rate of a PVD
R	Shape parameter
r_e	Equivalent radius of the unit cell
S	PVD spacing
r_w	Unit weight of water
r_s	Radius of the smear zone
Δt	Time increment
$\bar{t}$	Reference time
T_h	Time factor for consolidation analysis
u	EPP
U_h	Degree of consolidation in radial direction
U_v	Degree of consolidation in vertical direction
α	Creep coefficient in the natural log scale
κ	Re-compression index in the natural log scale
λ	Compression index in the natural log scale
γ_{sat}	Saturated unit weight
γ_w	Unit weight of the water
η	Conversion factor of permeability from axisymmetric to PS
ε	Strain
$\dot{\varepsilon}$	Strain rate
ε_v	Volumetric strain
$\dot{\varepsilon}_v^{vp}$	Viscoplastic volumetric strain rate
ε_{ver}	Vertical strain
ε_h	Horizontal strain
v	Poisson's ratio
σ	Stress
σ_v	Vertical stress
σ_h	Horizontal stress

σ_{vac}	Stress due to vacuum
σ_s	Stress due to surcharge
ϕ	Rate sensitivity function

List of relevant publications

Kumarage, P.I., and Gnanendran, C.T. 2019b. Long-term performance predictions in ground improvements with vacuum assisted Prefabricated Vertical Drains. Geotextiles and Geomembranes, **47**(2): 95–103. Elsevier. doi:10.1016/j.geotexmem.2018.11.002. [Based on Chapter 3 and 4].

Kumarage, P.I., and Gnanendran, C.T. 2019c. Plane strain analysis of an embankment with vacuum-assisted PVDs using an elasto-viscoplastic model. Submitted for the Computers and Geotechnics Journal. Manuscript No. COGE-D-19-01019. [Based on Chapter 4 and 5].

Kumarage, P.I., and Gnanendran, C.T. 2017. Viscoplastic behaviour of soft soil in vacuum consolidation. *In* Proceedings of the 70th Canadian Geotechnical Conference. Canadian Geotechnical Society (CGS), Ottawa, Canada. [Based on Chapter 3 and 4].

Kumarage, P.I., and Gnanendran, C.T. 2018b. Numerical modelling of vacuum suction distribution and its effects in ground improvement with PVD vacuum consolidation. *In* Proceedings of the 11th International Conference on Geosynthetics. Seoul, Korea. [Based on Chapter 7].

Kumarage, P.I., and Gnanendran, C.T. 2018a. Creep based viscoplastic numerical modelling of soil deformations in vacuum application and removal. *In* Proceedings

of the 71st Canadian Geotechnical Conference. Edmonton, AB, Canada. [Based on Chapter 6].

Kumarage, P.I., and Gnanendran, C.T. 2019d. Predicting deformations in vacuum assisted ground improvements using an elasto-viscoplastic numerical model. Accepted for the Proceedings of the XVI Panamerican Conference on Soil Mechanics and Geotechnical Engineering. Cancún, México. [Based on Chapter 6].

Kumarage, P.I., and Gnanendran, C.T. 2019a. Plane strain viscoplastic modelling in vacuum consolidation. *In* Proceedings of the 17th African Regional Conference on Soil Mechanics and Geotechnical Engineering. Cape Town, South Africa. [Based on Chapter 4 and 5].

Chapter 1 : Introduction

1.1 General

Rapid urbanisation has moved construction works towards areas that are not readily suitable for such development. As marshy lands, river floodplains and shallow ocean are being used to create additional usable land mass, one significant problem engineers face in improving these grounds is the underlying soft clay. These soft clays are often characterised by its low shear strength (typically below 25 kPa), high compressibility and often found with high water content (Flodin and Broms 1981). Due to these undesirable properties, these soils are not readily suitable to be used to build structures on them. The process and technique to convert these unsuitable ground conditions to safe and usable platform to build structures on them, is commonly referred to as ground improvement.

Prefabricated vertical drains (PVDs) were often regarded as a successful method of ground improvement to treat foundations with saturated soft clays. Essentially these drains make shorter paths for the excess pore pressure (EPP) to dissipate during soil consolidation, thereby greatly reducing the time for consolidation. Hence, using PVDs in building embankments like geo-structures for ground improvements has gained popularity in the last three decades.

Conversely, first experiment to use atmospheric pressure for ground improvement was carried out by Kjellman (1952). This technique is now commonly referred as vacuum consolidation. Combining vacuum with PVDs can further accelerate the consolidation process. This system can be called as vacuum-assisted PVDs. Using vacuum-assisted

PVDs can be beneficial in a number of ways, as it reduces the time required for ground improvement, lowers costs due to using less embankment fill material, reduces lateral displacements and limits the use of eco-unfriendly heavy machinery. These factors will be reviewed further in Chapter 2).

Although several laboratory results and field projects have been reported in the literature having assessed vacuum-assisted PVDs, no collective agreement exists between the research community regarding the numerical modelling of this technology. Throughout the early 2000s research activities were mainly focused on understanding the mechanism of vacuum consolidation through laboratory and field experiments. Differing opinions between Mohamedelhassan and Shang (2002) and Chai et al. (2005b) encapsulate the dissension on vacuum consolidation and its efficiency compared to surcharge loading of the same magnitude. Evidently, it appears that the accuracy of numerical modelling was of less concern in those years. Throughout the last two decades, several models including closed-form solutions, elastic models and elasto-plastic models have been tested used to numerical simulattions. However, since vacuum consolidation is used for soft clays, it remains a question as to whether these models are the best solutions in this context. Particularly since soft clay, can exhibit time-dependent phenomena such as creep, a creep-based model would be a better choice. This approach unfolds the possibility of carrying out predictions for several years, which constitutes a major concern in ground improvements with soft clay.

There is a number of ways to numerically simulate vacuum-assisted PVDs using the finite element method (FEM) (reviewed in Chapter 2). As identified, most of these methods lack accuracy; and either focus on settlements or EPP only. Also, they are typically built

for very simple, idealised scenarios and do not serve to numerically simulate the practical and complex situations that arise in actual ground-improvement projects, such as a change in vacuum suction intensity with time and depth, vacuum pump breakdowns and long-term effects such as creep among other phenomena. Another recent improvement in the geosynthetic technology is the use of capped-PVDs (Chai et al. 2008). This system permits each PVD to be connected to the vacuum line directly and thereby transport vacuum suction to a greater depth with minimum loss. Yet, modelling of these state-of-art technologies has not been sufficiently explored.

As such, the research carried out in this thesis is focused on the numerical modelling of vacuum-assisted PVDs. Time-dependent boundary conditions have been introduced to a creep-based EVP model to numerically simulate practical ground improvement projects. This is a unique combination to the geo-technical engineering field with comparatively limited existing research reported.

1.2 Major contributions

This thesis offers the following major contributions to the literature:

(i) An EVP model with time-dependent boundary conditions is developed for the purpose of analysing and predicting the behaviour of soft clays stabilised using vacuum consolidation. The model can be used to predict both short and long-term soft soil consolidation with vacuum. An EVP model with time-dependent boundary conditions for vacuum consolidation is a unique, useful and powerful combination. The model is implemented in a FE program AFENA (Carter and Balaam 1995),

through a newly written subroutine which can be called upon to change the boundary conditions as necessary.

(ii) The Ballina test embankment (Kelly and Wong 2009) in New South Wales, Australia is analysed using the axisymmetric unit cell idealisation for a duration of three years for the first time. The first year of the embankment is relatively easy and has been a popular topic among researchers (Kelly et al. 2018); but the long-term behaviours had not been given reasonable attention. Historically, achieving good FEA predictions for both settlement and EPP has posted a significant challenge but was achieved in the research work reported in this thesis. Predictions are compared with previous modelling attempts to illustrate the improvements made. Importance of a non-linear creep model in the relative to vacuum consolidation is illustrated and the influence of the vacuum intensity for the said project is also analysed.

(iii) Vacuum consolidation is investigated in plane strain (PS) idealisation. The results obtained from the axisymmetric FEA of the Ballina embankment are compared in PS conditions and the influence of unit cell width is illustrated relative to the vacuum consolidation, which is expected to provide useful guidance for similar FEA works. Lateral displacement profiles are also compared with field data, and embankment stability is discussed for the total project duration for the first time.

(iv) Numerical instability in vacuum application and removal as a boundary value modification has not been thoroughly discussed in the literature. Repercussions of numerical non-convergence are illustrated. Vacuum surcharge ratio (VSR) is introduced as an indicator to pre-determine numerical instabilities. A simple yet

effective algoritm is proposed for the iteration process to converge to the correct solution. Validation of such proposed methods are also carried out.

(v) The intensity of vacuum suction can reduce with the depth along the PVD, especially for long drains (i.e. >10 m). This reduction can be linear or non-linear depending on the soil strata being treated. As such, the implications of the non-linear reduction of vacuum intensity are discussed using FEA. Moreover, a convenient method to model such non-linearity using nodal-constraining is proposed and validated.

1.3 Thesis outline

The thesis consists of eight chapters. Following this chapter,

Chapter 2 carries out a comprehensive review of the literature related to soft soil consolidation. Literature related to the use of vacuum suction as a ground improvement method is given an emphasis. Different numerical methods adopted in literature to model vacuum-assisted PVDs are thoroughly reviewed. Next,

Chapter 3 introduces time-dependent boundary conditions to an EVP model. FE implementation of the model with said boundary conditions are implemented in AFENA numerical algorithm and the formulation of the coupled analysis is presented. Basic illustrations on settlement and EPP behaviour using the developed methodology is also presented.

The Ballina test embankment is analysed in Chapter 4 using the axisymmetric unit cell idealisation and the developed EVP model. Settlements and EPP measurements are compared against field data, along with an analysis of settlement behaviour in different places along the embankment centreline. Influence of a fine-tuned non-linear creep function and the intensity of vacuum towards FEA results are illustrated.

Chapter 5 then presents PS modelling of the Ballina embankment. Since the unit cell idealisation (assumed in Chapter 4) limits the analysis only to the centreline of the embankment, PS analysis is carried out to analyse the effects such as the influence of unit cell width, lateral displacement and embankment stability. Conversion procedure is presented and FEA are compared against field data and axisymmetric FEA results obtained from Chapter 4.

Chapter 6 discusses numerical modelling of the application and removal of vacuum. Due to sudden changes in the boundary conditions, numerical instability can occur and thus, result in either non-convergence or convergence to an erroneous value. These instances are presented, numerical treatments for such cases are proposed and validated in this chapter.

Chapter 7 follows to discuss vacuum distributions and their effects. It can be cumbersome to implement time-dependent boundary conditions with different vacuum distributions, so a convenient FE implementation is proposed and validated in this chapter to model complex, yet practical vacuum distributions. The implications of said vacuum reductions (both linear and non-linear) are also illustrated.

Finally, Chapter 8 summarises the research work carried out in this thesis. Conclusions are drawn and some recommendations for future works are also proposed.

Regarding the supplementary material,

Appendix A presents details of r_s/r_w and k_s/k_h ratios adopted by researchers in various PVD-related numerical modelling tasks.

Appendix B presents a summary of recent vacuum-assisted ground-improvement projects carried out globally, with their references and salient features included.

Appendix C sets out the elastic moduli tensor.

Chapter 2 : Literature review

2.1 General

Currently, about 40% of the world population living in coastal areas (UN 2017). According to the Australian Bureau of Statistics, this figure was more than double in Australia in 2001, with approximately 85% of the population living within 50 kilometres of the coastline in 2001 and increasing approximately 1-2% each year (Australian Bureau of Statistics 2001). With increasing population comes added infrastructure such as roads and railways, built to accommodate for change in coastal areas. However, some of these regions are not readily suitable for constructions. In particular, soft marine clay soils, which are predominant in most parts along the coast, have high compressibility characteristics and low shear strength. Thus, these soils need to be improved before starting any constructions. In civil and geotechnical engineering, this practice is commonly known as ground-improvement.

Various techniques have been developed to improve soft soil foundations, some of which include, soil mixing, stone columns, sand drains and wick drains. Vertical drains provide an easy, shorter path for any excess water to drain out during ground-improvement thus, accelerating the consolidation process. In particular, PVDs provide a more economical way of creating a drainage path to dissipate EPP. In the 1950s, these were made of cardboard but nowadays they are being created from composite plastics and fibres. As PVDs were and remain easier to install and are comparatively inexpensive compared to sand drains, they entirely replaced the latter within a decade following their introduction.

Kjellman (1952) first utilised the atmospheric pressure for ground-improvement by applying a vacuum suction on the ground surface using a geosynthetic sealing layer and a vacuum pump. Although the technique had a sound theoretical background, it could not be implemented in practice successfully due to the unavailability of proper geosynthetic materials. In addition, due to poor sealing material, air leakages were a common observation. Even by early 2000, there were differing opinions regarding the effectiveness of the vacuum-consolidation method compared to preloading and surcharging. Research conducted throughout those years mainly focused on effectiveness and in understanding soil behaviour in the presence of vacuum, rather than the accuracy of the numerical modelling of the method.

As such, this chapter comprehensively reviews the method of ground-improvement using vacuum-assisted PVDs. Since vacuum is essentially applied through these drains, their characteristics are also reviewed. Likewise, numerical modelling of this vacuum-assisted PVD method and soil models available to perform such modelling are also reviewed.

2.2 Role of vertical drains in ground improvement

Soft clays have very low permeability generally in the order of 10^{-4} m/s to 10^{-10} m/s. If the ground being improved has only one drainage surface at ground level, excess pore water must travel vertically from deep clay layers to the ground surface to dissipate. This may take several months or years depending on the depth of the ground being improved.

Installing PVDs provides a shorter horizontal path for excess water to dissipate. In addition, horizontal permeability in undisturbed soil can generally be several times higher

than vertical permeability. Hence, facilitating horizontal dissipation of excess water can greatly enhance the speed of consolidation.

Barron (1948) introduced the theory of radial consolidation, such that total consolidation at a given time is can be calculated as in Eqn. (2.1),

$$U = U_v.U_h \tag{2.1}$$

where, U is the total degree of consolidation, U_v is the degree of consolidation in the vertical direction and U_h is the degree of consolidation in horizontal (radial) direction. Employing PVDs introduces few more parameters such as, equivalent radius, smear zone, and the discharge capacity of the drain, among others.

2.2.1 Influence zone or the equivalent diameter of the unit cell

PVDs are installed either in a square or triangular pattern. When a unit cell is concerned, an influence zone or equivalent diameter can be identified for each drain. This can be achieved by considering the area influenced by an individual PVD. For a square pattern, it can be shown that the equivalent diameter can be calculated as per Eqn. (2.2), and the triangular pattern follows Eqn. (2.3):

$$De = \frac{2}{\sqrt{\pi}} S \tag{2.2}$$

$$De = \sqrt{\frac{2\sqrt{3}}{\pi}} S \tag{2.3}$$

where, D_e is the equivalent diameter of the unit cell and S is the actual PVD spacing in the ground. This is commonly expressed approximately as $D_e = 1.13S$ and $D_e = 1.05S$ for square and triangular patterns respectively.

In most ground-improvement projects, square pattern is adopted due to the convenience in layout (Chu and Yan 2005b, Karunawardena and Nithiwana 2009, Kelly and Wong 2009, Indraratna et al. 2011, Sun et al. 2018). Conversely, triangular pattern provides a more uniform effect of PVDs to the entire foundation soil being improved (Bamunawita 2004), despite their limited application (such as Saowapakpiboon et al. 2010, López-Acosta et al. 2019) in the industry.

2.2.2 Equivalent well diameter

PVDs are generally rectangular in shape. For convenience in modelling, this is converted to an equivalent circular shape. If the height and width of the PVD are a and b respectively, the equivalent diameter of the drain can be expressed according to Eqn. (2.4) as a function of a and b such that:

$$d_w = f(a,b) \tag{2.4}$$

where, d_w is the equivalent well diameter of the drain. In the literature, well radius (r_w) is also commonly referred to where $r_w = d_w / 2$. Table 2-1 summarises the methods reported in literature to quantify d_w.

Additionally to the methods summarised in Table 2-1 , Pradhan et al. (1993) proposed an expression considering the net flow around a soil cylinder. However, it has not been a

popular method due to complexity. Huang et al. (2016) suggested to use an elliptical approximation to model PVDs, rather than approximating a rectangular PVD to a circular one. However, owing to the complexity of the formulation and failing to provide significantly different results from those of simpler methods such as of Long and Covo (1994), the elliptical assumption is not commonly used.

Table 2-1: Expressions for the equivalent drain diameter.

Expression for d_w	Reference
$2(a+b)/\pi$	Hansbo (1979)
$\sqrt{4ab/\pi}$	Fellenius and Castonguay (1985)
$0.5(a+b)$	Rixner et al. (1986)
$0.5a + 0.7b$	Long and Covo (1994)
$0.45b$	Abuel-Naga and Bouazza (2009)

One exception of this formulation regards the use of circular drains (Indraratna et al. 2012b). In these instances, there is no need to consider an equivalent d_w, as the diameter of the circular drain itself can be considered as d_w. Figure 2-1 illustrates an example of a circular drain recently reported.

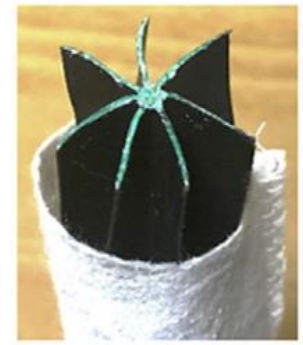

Circular drain with filter material

Schematic diagram of a circular drain

Figure 2-1: Example of a circular drain (modified from López-Acosta et al. 2019).

2.2.3 Smear zone

Smear zone denotes the area surrounding the immediate vicinity of the PVD that is disturbed upon installation. A mandrel is used to drive PVDs to foundation soil and the amount of disturbance inflicted can vary due to the size and shape of the mandrel. Generally, this smear zone can be represented as a ratio to the diameter of the PVD ($s = d_s/d_w$). According to literature (Hird and Moseley 2000a, Parsa-Pajouh et al. 2014) this ratio varies significantly from 1 to 7.

Understanding certain characteristics in this zone are essential for successful modelling of soil behaviour. First is the reduced permeability in the smear zone (k_{hs}) which can also be represented as a ratio to the undisturbed soil permeability (k_h) as k_{hs}/k_h. Second is the ratio of horizontal permeability to vertical permeability (k_{hs}/k_{vs}) inside the smear zone

which is less frequently used as the ratio can be assumed as 1, as the smear zone primarily composed of remoulded clay, thus such distinction between the two permeabilities may not be necessary and could be assumed equal. The next important characteristic is the extent of the smear zone, which is often expressed as r_s/r_w, where r_s is the radius of the smear zone and $r_w = d_w/2$.

An intensive literature review was carried out for the k_s/k_h and r_s/r_w ratios as these represent two important factors for the modelling works presented in this thesis. The results of the statistical analysis are presented in the form of a normal distribution (see Figure 2-2), and the raw data collected from the literature review are provided in Appendix–A.

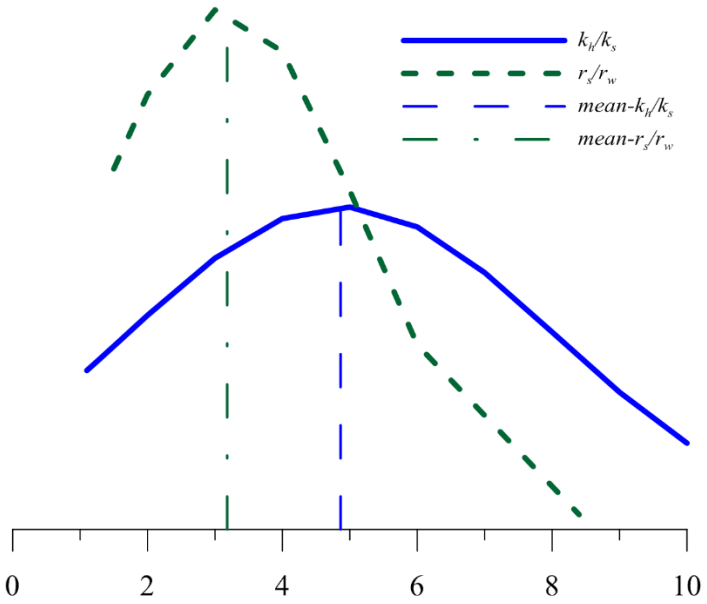

Figure 2-2: Normal distribution of the k_h/k_s ratio and r_s/r_w ratio reported in the literature (plotted from the data in Appendix–A).

Synthesis of the reported values reveals that the extent of the smear zone and its permeability vary widely. Rounded off to a whole number, the mean values are $r_s/r_w = 3$

and k_h/k_s = 5. Due to uncertainty of these factors, some trial and error appears unavoidable when quantifying these parameters in numerical modelling.

2.2.4 Drain discharge capacity

The capacity of a PVD to discharge water depends primarily on its effective size, geometry and the material being used (Rixner et al. 1986, Holtz et al. 1991). Generally, the discharge capacity (q_w) will vary from 50 – 1500 m^3/year. Whether this property should be considered depends on how the drain performs over time. In numerical modelling for ground-improvement with PVDs, it is commonly argued among researchers that as long as the discharge capacity exceeds 100–150 m^3/year, the drain is sufficiently less resistant, and the effect of discharge capacity can be safely ignored. Notably, Chai et al. (2001) suggested that q_w = 100 m^3/year can be adopted if no data are available, whereas Indraratna and Redana (2000) have demonstrated how well-resistance can become significant, especially if q_w < 40-60 m^3/year.

Futher, Hansbo (1979) recommended that the permeability of the PVD filter must be at least 100 times higher than the clay being treated. Chai and Miura (1999) reported results listing various factors that affect the PVD behaviour, including the discharge capacity.

2.3 Ground improvement with vacuum consolidation

The principle behind vacuum consolidation is to reduce the pore pressure within the soil and thereby use the atmospheric pressure to exert stress on the ground. This was experimentally conducted by Kjellman (1952). Main limitation was the air leaks encountered during the operation of vacuum suction. This limited the use of vacuum-consolidation technology as a successful ground-improvement method. Around early

2000, the method was brought back to attention since the method had the potential of being a successful ground-improvement method with the developments made in geosynthetic technology. Three factors can be identified as responsible for its recent surge in popularity:

(i) development of geosynthetic technology, which reduced air leakages and enabled vacuum suction to be applied effectively to the ground,

(ii) increasing need of land requirements for human settlements and infrastructure, which led policymakers to select area that were not readily suitable for such application; this includes lands with deeply buried clay layers, which are extremely time consuming to be consolidated only with conventional PVDs,

(iii) increasing cost of fill materials and the cost of surcharge application and removal.

2.3.1 Combination of vacuum and surcharge as a ground improvement method

Generally, in a ground-improvement project, vacuum is not applied alone. Instead it is combined with surcharge using an embankment. This combination is preferred over the former due to a few reasons as follows.

First, there is an upper limit for vacuum intensity that can be successfully applied to the ground. Theoretically, this is equal to the atmospheric pressure (101.3 kPa), but practically soil desaturation occurs at around 80–90 kPa vacuum intensity (Cognon et al. 1994, Leong et al. 2000). Thus, throughout all previous ground-improvement projects, vacuum suction has been limited to this upper limit (Kelly et al. 2008, Karunawardena and Nithiwana 2009, Indraratna et al. 2011, 2012a).

This represents a significant limitation, and implies that vacuum consolidation cannot eliminate the need of an embankment preloading, hence why vacuum suction is routinely combined with an embankment construction in almost all ground-improvement projects. Although this can be uniquely identified as the vacuum-surcharge method, in the context of ground-improvements, 'vacuum-consolidation' generally suggests that vacuum is being applied using PVDs and surcharge by an embankment.

Three distinct advantages of the vacuum-surcharge combination can be identified as follows:

(i) Combination of vacuum and embankment can impose greater stress on foundation soil than vacuum alone.

(ii) Vacuum tends to form inward lateral deformations (This will be reviewed later in Section 2.8), which can lead to cracking of the ground surface and shallow depths (Chai et al. 2005a, López-Acosta et al. 2019). Conversely, surcharge results in outward lateral displacements. Thus, combining vacuum with surcharging, inward-lateral displacements can be compensated with outward-lateral displacements, consequently minimising net lateral displacements.

(iii) In the case of an embankment construction is necessary, embankment construction can be carried out at a faster rate than conventional PVD alone due to the rapid dissipation of EPP and soil stabilisation due to vacuum.

2.3.2 Understanding the mechanism in vacuum consolidation

Several analogies have been proposed in the literature to understand the mechanism involved in vacuum consolidation. The easiest involves a one-dimensional (1D) perspective of the process. Mohamedelhassan and Shang (2002) idealised vacuum and

surcharge by the principal of superposition as the simple summation of the two. Figure 2-3 is an illustration of the method.

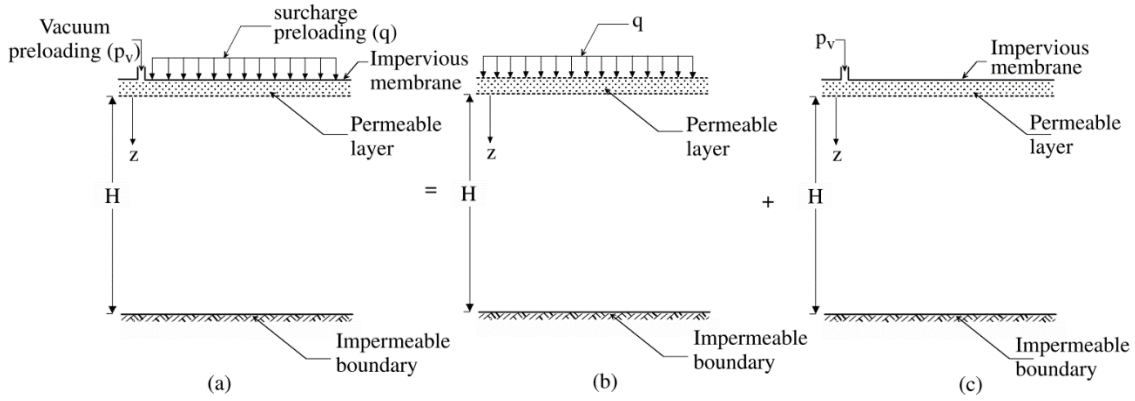

Figure 2-3: Mechanism of vacuum consolidation(modified from Mohamedelhassan and Shang 2002).

Another analogy can be described as follows: let us employ a total stress change of Δp to the system. Without vacuum suction, the change in EPP (Δu) would momentarily be Δp and would dissipate depending on the boundary conditions and permeability of the soil, and eventually will become $\Delta u = 0$. In vacuum consolidation for the same stress change, the initial EPP would be $\Delta u = \Delta p - p_{vac}$ where p_{vac} is the vacuum suction. Over the time, EPP of the system will be equal to p_{vac}.

To illustrate the above concept, generic graphs for EPP dissipation can be illustrated as follows. In Figure 2-4, p_v is the vacuum suction; for comparison $p_0 = p_1 + p_v$ has been assumed.

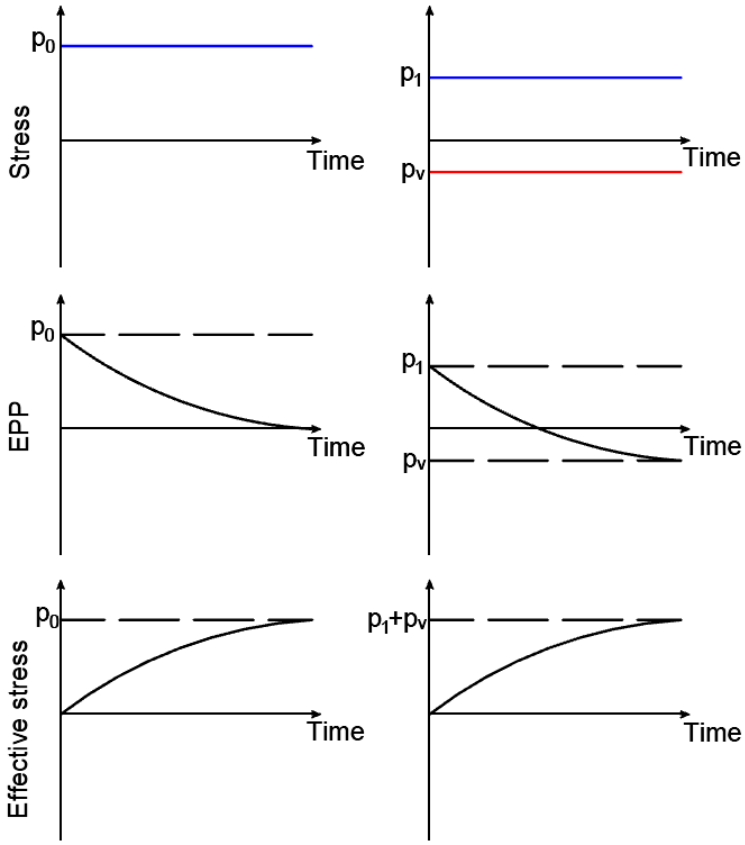

Figure 2-4: Generic pattern of EPP dissipation and effective stress development in vacuum consolidation.

With current knowledge, the generic graphs in Figure 2-4 have been challenged. It has been reported that EPP dissipation is faster in vacuum consolidation compared to surcharge alone, in that greater effective stress can be transferred thus, achieving higher over-consolidation ratio (OCR) than a surcharge of the same magnitude (Indraratna et al. 2013, Kianfar et al. 2015).

In the literature, researchers have shown differences in stress paths from conventional preloading. Notably, Robinson et al. (2012) suggested the following expressions in Eqn. (2.5) and Eqn. (2.6) for vertical and horizontal effective stresses (i.e. σ_v', σ_h') respectively.

$$\sigma'_v = \sigma'_o + \sigma_{vac} \tag{2.5}$$

$$\sigma'_h = K_0 \left(\sigma'_{vo} + \sigma_{vac} \right) \tag{2.6}$$

where, $K_0 = \sigma'_h / \sigma'_v$. However, Robinson et al. (2012) validated their results only for deformations and not for EPP.

When considering the practical application of vacuum for foundation soil in a ground-improvement project, two methods can be identified, namely: the membrane method and the membrane-less method.

2.3.3 Membrane method

In the membrane method, an airtight sheet or membrane is placed on the ground surface and vacuum is applied below the membrane (Figure 2-5[a]). Vacuum suction then travels along the PVDs to reach deeper levels in the ground. Domestic (Australian) examples of ground-improvement using this method include the port of Brisbane in Queensland and the Ballina bypass in New South Wales. Generally, high-density polyethylene is used as the membrane.

The main challenge in membrane method is to overcome the air leaks. Hence, to make the membrane airtight, it is very common to make a trench and flood the boundaries of the membrane with bentonite slurry.

2.3.4 Membrane-less method

In the membrane-less method, vacuum suction is applied to individual PVD and use clayey soil as the sealing layer (Figure 2-5[b]). This method is also known as the Capped-PVD or CPVD method, since vacuum lines are connected to each drain using a geosynthetic cap (Chai et al. 2010). One key advantage resides in its ability to minimise air leaks since each PVD acts independently. However, compared to the membrane method, an intensive amount of piping connections must be made, which can be relatively costly.

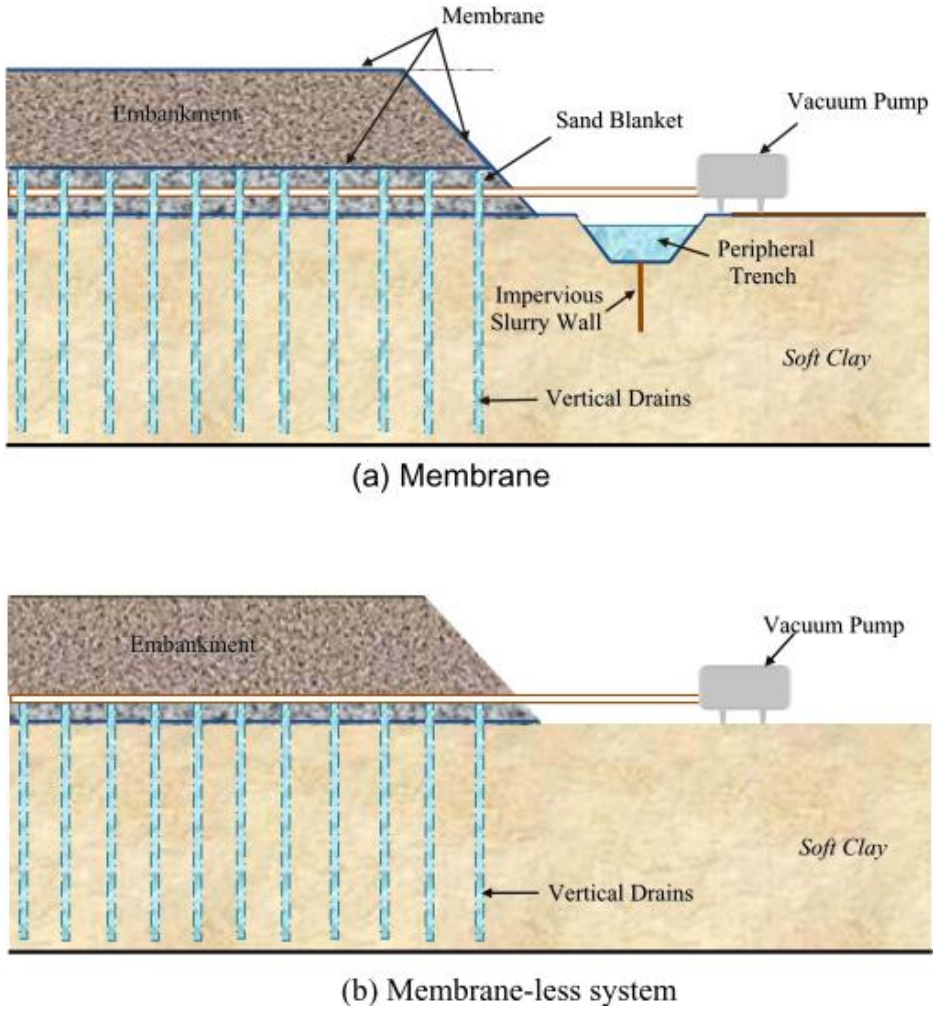

Figure 2-5: Vacuum-assisted PVDs, (a)Membrane method and, (b) membrane-less method (from Kianfar 2013).

This method has been used when the treated area is susceptible to flooding or changes in water table, resulting the treated area being inundated. In addition, if the foundation soil has sand layers, piping should be extended to pass these layers and apply the vacuum directly to the clay layer (e.g. Lam et al. 2018).

2.4 Finite element numerical modelling of vacuum preloading

In FE modelling of vacuum consolidation, four distinct methods can be found in the literature. They are:

(i) treating vacuum as an equal vertical stress,

(ii) calculating an equivalent permeability value considering the effect of PVDs and vacuum;

(iii) defining a pseudo water table for the PVDs beneath the foundation so that it imposes additional stress around the selected area (e.g. PLAXIS 2016),

(iv) considering vacuum as a change in EPP.

2.4.1 Treating vacuum as an equal vertical stress

Treating the vacuum in this sense likely represents the simplest method in modelling its effects. In this method, vacuum suction is treated as an equal vertical stress on the ground surface. Mohamedelhasan and Shang (2002) claimed that equivalent vertical stress could be used to predict both settlement and EPP in vacuum preloading. Conversely, Bamunawita (2004) and Indraratna et al. (2004) emphasised that although reasonable settlement predictions were possible using this approach, accurate calculation of EPP was not possible, and often some mathematical treatment would be necessary to correct the resulting EPP values. Nonetheless, they reported that the overall rate of EPP dissipation was similar for practical purposes.

This method could not explain a number of observations including the different lateral displacements, cracking of the edges in improved ground with vacuum (Chai et al. 2005a, López-Acosta et al. 2019), the accelerated degree of consolidation than that using an equivalent surcharge (Kianfar et al. 2015) and different degrees of consolidation at different depths due to vacuum suction reduction (Indraratna et al. 2012b).

2.4.2 Calculating an equivalent permeability value considering the effect of PVD and vacuum

Chai et al. (2001) introduced a relatively simple method to approximate ground behaviour by calculating an equivalent permeability of soil due to PVDs. In this method, modelling of PVDs is not necessary which is highly convenient for a large structure such as an embankment. Later, Chai et al. (2006) extended this technique to incorporate vacuum suction, making possible predictions for ground settlements with vacuum-assisted PVDs.

2.4.3 Modelling vacuum as a change in EPP

In the membrane method, the ground surface is subjected to vacuum suction. To model this in FEA, EPP of the ground surface can be set to respective vacuum value (e.g. Saowapakpiboon et al. 2011). However, since vacuum is commonly applied for grounds where PVDs have been installed, it is arguable that this vacuum could be transported beneath the ground surface along the vertical drains. This idea was confirmed with laboratory and field experiments (Tang and Shang 2000, Chu et al. 2000, Chen et al. 2019). The EPP along each line in FE mesh to represent a PVD can also be modelled as a drainage line by setting EPP to zero.

2.5 Analytical methods for modelling vacuum consolidation

It is beyond the scope of this thesis to develop a rigorous analytical formulation for vacuum consolidation. Owing to changing boundary conditions in vacuum consolidation, such derivation is far less practical. That said, some analytical methods exist as convenient approximations. These are referred to as such (i.e. approximations even though they are analytical models) because they do not necessarily represent the conditions (e.g. stress path) to which soil elements are subjected, with changing boundary conditions.

One closed form solution is to use the Terzaghi's theory of one-dimensional consolidation, assuming that vacuum act as additional vertical stress on the material surface (Mohamedelhassan and Shang 2002). As a continuation of this method, Barron (1948) consolidation formulation for radial consolidation can also be adopted when PVDs are employed. Chen et al. (2019) claimed that using the 1D idealisation (Eqn. (2.7)), the calculated settlements can deviate as much as 26%.

$$S_p = \frac{C_c H}{1+e_0} \log\left(\frac{\sigma_0' + \Delta\sigma}{\sigma_0'}\right) \tag{2.7}$$

where, C_c is the compression index, H is the height of the soil layer, σ_0' and $\Delta\sigma$ represent the current and change in vertical effective stress and e_0 is the initial void ratio. Historically, researchers (e.g. Mohamedelhassan and Shang 2002, Chai et al. 2005b, Robinson et al. 2012) have discussed and expressed differing opinions about the use of 1D idealisation for vacuum consolidation. The main limitations concerned the EPP values that resulted from these methods are obviously wrong as further confirmed by

Bamunawita (2004). Conversely, focusing on EPP dissipation Indraratna et al. (2005a) proposed an analytical solution for a single vertical drain as in Eqn. (2.8),

$$\frac{\bar{u}}{\sigma_1} = \left[1 + \frac{(1+k_1)\, p_{o-ax}}{2\sigma_1}\right] \exp\left(\frac{-8T_{h-ax}}{\mu_{ax}}\right) - \frac{(1+k_1)\, p_{0-ax}}{2\sigma_1} \tag{2.8}$$

where, $\bar{u}$ is the average EPP, σ_1 is the vertical stress, $p_{o\text{-}ax}$ is the vacuum intensity, k_1 is the factor for reduction in vacuum along the depth of the drain and $T_{h\text{-}ax}$ is the time factor. Recent research has proven that this observation is only partially correct. For example, Kianfar et al. (2015) showed that higher amount of effective stress can be transferred to the soil skeleton using a combination of vacuum and fill surcharge, rather than the equivalent surcharge alone and thereby after removing the induced stresses, vacuum treated soil reach a higher OCR (Figure 2-6). Although the reason for this is still unclear, it could be due to the higher k_h in in-situ ground conditions than k_v thus, with vacuum suction, horizontal water flaw dominate in a greater extent than PVDs alone, resulting quicker EPP dissipation, transferring the stress to the soil skeleton.

Indraratna et al. (2005b) proposed a rigorous analytical solution for soil consolidation with vacuum-assisted PVDs. One key benefit of this formulation is, it permitted users to apply a linear vacuum reduction along the PVD depth. Similarly, Geng et al. (2012) proposed analytical solutions for both membrane and membrane-less systems. Zhou et al. (2017) made further improvements by introducing consolidation of a multi-layer soil system under surcharge combined with vacuum.

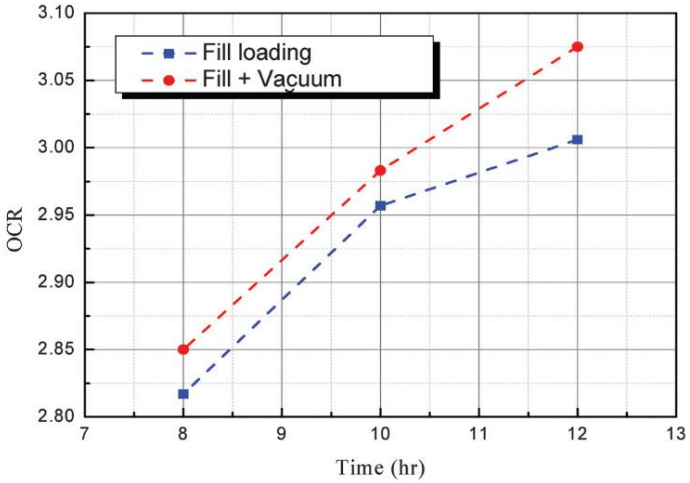

Figure 2-6: Average OCR after removing fill loading and vacuum + fill loading (from Kianfar et al. 2015).

The primary disadvantage of applying analytical solutions for vacuum-assisted PVDs regard the inherent limitation that they are all formulated for fixed and simple boundary conditions that do not represent actual field conditions. Analytical models based on the principle of superposition lack the accuracy in EPP predictions. Hence, in modelling vacuum-assisted PVDs, numerical methods such as FEA are more popular and preferred.

2.6 Soil models for numerical modelling of vacuum consolidation

Vacuum consolidation is adopted mainly for thick, soft clay layers. As soft soil undergoes a significant amount of plastic deformation before failure, elastic or elastic-perfectly plastic models are not an option modelling vacuum consolidation, despite their application in some researchers' models.

In selecting or developing a soil model, it is crucial that decisions are made according to the accuracy, simplicity and validity of the model throughout different phases in the selected materials' behaviour (e.g. elastic, plastic and creep, among others). With the

development of critical-state soil mechanics, Cam-clay (CC) and modified Cam-clay (MCC) was introduced (discussed in section 2.6.1) to represent the soft clay behaviour and gained significant popularity.

2.6.1 Modified Cam-clay model

The original CC model was proposed by Roscoe and Schofield (1963) and later modified by Roscoe and Burland (1968) to produce a version now commonly known as MCC. Both models assume a linear relationship between the void ratio (*e*) and logarithm of the mean effective stress. Notably, their mathematical formations appear similar except for the shape of the yield surface (see Figure 2-7). Undoubtedly, MCC is the most widely used soft soil model of the last two decades. In early 2000, when most modelling attempts on vacuum consolidation began, many researchers experimented with simple elastic models before and moved towards critical state models such as MCC in mid-2000. Some improvements were made upon introducing different yield curves along the dry side, introducing anisotropy and de-structuring. In the recent past a number of research has been reported using MCC to model vacuum-assisted PVDs (e.g. Bamunawita 2004, Indraratna et al. 2004, 2011, 2012a, Chai et al. 2006, Saowapakpiboon et al. 2011, Lam et al. 2015, Deng et al. 2017).

One significant drawback in MCC is the inability to model long-term deformations in soft clays. Since vacuum consolidation is often used for thick soft clay deposits which exhibit time-dependent phenomena such as creep, a more suitable model is necessary.

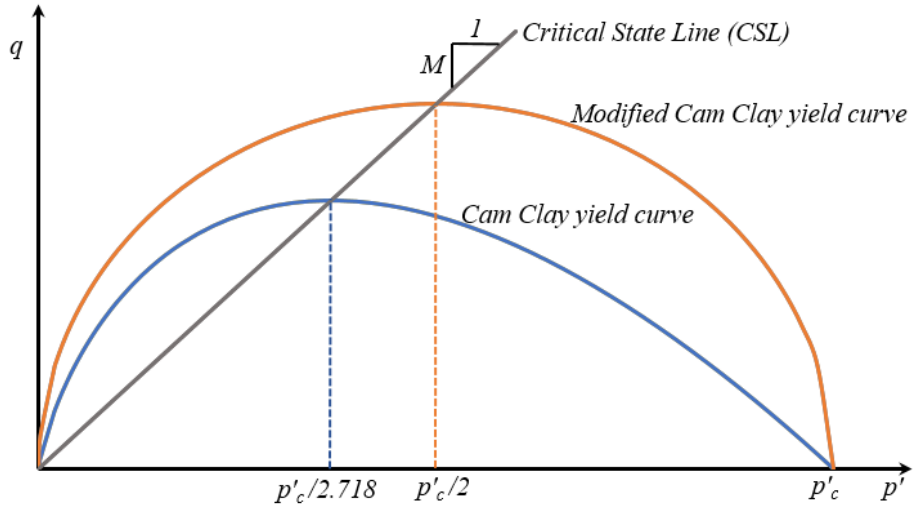

Figure 2-7: Yield curves for Cam-Clay and MCC in p'- q space.

2.6.2 Elastic viscoplastic models

EVP models take the viscous behaviour of soil into account. Although different categorisations can be adopted, for the work in this thesis, such models can be broadly categorised into two classes: rate-based models and creep based models (Gnanendran et al. 2006). As the name implies, rate-based models focused more on the rate-dependency of material, whereas creep-based models focus on creep behaviour. The literature review primarily explored the latter since the formulation adopted in this thesis follow a creep-based approach.

Based on Bjerrums' (1967) concept of delayed compression (Figure 2-8), a series of development can be identified in EVP modelling by Yin and others (Yin and Graham 1989, 1994, 1999, Yin et al. 2002). The three main criticisms about these formulations were the so-called equivalent-time concept lagging a physical meaning, complexity of the models resulted by deviating from the conventional parameters (e.g. λ/v, κ/v etc.) and the

creep strain approaching infinity as time passes, which does not make physical sense. Although Yin et al. (2002) introduced a non-linear creep function to rectify this limitation, the model was too complex with the need of 10 material parameters.

Conversely, Kutter and Sathialingam (1992) proposed a new EVP model likewise based on Bjerrum's (1967) concept of delayed compression and Perzyna's (1963) formulation of viscoplasticity on the MCC framework. Creep-based EVP models use secondary compression (C_α) as the input parameter to represent the viscous behaviour of soil. The fact that C_α being able to be obtained relatively easily and having empirical formulae, such as the ratio of compression index (C_c) to C_α (Mesri and Godlewski 1977) has increased the popularity of these models. Kutter and Sathialingam (1992) used a constant value for the C_α which was later pointed out as a limitation by Karim et al. (2010). Yin et al. (2002) also faced the same problem of using a constant value for C_α, so it is worth reviewing the possible options to incorporate C_α in to EVP models.

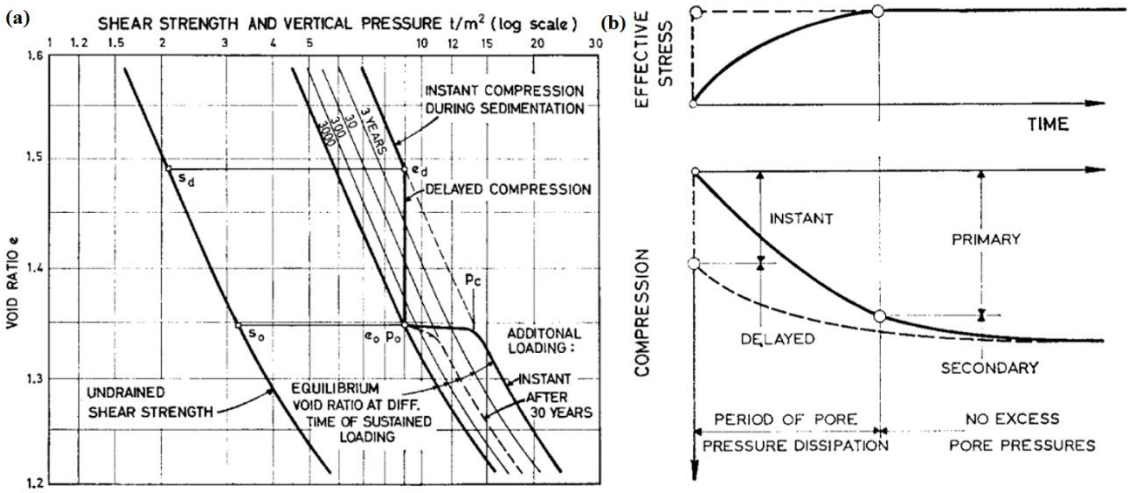

Figure 2-8: Delayed compression concept by Bjerrum (1967).

2.6.2.1 Incorporating secondary compression into EVP modelling

Secondary compression as a fixed ratio to compression index (C_α/C_c) proposed by Mesri et al. (1997) has gained popularity among researchers due to its simplistic approach. As the time duration is long-term (e.g. spanning several years), it is arguable whether this fixed ratio would actually be suitable. Other than the abovementioned approach, several methods can be found in the literature to model C_α. These can be summarised as follows.

Gao et al.(2006) proposed a creep function with a relationship to OCR and 1D creep compression ($C_{\alpha 0}$) as in Eqn. (2.9);

$$C_\alpha = C_{\alpha 0}\left(OCR\right)^{-m} \tag{2.9}$$

where, m is the slope of log C_α - log OCR plot.

Meanwhile, Alonso et al. (2000), Karim et al. (2010, 2011), presented non-linear creep functions using OCR and $C_{\alpha 0}$, generally in the form of Eqn. (2.10):

$$C_\alpha = C_{\alpha-\max}\, e^{-b_1 (OCR-1)} \tag{2.10}$$

where, $C_{\alpha\text{-}max}$ is the maximum value of C_α at the time of yielding begins and b_1 is a fitting constant. Wu et al. (2013) later proposed and validated a creep function based on the change in void ratio, as in Eqn. (2.11):

$$\frac{C_\alpha}{C_{\alpha NC}} = \left(\frac{1+e}{1+e_0} \right)^{m^*} \tag{2.11}$$

where, m^* is the slope of log C_α - log e.

Islam and Gnanendran (2017) adopted a creep function analogous to Nash (2001), which they validated against laboratory and field data and can be expressed as in Eqn. (2.12):

$$\frac{C_\alpha}{C_{\alpha i-1}} = \left(\frac{p_i}{p_{i-1}} \right)^{\frac{\lambda-\kappa}{\alpha_{i-1}}} \tag{2.12}$$

Islam and Gnanendran (2017) defined p_i and p_{i-1} as the creep inclusive pre-consolidation pressure at two consecutive time steps while the given material is hardening.

2.6.2.2 Secondary consolidation in the presence of vacuum suction.

To date, no evidence has proven a difference in C_α in the presence of vacuum. However, in synthesising the literature, it is possible to create an indirect relationship between these two variables. Since vacuum consolidation can yield higher OCR (Kianfar et al. 2015), which is linked to C_α such as through Eqn. (2.9) and (2.10), it can be argued that the vacuum consolidation can actually reduce C_α and thus reduce the long-term creep settlements. That said, still there remains limited experimental evidence (e.g. Karunawardena and Nithiwana 2009, Kosaka et al. 2016) to confirm this argument.

2.7 Vacuum distribution

When dealing with long PVDs, a certain amount of vacuum loss can occur along the drain for several reasons. Generally, sandwiched sand layers, imperfections of the PVD system and generation of surface cracks are noted as the main causes (Sun et al. 2017, López-Acosta et al. 2019).

Both for membrane and membrane-less methods, vacuum suction may not penetrate equally to the full depth of the PVD. Several researchers have reported vacuum suction getting lost along the depth of the drain in both laboratory experiments and in field cases (e.g. Indraratna et al. 2004, Chai et al. 2006, 2008). This was noted both from low strain rate at deeper depths such as that reported by Indraratna et al. (2012) and inferred from changes in soil index properties after vacuum consolidation (e.g. Chu et al. 2000). Such observations encouraged further study of this phenomenon.

Recent developments in geosynthetic technology (such as CPVDs) have allowed vacuum suction to be applied to individual PVDs, resulting in more effective vacuum application. Despite this progression, a certain percentage of vacuum loss is still inevitable.

In the modelling of vacuum suction, a constant vacuum along the PVD was adopted due to convenience. Later, with experimental evidence (e.g. Chu et al. 2000, Indraratna et al. 2004), linear decay of vacuum loss was applied as a reasonable approximation (Figure 2-9[a–b]).

Chai et al. (2006) proposed a method to quantify vacuum distribution for a partially penetrated PVD system in a layered soil mass (Figure 2-10), using the relative

permeability of each soil layer. The relationship between the parameters was proposed as in Eqn. (2.13):

$$k_{v1}\frac{p_{v0}-p_{v1}}{H_1}=k_{v2}\frac{p_{v1}}{H-H_1} \tag{2.13}$$

where, k_{v1} and k_{v2} are the permebilities of the each soil layer, p_{vo} is the vacuum at the grouns surface and p_{v1} is the vacuum at the interface of the two soil layers, H is the total thicknes of the foundation soil and H_1 is the depth improved by PVDs. Chen et al. (2019) later reported a comprehensive observation on the evolvement of vacuum distribution with time in a ground-improvement project. This is illustrated in Figure 2-11(a–b).

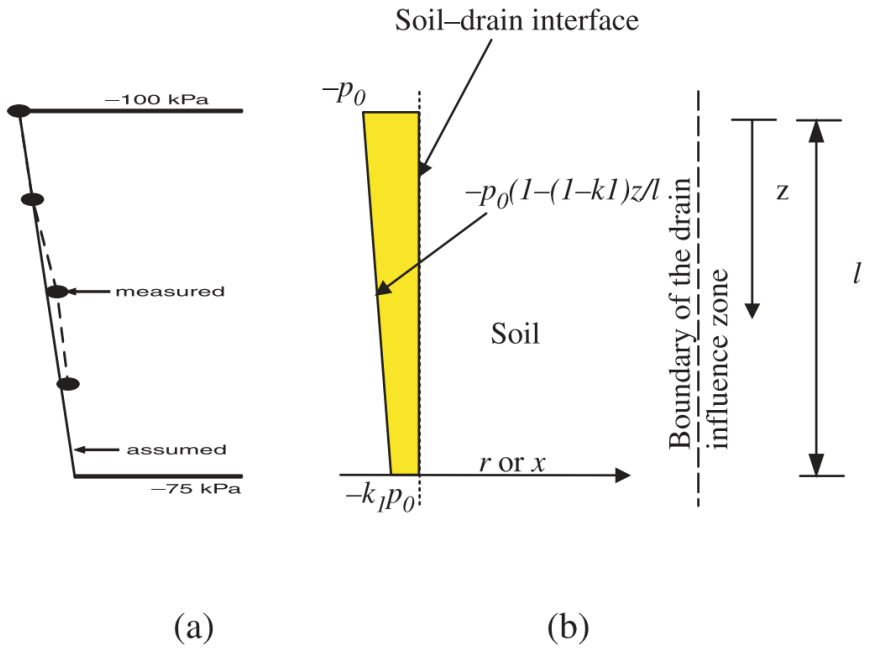

Figure 2-9: (a) Measured and (b) analytically modelling of linear reduction in vacuum consolidation (after Indraratna et al. 2005a).

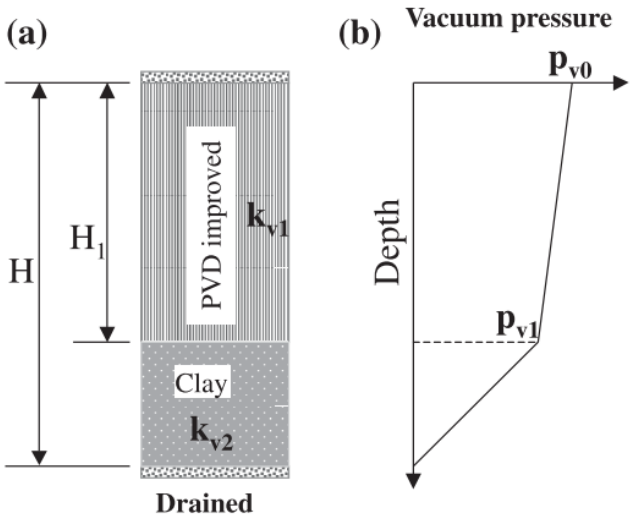

Figure 2-10: Illustration of vacuum pressure distribution in two-layer system (from Chai et al. 2006).

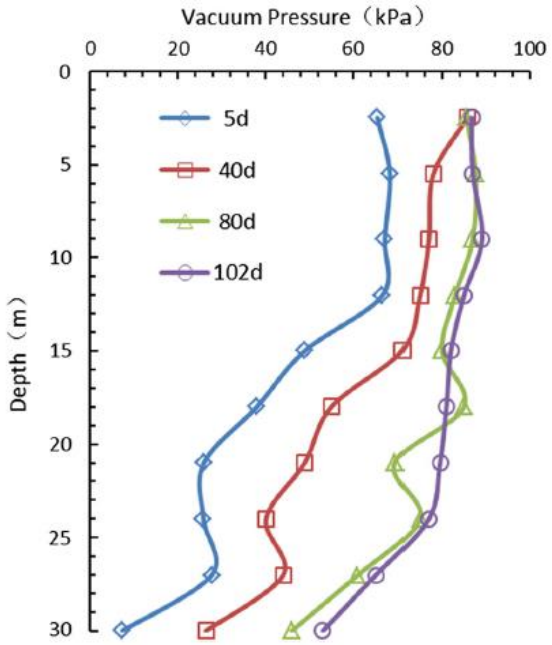

Figure 2-11: Evolvement of vacuum distribution against time and depth reported from a case study (from Chen et al. 2019).

However, in CPVDs the geosynthetic cap is buried by the sealing layer, and vacuum starts from a few metres below the ground surface (Chai et al. 2010). This makes vacuum distribution somewhat complex in shape. Also, partially penetrated PVDs in a high permeable layer at the bottom of a clay deposit can contribute to producing complex vacuum distributions along the depth of the PVD. Chai et al. (2010) simplified these types of elliptical vacuum distributions to a three zone linear variation in which the vacuum increases from the ground surface to its maximum value, then maintains a constant along the PVD and start diminishing from the end of the PVD to the drained bottom surface as shown in Figure 2-12.

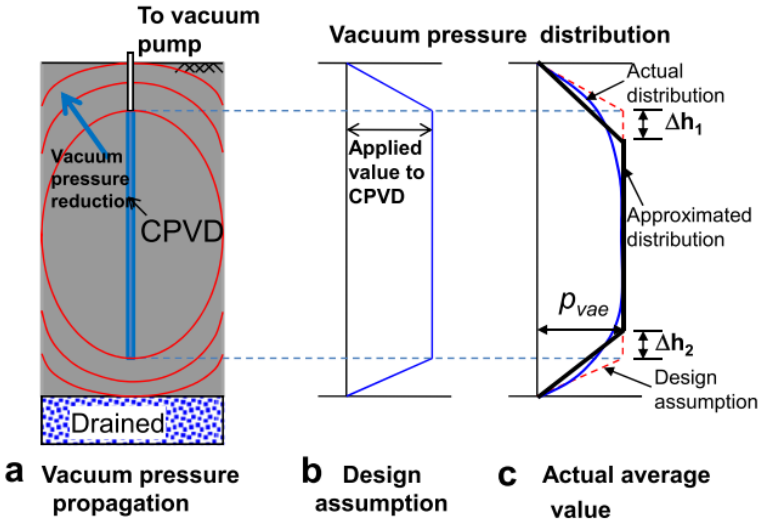

Figure 2-12: Elliptical shape vacuum distribution in two-way drainage system (from Chai et al. 2010).

Chai et al. (2010) also proposed a function to quantify Δh_1 and Δh_1 as shown in Eqn. (2.14),

$$\Delta h = \Delta h_0 \left(\frac{D_e}{1.36} \right)^{n1} \left(\frac{k_h}{k_s} \right)^{n2} \left(\frac{k_h / k_v}{1.5} \right)^{n3} \quad (2.14)$$

where, Δh_0, *n1*, *n2* and *n3* are constants. With a series of FE simulations, Chai et al. (2010) offered average values for the above constants as 1.0, 0.45 and –0.65 respectively.

2.8 Modelling lateral deformations in vacuum consolidation

Lateral deformations are measured in the field through geodetic landmark on the earth surface, using pipe strain gauges, and by employing inclinometers and extensometers in boreholes etc.

Due to the embankment load, foundation soil tends to move laterally outwards. Applying a vacuum introduces negative pressure along the PVD, which may help to compensate for any outward lateral displacement. However, in shallow depth, due to low vertical stress and high inward lateral stress by vacuum, soil tends to deform laterally inwards. That said, the term 'shallow' itself within this context requires further explanation.

When Mohamedelhassan and Shang (2002) reported that vacuum suction can produce identical results to surcharge pressure, they did not consider lateral deformations since the study was limited to 1D conditions. However, Chai et al. (2005b) claimed that vacuum suction can only reach 80% of the final settlement compared to a surcharge of the same magnitude. They continues noting cracking of the earth's surface when vacuum suction is applied (Figure 2-13[a–b]). Recently this finding was echoed in López-Acosta et al. (2019) wherein the same observation was noted in a field experiment (see Figure 2-14).

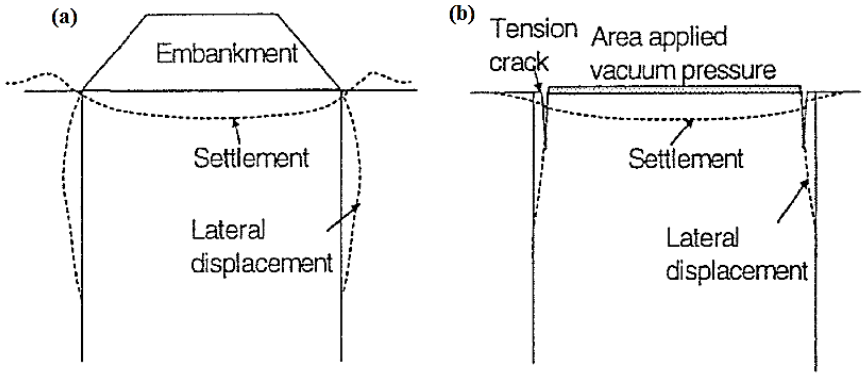

Figure 2-13: (a)-Outward lateral displacements with embankment surcharge and (b)-inward lateral displacements and surface cracking with vacuum suction (modified from Nguyen et al. 2017).

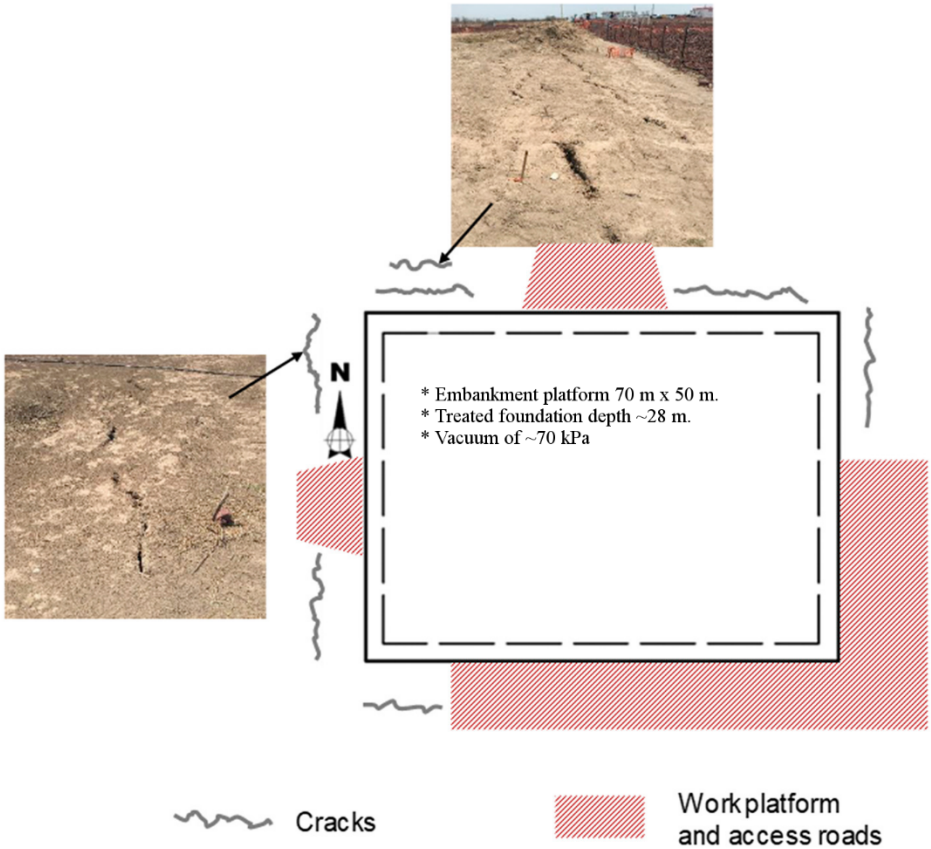

Figure 2-14: Example of surface cracking due to vacuum (modified from López-Acosta et al. 2019).

Contradictory opinions between Mohamedelhassan and Shang (2002) and Chai et al. (2005b) were later clarified by Chai et al.(2005a) by defining the condition to actuate inward lateral deformations in vacuum consolidation as in Eqn. (2.15):

$$\Delta\sigma_{vac} \geq \frac{K_0\sigma'_{vo}}{1-K_0} \tag{2.15}$$

where, $\Delta\sigma_{vac}$ is the vacuum intensity at and beyond which it violates the K_0 condition and actuates inward lateral deformations.

Still, there is a significant level of uncertainty in calculating lateral displacements in vacuum consolidation. The rationale behind most approximations is the creation of a ratio between horizontal displacements to vertical displacements.

Extending the method by Poulos and Davis (1974), Robinson et al. (2012) proposed a lateral strain factor (*LF*) as in Eqn.(2.16):

$$LF = \frac{\varepsilon_h}{\varepsilon_v} = 0.5\left[1 - \frac{(1-2\alpha_1\nu)}{1+2\alpha_1 - 2(1+2\alpha_1\nu)}\right] \tag{2.16}$$

where, ε_h and ε_v are horizontal and vertical strains respectively, $\alpha_1 = 1$ represents isotropic consolidation and $\alpha_1 = K_0$ represents K_0 consolidation, and ν is Poisson's ratio. It was claimed that $\alpha_1 = 0.62$ can predict lateral displacements well. However, their

validation was limited to lateral displacements sonly and did not present other results such as EPP and vertical displacements.

2.9 Modelling application and removal of vacuum

Very limited discussion is available on modelling the deformation of soil upon application and removal of vacuum. Chai et al. (2005a) mentioned that volumetric strain needs some correction in the presence of vacuum and proposed these adjustments as a multiplication factor.

Kianfar et al. (2015) carried out laboratory experiments on EPP and deformation analysis on application and subsequent removal on vacuum. Despite this, numerical simulations were not carried out, and the researchers instead recommended it for future research work. In discussing this phenomenon, it must be highlighted that the magnitude of the vacuum suction must be significantly higher compared to the surcharge (if surcharge is applied) to qualify for further research. In the case of high surcharge and relatively smaller vacuum suction, researchers may not experience difficulties in numerical modelling–hence why this phenomenon has not typically drawn much research attention. Nonetheless, with the development of geosynthetic technology, higher vacuum intensities can be applied, a factor particularly relevant when used in laboratory environments where higher vacuum intensity compared to surcharge is a common occurrence.

2.10 Limitations and disadvantages of vacuum preloading

Vacuum suction alone may not be sufficient to consolidate the ground. If preliminary calculation shows a vacuum of 100 kPa or more is necessary for the target settlement, it is practically impossible to consolidate the ground with vacuum suction alone. This is

primarily because attempts to apply a vacuum at a greater intensity than the atmospheric pressure will induce cracks and result in less settlements compared to surcharge preloading. This limitation has been experimentally shown in the literature (e.g. Chu and Yan 2005a, Zhou et al. 2017). In practice, where more than 80 kPa of suction is necessary, it is preferred to combine vacuum with conventional preloading. From resent vacuum consolidation projects (shown in Appendix B) it confirms that most projects used a vacuum intensity in the rage of 60–70 kPa to avoid this problem.

When a membrane is used as a sealing layer, the effectiveness of the method mainly depends on the air tightness of the membrane. Vacuum losses have been reported in several ground-improvement cases (e.g. Karunawardena and Nithiwana 2009, López-Acosta et al. 2019). Notably, Karunawardena and Nithiwana (2009) reported significant (about 80%) vacuum loss due to air leaks which hindered the effectiveness of the ground-improvement process.

Vacuum pump breakdowns and electrical downtimes (among other factors) can also affect the consolidation process. While the vacuum pumps are running, some manned observation must also be placed. Hence, the process can be interrupted various times throughout the year (e.g. during long holiday seasons). These disturbances have also been reported in literature (e.g. Chai et al. 2006, Lam et al. 2018) and can be identified as a limitation in vacuum consolidation technique.

Although exact cost figures are not readily available, it is generally accepted that the CPVD method is comparatively costlier than the membrane vacuum method. Extensive tubing in the former method can be cumbersome and slow to implement.

2.11 Main research gaps in the literature

The primary research gaps identified in the current literature can be pointed out as follows:

(i) Extremely limited numerical modelling that considering long-term (more than one year) deformation predictions have been published relative to vacuum consolidation.

(ii) Elasto-plastic models limit the duration of predictability for a relatively short term. Since vacuum consolidation accelerates the consolidation process, settlements without significant change in EPP dissipation can be observed, and modelling such instances (e.g. creep) have not been sufficiently explored in the literature.

(iii) Despite numerous previous research attempts, predicting both EPP and settlement are still challenging, especially when long-term ground performance is concerned. Sustained EPP is a common observation in ground-improvement cases histories with deep buried soft clays. Mere modification or fine-tuning input parameters would not effectively produce accurate settlement and EPP predictions, as evident from Kelly et al. (2008) and Kelly and Wong (2009).

(iv) EVP models have been identified and suggested as a potential improvement for modelling accuracy in vacuum consolidation (e.g. Parsa-Pajouh et al. 2014). However, limited research has evaluated its success. Yin (2015) has also

suggested carrying out additional studies using EVP models for vacuum consolidation.

(v) Numerical modelling with significant changes in vacuum suction intensity compared to surcharge is challenging to numerically simulate. Although Kianfar et al. (2015) completed experimental work, they did not carry out numerical simulations. Instead they recommended to carryout numerical modelling of vacuum application and removal to fill the gaps in the literature.

(vi) Numerical modelling and implications of rather complex yet practical vacuum distributions have not been sufficiently explored.

2.12 Summary

This chapter critically discussed the relevant literature for the work presented in this thesis. First, it appears that vacuum application in a ground-improvement project is often carried out using two methods: the membrane and membrane-less method. The former is relatively easy to implement, but susceptible to air leakages, while the latter utilises extensive tubing, with less susceptibility to leakages. When dealing with highly permeable sand layers or if the ground being treated has the possibility being inundated, membrane-less method again proves more suitable.

Several numerical methods have been adopted to model vacuum consolidation. Advantages and disadvantages of these each method were discussed. Approaches such as treating vacuum application as additional vertical stress, lacks the accuracy of predicting EPP and lateral displacements. During the last few decades, most research has focused

on understanding the mechanisms involved in vacuum consolidation through laboratory and field cases, rather than on increasing the accuracy of numerical modelling.

It was identified, although soil responses upon application and removal vacuum in large magnitudes are available, the numerical modelling of the same has not been carried out in the literature.

Although vacuum consolidation is implemented for soft clays that can exhibit long-term settlement behaviours such as creep, almost all analyses related to vacuum consolidation are limited to elastic or elasto-plastic models, which are not suitable for predicting long-term ground performance. This is a clear contradiction and a research gap that must be explored in detail within the context of vacuum assisted PVDs. Several similar research gaps were also identified and pointed out in this literature review.

Upon identified the above research gaps, in the next chapter (Chapter 3) introduces a creep-based EVP model with time-dependent boundary conditions. This includes basic illustration on its potential to model vacuum consolidation. The model is then extensively applied in later chapters to address the persisting research gaps.

Chapter 3: EVP model with time-dependent boundary conditions for vacuum consolidation[1]

3.1 General

The boundary condition for conventional PVDs is typically modelled as a drained boundary. In a coupled analysis, this can be achieved by setting the respective degree of freedom (DOF) representing the EPP of the nodes along the PVD-soil interface to zero. Generally, this is a set boundary condition which prevails from the start to the end of an analysis. Importantly, such simplicity no longer exists in soil consolidation with vacuum-assisted PVDs. Hence, in this chapter proposes an EVP model with time-dependent boundary conditions. FE implementation is discussed and basic validation is also illustrated.

3.2 Importance of time-dependent boundary conditions for vacuum consolidation

Vacuum suction is applied through a vacuum pump and will not invariably prevail from the start to the finish in a ground-improvement project. As such, the same should be followed in numerical analysis. The vacuum application cannot be started until the main tasks of ground preparation are completed. This necessitates working platform, fully laying of all the tubing (if membrane-less vacuum-consolidation method is used),

[1] Material discussed in this chapter form part of the following publications:

Kumarage, P.I., and Gnanendran, C.T. 2019b. Long-term performance predictions in ground improvements with vacuum assisted Prefabricated Vertical Drains. Geotextiles and Geomembranes, **47**(2): 95–103. Elsevier. doi:10.1016/j.geotexmem.2018.11.002.

Kumarage, P.I., and Gnanendran, C.T. 2017. Viscoplastic behaviour of soft soil in vacuum consolidation. *In* Proceedings of the 70th Canadian Geotechnical Conference. Canadian Geotechnical Society (CGS), Ottawa, Canada.

trenches and sealing membrane (if membrane method is used). Generally, the vacuum pump is started soon after the embankment building commences.

Switching the vacuum pump on and off during long holiday periods and changing vacuum intensity over time are evident in most ground-improvement projects. Notably, vacuum consolidation project in Saga, Japan (Chai et al. 2006) provides a classic example of variable vacuum applications. Here, a vacuum pump was in operation only during the daytime from November to late December 2003. From January to March 2004, the pump was in operation 24 hours each day, sparking a mechanical failure from 31 January to 4 February. Similarly, the ground-improvement project reported in Lam et al. (2018) also noted a vacuum-pump failure(numerical simulation of this project is carried out in this thesis and discussed in Chapter 6).

Further, vacuum leaks can occur at many locations depending on the vacuum-consolidation technology being used. In the membrane method, leaks mainly occur at the sealing membrane, whereas the connection lines are most vulnerable in the membrane-less set-up. Even after vacuum suction reaches the PVD, significant vacuum loss can occur along the depth of the drain due to sandwiched sand layers or imperfections in the drain core.

Together, these examples prove that researchers should not solely perceive vacuum application as a constant value with time. It instead should be treated as a function of both time and depth. Thus, the boundary condition representing the vacuum application should also be considered as a time-dependent boundary condition. This approach helps in following the actual stress path the soil will likely undergo in vacuum consolidation.

It is important to highlight the differences in the approach undertaken in the literature. For example, Mesri and Khan (2012) simulated vacuum consolidation by modifying EPP as in the Eqn. (3.1):

$$u = |p_v| + \Delta\sigma_v \tag{3.1}$$

where, $|p_v|$ is the absolute value of vacuum intensity applied to the ground and $\Delta\sigma_v$ is the change in total vertical stress. In this approach, the solution for settlement and EPP is obtained as if the soil had been subjected to a fill load equivalent to $|p_v| + \Delta\sigma_v$. In case of instantaneous stress application, the initial EPP just after the application of vacuum and surcharge will be equal to $|p_v| + \Delta\sigma_v$. A correction is necessary to obtain the actual EPP. The approach undertaken in this thesis is different to the above, and is described in the following Section 3.3.

3.3 EVP model with time dependant boundary conditions

Let each node in the FE mesh have three DOFs. The first and second DOFs can be set at the users' preference (Typically the former denotes *x*-displacement and the latter is the y-displacement). The boundary condition for the third DOF (i.e. the EPP) for the nodes along the PVD-soil interface is defined in Eqn. (3.2):

$$u = p_{vac}(t, z) \tag{3.2}$$

where, *u* is the EPP and $p_{vac}(t,z)$ denotes vacuum function.

Meanwhile, the mean effective stress (p') is conventionally defined as the difference between the total mean stress (p) and the EPP (u), (i.e. $p' = p - u$). Unlike in conventional preloading with PVDs, p' is presented as in Eqn. (3.3):

$$p' = \begin{cases} p - (-p_{vac}) \\ p - u \end{cases} \tag{3.3}$$

where, p is the total mean stress and p' has two conditions as illustrated in Eqn. (3.3). At the PVD-soil boundary interface, there exists no EPP. Instead, the EPP values are equal to the respective vacuum suction at that particular time and depth. In the rest of the soil skeleton, p' is calculated as usual–that is as the difference between the total mean stress and the EPP.

3.3.1 Defining reference and loading surfaces

The reference surface and loading surface can be introduced in Eqn. (3.4) and Eqn. (3.5) respectively:

$$\bar{f} = \bar{p}^2 - \bar{p}_0 \bar{p}' + \left(\frac{\bar{q}}{M} \right)^2 \tag{3.4}$$

$$f = p^2 - p_L p' + \left(\frac{q}{M} \right)^2 \tag{3.5}$$

where, $\bar{p}'$ and p' are the mean effective stresses in $\overline{f}$ and f respectively, $\overline{q}$ and q are their corresponding deviatoric stresses. Meanwhile, $\bar{p}_0$ and p_L represent the intersection of the $\overline{f}$ and f surfaces with the positive p' axis, and M is the slope of the critical state line (CSL).

To calculate plastic (or viscoplastic) strains, a plastic potential function ($\hat{f}$) needs to be defined. For the research carried out in this thesis, the associated-flow rule (AFR) was instead assumed. Thus, it is considered that $\hat{f} \equiv f$.

Another possibility in defining $\bar{f}$ and f is to modify Eqn. (3.4) and (3.5) to incorporate a shape parameter (R). However, as previous research (e.g. Islam 2014, Islam and Gnanendran 2017) has shown R typically carries values very close to two, where incorporating $R = 2$ reduces the unnecessary complexities in the model. For this, a cross-check is carried out in Chapter 4 to calculate R, and to confirm whether $R \approx 2$ in the respective clay being used for the analysis.

3.3.2 Strain rate tensors

In the general stress space, the total strain rate tensor ($\dot{\varepsilon}_{ij}$) is assumed to be consisted of two components: the elastic strain rate tensor ($\dot{\varepsilon}_{ij}^{e}$) and viscoplastic strain rate tensor ($\dot{\varepsilon}_{ij}^{vp}$), as in Eqn. (3.6):

$$\dot{\varepsilon}_{ij} = \dot{\varepsilon}_{ij}^{e} + \dot{\varepsilon}_{ij}^{vp} \tag{3.6}$$

$\dot{\varepsilon}_{ij}^{e}$ is calculated according to Hooke's law as in Eqn. (3.7),

$$\dot{\varepsilon}_{ij}^{e} = C_{ijkl}\,\dot{\sigma}'_{kl} \tag{3.7}$$

where, $\dot{\sigma}'_{kl}$ is the effective stress rate tensor and C_{ijkl} is the elastic moduli tensor (given in Appendix–C).

Adopting Perzyna's (1963) formulation, the viscoplastic strain rate ($\dot{\varepsilon}_{ij}^{vp}$) can be defined using Eqn. (3.8),

$$\begin{aligned} \dot{\varepsilon}_{ij}^{vp} &= \langle \phi(F) \rangle \frac{\partial f}{\partial \sigma'_{ij}} \\ \langle \phi(F) \rangle &= \begin{cases} \phi(F) : F > 0 \\ 0 \quad\;\; : F \le 0 \end{cases} \\ F &= \frac{f - \bar{f}}{\bar{f}} \end{aligned} \tag{3.8}$$

where, ϕ is the rate sensitivity function, F is the overstress function and σ'_{ij} is the effective stress tensor.

As in Eqn. (3.8), if $f < \bar{f}$, then $F = 0$ and material behaves elastically. If $f > \bar{f}$ viscoplastic deformations will subsequently actuate. In this instance, F is quantified as the normal distance between f and $\bar{f}$ and the direction of the strain rate is determined by $\partial f / \partial \sigma'_{ij}$. However, this procedure inherently makes the assumption of AFR.

With the same stipulated conditions for *F*, in triaxial stress space, the viscoplastic volumetric strain rate ($\dot{\varepsilon}_v^{vp}$) can be defined by modifying the Eqn. (3.8) as,

$$\dot{\varepsilon}_v^{vp} = \langle \phi(F) \rangle \frac{\partial f}{\partial p'} \tag{3.9}$$

where, p' is the mean effective stress as calculated in Eqn. (3.3).

3.3.3 Deriving an expression for ϕ

According to Bjerrum's (1967) delayed concept, C_α can be defined as in Eqn. (3.10),

$$C_\alpha = \frac{\bar{e} - e}{\log t - \log \bar{t}} \tag{3.10}$$

where, $\bar{t}$ is the reference time and $\bar{e}$ is the void ratio at the reference time.

By substituting $\alpha = C_\alpha / \ln(10)$ and with subsequent re-arrangement, Eqn. (3.11) can be obtained:

$$\frac{t}{\bar{t}} = \left(\frac{\bar{e} - e}{\alpha} \right) \tag{3.11}$$

Differentiating Eqn. (3.11) with respect to time (*t*) and further re-arrangement obtains Eqn. (3.12):

$$\frac{de}{dt} = -\frac{\alpha}{\bar{t}} \exp\left(\frac{e-\bar{e}}{\alpha}\right) \tag{3.12}$$

Consider a clay sample is at point *A* (see Figure 3-1) at a reference time of $\bar{t}$ with a reference void ratio of $\bar{e}$. Due to creep, within a Δt duration, void ratio reduces from $\bar{e}$ to *e*. Consequently, the pre-consolidation pressure apparently increases from p_L to $\bar{p}_0$. Using Figure 3-1, expressions for $\bar{e}$ and *e* can be conveyed as in Eqn. (3.13) and (3.14) respectively:

$$\bar{e} = e_N - \lambda \ln p_L + \kappa \ln\left(\frac{p_L}{p'}\right) \tag{3.13}$$

$$e = e_N - \lambda \ln \bar{p}_0 + \kappa \ln\left(\frac{\bar{p}_0}{p'}\right) \tag{3.14}$$

where, e_N is the void ratio in the normal consolidation line (λ line) at $p' = 1$, λ and κ denote the compression and re-compression indices respectively according to the conventional theory of critical-state soil mechanics.

Combining Eqn. (3.13) and (3.14) consequently obtains Eqn. (3.15):

$$e - \bar{e} = (\lambda - \kappa) \ln\left(\frac{p_L}{\bar{p}_0}\right) \tag{3.15}$$

From the definition of viscoplasticity, Eqn. (3.16) contends the following:

$$\dot{\varepsilon}_v^{vp} = -\frac{de}{dt}\frac{1}{(1+e_0)} \tag{3.16}$$

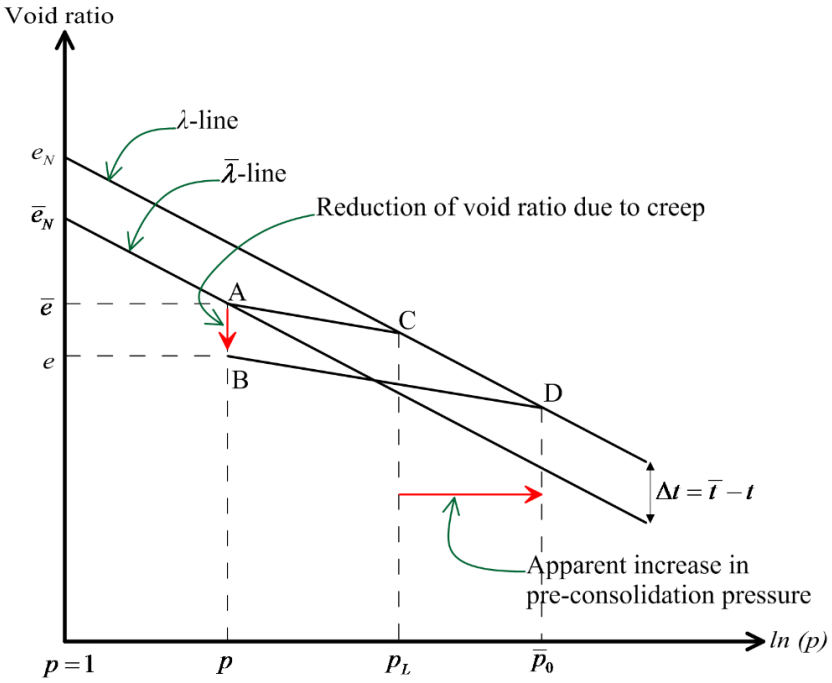

Figure 3-1: Illustration of the normal and reference consolidation lines in the *e-ln(p)* space.

Further by substituting Eqn. (3.12) to (3.16), Eqn. (3.17) is obtained:

$$\dot{\varepsilon}_v^{vp} = \frac{\alpha}{\bar{t}(1+e_0)}\exp\left(\frac{e-\bar{e}}{\alpha}\right) \tag{3.17}$$

Substituting Eqn. (3.15) to Eqn. (3.17) an expression for $\dot{\varepsilon}_v^{vp}$ can be obtained as in Eqn. (3.18):

$$\dot{\varepsilon}_v^{vp} = \frac{\alpha}{\bar{t}\left(1+e_0\right)}\left(\frac{p_L}{\bar{p}_0}\right)^{\frac{\lambda-\kappa}{\alpha}} \tag{3.18}$$

Meanwhile, rearranging Eqn. (3.9) ϕ can be expressed as,

$$\phi = \frac{\dot{\varepsilon}_v^{vp}}{\left(\frac{\partial f}{\partial p'}\right)} \tag{3.19}$$

Now, combining Eqn. (3.18) and Eqn. (3.19), an expression for ϕ can be obtained as in Eqn. (3.20):

$$\phi = \frac{\alpha}{\bar{t}\,\nu_0\left(\frac{\partial f}{\partial p'}\right)}\left(\frac{p_L}{\bar{p}_0}\right)^{\frac{\lambda-\kappa}{\alpha}} \tag{3.20}$$

where, $\nu_0 = \left(1+e_0\right)$.

3.4 Numerically modelling C_α

As shown in Eqn. (3.10), C_α is often treated as a constant and related to natural logarithm scale, where a change in void ratio of $\bar{e}-e$ occurs at a time interval of $\bar{t}-t$ under constant effective stress. When predicting the long-term deformational behaviour of soft clay, the assumption of a constant C_α value can provide misleading results (Yin 1999, Karim et al. 2010). Moreover, in vacuum consolidation, stresses in the soil element can

significantly change upon application and removal of vacuum. There are several ways of modelling a linear or non-linear change in C_α, as discussed in Chapter 2. Consequently, in this thesis C_α in vacuum consolidation has been modelled using the following Eqn. (3.21):

$$C_\alpha = C_{\alpha-\max} EXP\left[-N\left(\bar{p}_0 - p_L\right)\right] \tag{3.21}$$

where, $C_{\alpha\text{-}max}$ is the maximum value of C_α generally at the time yielding commencement, and N is a numerical constant. Eqn. (3.21) is analogous to the function proposed in Karim et al. (2010); however, the two constants $C_{\alpha\text{-}max}$ and N were modified to match the particular clay type. Parameter $\bar{p}_0 - p_L$ can be considered as a measure of the extent creep has occurred (Karim et al. 2010) and is a helpful measure in long-term EVP modelling. To determine $C_{\alpha\text{-}max}$ and N it is necessary to conduct long-term consolidation tests at different vertical stresses. These stresses should be chosen such that they cover the entire stress range the clay is expected to undergo in the field. C_α determined from each test can then be plotted against $\bar{p}_0 - p_L$ to determine $C_{\alpha\text{-}max}$ and N. Generally, $C_{\alpha\text{-}max}$ is observed as the material commence yielding i.e. when $\bar{p}_0 - p_L = 0$. Relevant experimental data were used to calibrate the above function in the subsequent FEA reported in this thesis.

In numerical implementation, Eqn. (3.21) also proposes that researchers question an outcome if $\bar{p}_0 - p_L < 0$. Indeed, this would result in creep values even higher than the set maximum, hence prompting the necessity of error trapping in the numerical coding of this equation. However, $\bar{p}_0 - p_L < 0$ condition also implies that $f < \bar{f}$, thus $F = 0$ and

consequently the material will behave elastically; hence the value of the C_α is immaterial. As such, in the FE code, it was defined as $C_\alpha = C_{\alpha-\max}$ when $\bar{p}_0 - p_L \le 0$.

Figure 3-2 is a visual illustration of the creep function in Eqn. (3.21) within a reasonable range. However, with specific data, this 3D surface can be deduced to a line.

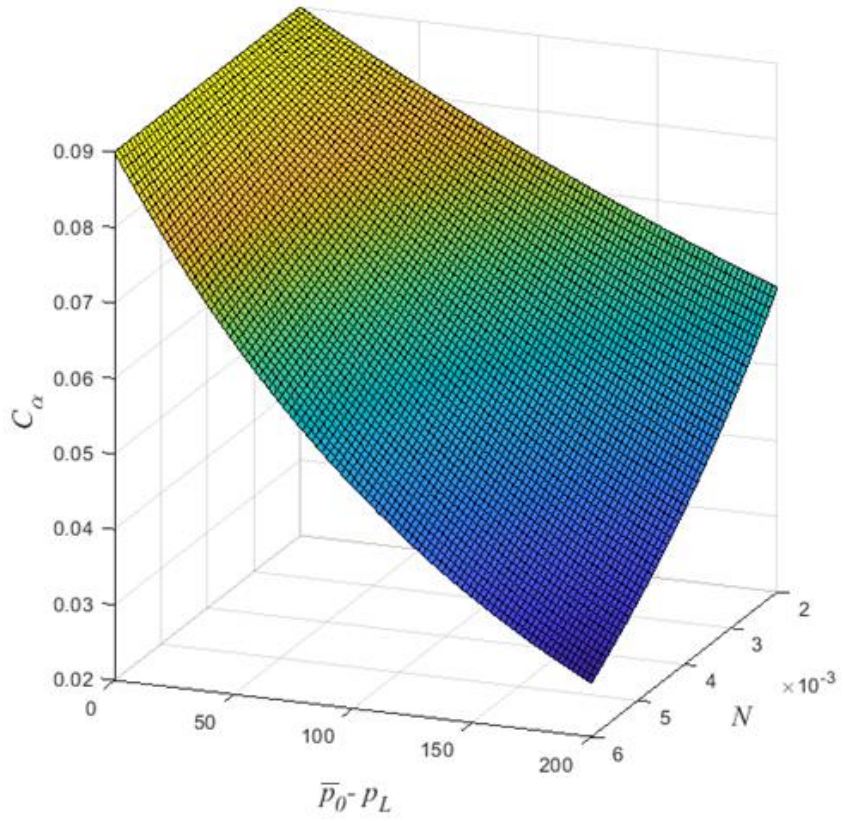

Figure 3-2: Visual 3D presentation of the creep function.

3.5 FE implementation

The model was implemented in modified version of AFENA (Carter and Balaam 1995, Islam 2014). Importantly, the said version of the AFENA program could not simulate vacuum consolidation.

3.5.1 Viscoplastic strain increments

For a time increment, $\Delta t = t_{n+1} - t_n$, the viscoplastic strain rate increment $\Delta\varepsilon_n^{vp}$ can be defined as in Eqn. (3.22):

$$\Delta\varepsilon_n^{vp} = \Delta t_n \left[\left(1-\theta_d\right)\dot{\varepsilon}_n^{vp} + \theta_d \dot{\varepsilon}_{n+1}^{vp} \right] \tag{3.22}$$

where, θ_d is a constant, θ_d = 0 and θ_d = 1 represent fully explicit and fully implicit Euler time integration schemes. There is no restriction in using any value as $0 \le \theta_d \le 1$; however, to make the integration scheme unconditionally stable, $\theta_d \ge 0.5$ can be adopted. As such, θ_d = 0.5 is used throughout this thesis.

The term $\dot{\varepsilon}_{n+1}^{vp}$ (at the time step $n+1$) can be calculated using the Taylor series expansion as in Eqn. (3.23);

$$\dot{\varepsilon}_{n+1}^{vp} = \dot{\varepsilon}_n^{vp} + \frac{\partial \dot{\varepsilon}_n^{vp}}{\partial \sigma}\Delta\sigma_n + \frac{\partial^2 \dot{\varepsilon}_n^{vp}}{\partial \sigma^2}\frac{\left(\Delta\sigma_n\right)^2}{2!} + \frac{\partial^3 \dot{\varepsilon}_n^{vp}}{\partial \sigma^3}\frac{\left(\Delta\sigma_n\right)^3}{3!} + ... \tag{3.23}$$

Ignoring the higher order terms Eqn. (3.23) can be approximated as,

$$\dot{\varepsilon}_{n+1}^{vp} = \dot{\varepsilon}_n^{vp} + \frac{\partial \dot{\varepsilon}_n^{vp}}{\partial \sigma}\Delta\sigma_n \tag{3.24}$$

Substituting Eqn. (3.24) in Eqn. (3.22), the following (Eqn. (3.25)) can be obtained,

$$\Delta\varepsilon_n^{vp} = \Delta t_n \left(\dot{\varepsilon}_n^{vp} + \theta_d \frac{\partial \dot{\varepsilon}_n^{vp}}{\partial \sigma} \Delta\sigma \right) \tag{3.25}$$

3.5.2 FE formulation for coupled analysis

Since soil consolidation essentially involves a hydro mechanism (with or without vacuum), a coupled analysis is inevitable. Thus, Biot-type coupled solution is formulated for the vacuum consolidation analysis.

To satisfy the equilibrium condition it requires,

$$\begin{aligned} \frac{\partial \sigma_x}{\partial x} + \frac{\partial u_w}{\partial x} + \frac{\partial \tau_{xy}}{\partial y} + \frac{\partial \tau_{xz}}{\partial z} + \gamma_x = 0 \\ \frac{\partial \sigma_y}{\partial y} + \frac{\partial u_w}{\partial y} + \frac{\partial \tau_{xy}}{\partial z} + \frac{\partial \tau_{xz}}{\partial x} + \gamma_y = 0 \\ \frac{\partial \sigma_z}{\partial z} + \frac{\partial u_w}{\partial z} + \frac{\partial \tau_{xy}}{\partial x} + \frac{\partial \tau_{xz}}{\partial y} + \gamma_z = 0 \end{aligned} \tag{3.26}$$

where, γ_x, γ_y and γ_z are the components of the bulk unit weight of the soil acting in the *x*, *y* and *z* coordinate directions respectively.

The constitutive relationship can be expressed as in Eqn. (3.27):

$$\{\Delta\sigma\} = [D]\{\Delta\varepsilon\} \tag{3.27}$$

where, [*D*] is the material matrix for the EVP model.

For continuity, Eqn. (3.28) must be satisfied:

$$\frac{\partial v_x}{\partial x}+\frac{\partial v_y}{\partial y}+\frac{\partial v_z}{\partial z}-Q=\frac{\partial \varepsilon_v}{\partial t} \tag{3.28}$$

where, v_x, v_y and v_z are the velocities of the pore fluid in their respective coordinate directions and Q is the inflow or outflow from the system.

By application of the principle of virtual work to the equilibrium equation and the continuity equation, the following relationship in Eqn. (3.29) can be obtained:

$$\begin{aligned}\int_v \{\delta\varepsilon\}^T \{\Delta\underline{\sigma}\}\, dV &= \int_v \{\delta\varepsilon\}^T \{\Delta\sigma\}\, dV + \int_v \{\delta\varepsilon\}^T \{\Delta U_w\}\, dV \\ &= \int_v \{\delta\varepsilon\}^T \{\Delta F_b\}\, dV + \int_s \{\delta d\}^T \{\Delta T\}\, dS\end{aligned} \tag{3.29}$$

where, $\delta\varepsilon$ is the virtual strain vector, $\Delta\underline{\sigma}$ and $\Delta\sigma$ are the incremental total and effective stress vectors respectively, ΔU_w is the incremental pore water pressure vector, δd is the virtual displacement vector, F_b is the incremental body force vector and ΔT is the applied surface load incremental vector.

A shape function (N_s) can be used to vary the displacements within a finite element as,

$$\{\delta d\}=[N_s]\{\delta a\} \tag{3.30}$$

where, δa is the virtual nodal displacement vector.

Likewise, variation in pore pressure can be obtained by Eqn. (3.31):

$$\{\delta u_w\} = [N_s]\{\delta b\} \tag{3.31}$$

where, δb is the nodal EPP vector. Throughout this thesis, the same N_s was used for both the displacements and pore pressure variations within the element.

Corresponding strains within the element are obtained by,

$$\{\delta \varepsilon\} = [B_s]\{\delta a\} \tag{3.32}$$

where $[B_s]$ is the strain-nodal displacement transformation matrix.

The incremental volumetric strain vector (δv) is calculated as in Eqn. (3.33):

$$\{\delta v\} = \{m\}^T [B_s]\{\delta a\} \tag{3.33}$$

where, the vector $\{m\}^T$ is defined as,

$$\{m\}^T = [1 \quad 1 \quad 1 \quad 0] \tag{3.34}$$

Eqn. (3.29) can now be written by substituting Eqn. (3.30), (3.31), (3.32) and (3.33) as,

$$\left[K^e\right]\{\delta a\}+[L]\{\delta b\}=\{\Delta F\} \tag{3.35}$$

where,

$$\left[K^e\right]=\int_v [B_s]^T \left[D^e\right][B_s]\,dV \tag{3.36}$$

$$[L]=\int_v [B_s]^T \{m\}[N_s]\,dV \tag{3.37}$$

$$\{\Delta F\}=\int_v \{N_s\}^T \{\Delta F_b\}\,dV+\int_s \{N_s\}^T \{\Delta T\}\,dS+\int_v \{\Delta\sigma_{vp}\}dV \tag{3.38}$$

and σ_{vp} is the viscoplastic relaxation stress vector, which is defined as,

$$\{\Delta\sigma_{vp}\}=[B_s]^T \left[D^{vp}\right]\{\dot{\varepsilon}^{vp}\}\Delta t \tag{3.39}$$

where, $D^{vp}=\partial\dot{\varepsilon}_n^{vp}/\partial t$.

Applying the principle of virtual work to the 2D continuity equation gives,

$$\int_{vol}\{\delta b\}\left[\frac{k_{11}}{r_w}\frac{\partial^2 U_w}{\partial x_{11}^2}+\frac{k_{33}}{r_w}\frac{\partial^2 U_w}{\partial x_{33}^2}+\frac{\partial V_s}{\partial t}\right]d\,(vol)=0 \tag{3.40}$$

where, k_{11} and k_{33} are the hydraulic conductivities in the x and z directions respectively, and V_s is the seepage velocity.

The EPP gradient can be defined as in Eqn. (3.41):

$$\begin{bmatrix} \frac{\partial U_w}{\partial x_{11}} \\ \frac{\partial U_w}{\partial x_{33}} \end{bmatrix} = [E_s]\{\delta b\} \tag{3.41}$$

here, $[E_s]$ is the matrix containing the values obtained by differentiating the $[N_s]$ with respect to x_{11} and x_{33}.

Now from Eqn. (3.41), the Eqn. (3.42) is presented:

$$[L]^T \frac{d\{a\}}{dt} - \phi_k \{b\} = \int_s \{N_s\}^T \{V_n\} dA \tag{3.42}$$

where,

$$[L] = \int_v [B_s]^T \{m\}\{N_s\} dV \tag{3.43}$$

$$\phi_k = \int_{vol} [E_s]^T [K][E_s] \frac{1}{r_w} d(vol) \tag{3.44}$$

and V_n is the prescribed boundary seepage velocity, $[K]$ is the hydraulic conductivity matrix, given as,

$$[K] = \begin{bmatrix} k_{11} & 0 \\ 0 & k_{33} \end{bmatrix} \tag{3.45}$$

After integrating Eqn. (3.42), the following can be obtained,

$$\begin{aligned}&\left[L\right]^T\left\{\delta a\right\}-\phi_k\left[\left(1-\beta_1\right)\left\{b\left(t\right)\right\}+\beta_1\left\{b\left(t+\Delta t\right)\right\}\right]=\\&\int_s\left[N_s\right]^T\left[\left(1-\beta_1\right)\left\{V_n\left(t\right)\right\}+\beta_1\left\{V_n\left(t+\Delta t\right)\right\}\right]\Delta t\,dA\end{aligned}\tag{3.46}$$

where, β is a constant that defines how b varies during the defined time interval (Δt). As previous literature (e.g. Booker and Small 1975, Britto and Gunn 1987) suggest to use $\beta \geq 0.5$ to ensure the integration scheme remains stable. For the analyses carried out in this thesis $\beta = 1$ is adopted. It was noted that the same value has been used by Britto and Gunn (1987) and this having $\beta = 1$ simplifies Eqn. (3.46) as:

$$\left\{L\right\}^T\left\{\Delta a\right\}-\phi_k\Delta t\left\{\Delta b\right\}=\phi_k\Delta t\left\{b\right\}+\int_s\left\{L\right\}^T V_n\left\{t+\Delta t\right\}\Delta t dA=\left\{\Delta F_s\right\}\tag{3.47}$$

Now, the fully coupled FE formulation can be obtained as in Eqn. (3.48):

$$\begin{bmatrix}\left\{K_e\right\} & \left\{L\right\}\\ \left\{L\right\}^T & -\phi_k\Delta t\end{bmatrix}\begin{bmatrix}\left\{\Delta a\right\}\\ \left\{\Delta b\right\}\end{bmatrix}=\begin{bmatrix}\left\{\Delta F\right\}\\ \left\{\Delta F_s\right\}\end{bmatrix}\tag{3.48}$$

where $\left\{K_e\right\}$ is the element stiffness matrix.

3.6 Soil response with time-dependent boundary conditions

3.6.1 Simulating the EPP response with time-dependent boundary conditions

For a basic illustration of time-dependent boundary conditions and their respective EPP response, a FE simulation with a unit cell was carried out with the properties of soft Hong Kong marine deposit (HKMD) clay. Although no preference given, the primary reason for choosing HKMD clay lies is due to its well-established properties (presented in Table 3-1) which are readily available in the published literature (e.g. Yin and Zhu 1999, Yin et al. 2002).

Table 3-1: Adopted properties[1] for HKMD clay.

Property	Value	Property	Value
λ	0.1983	$\bar{t}$	1.0
κ	0.0451	M_c	1.265
ϕ'_{cs}	31.5^0	e_N	2.18
ν	0.3	R^2	2.0
C_α	0.0106	k_v	6.10E-08 cm/sec

[1]These properties were adopted from Yin et al. (2002); [2]Value of the shape parameter (R=2) was assumed.

The unit cell dimensions were 0.95 m in height and 0.02 m in radius which is close to the dimensions of a large consolidation cell reported in the literature (e.g. Indraratna and Redana 1998, Indraratna et al. 2004). The vertical drain assumed to run the full depth (i.e. 0.95 m) at the middle of the unit cell. Six-noded triangular elements were used in the

analysis, each node having three degrees of freedom per node. To represent the drain, the third degree of freedom of the elements along the axisymmetric boundary of the unit cell was modified. More details of the boundary value modification are given in Chapter 4, Section 4.6.1.

Four cases are presented for comparison. Case (i) is the simplest form with no vacuum applied. In this example, the third DOF of the nodes representing the PVD soil-boundary is set to zero and remains unchanged throughout the analysis. Conversely, Case (ii) sees –70 kPa of vacuum applied to the same nodes, which neither change over time. Numerical modelling of these scenarios are rather simple since the boundary condition is fixed with time. Figure 3-3(a) shows the EPP behaviour in these two cases.

Importantly, the second case (Case (ii)) is only practicable for numerically simulating laboratory experiments. In this scenario, vacuum can be applied for the total duration of the experiment (e.g. Saowapakpiboon et al. 2011). However, in most (if not all) ground-improvement projects, vacuum is applied after the main works of the ground preparation is completed and may not be applied with a fixed intensity. Simulation of these instances with time-dependent boundary conditions are illustrated as follows.

In Cases (iii) and (iv) vacuum was applied and removed during the total simulated time across 100 days. In Case (iii) vacuum was introduced at 10 days and removed at 60 days, while Case (iv) this occurred at 20 and 80 days respectively. In all of the above cases a surcharge of 100 kPa was maintained at the top most surface of the unit cell. For simplicity, characteristics of the unit cell (such as smear zone) are not considered and

more details are given in Section 3.6.2. A summary of simulated cases is given in Table 3-2.

Table 3-2: Summary of cases simulated with varying boundary conditions.

Case	Vacuum application on (day)	Vacuum removed on (day)
Case (i)	No vacuum applied	
Case (ii)	Constant –70 kPa vacuum applied	
Case (iii)	10	60
Case (iv)	20	80

From the FE simulation result (presented in Figure 3-3(a)), in Case (i), the EPP reduced from 100 kPa to zero, which is the set boundary condition to simulate conventional PVD. Similarly, in Case (ii) the solution converges to the applied vacuum of –70 kPa. EPP dissipation in Cases (iii) and (iv) significantly speeds up upon start of the vacuum application and reach the applied vacuum value of -70 kPa. Upon removing vacuum at 60 days and 80 days in these cases respectively, EPP reaches its natural stable value of zero.

The settlement pattern is also corresponding to the EPP dissipation as expected indicating the successful implementation of the coupled analysis with variable boundary conditions. Vacuum application contributes to reach a given settlement target in a shorter duration than the conventional methods without vacuum.

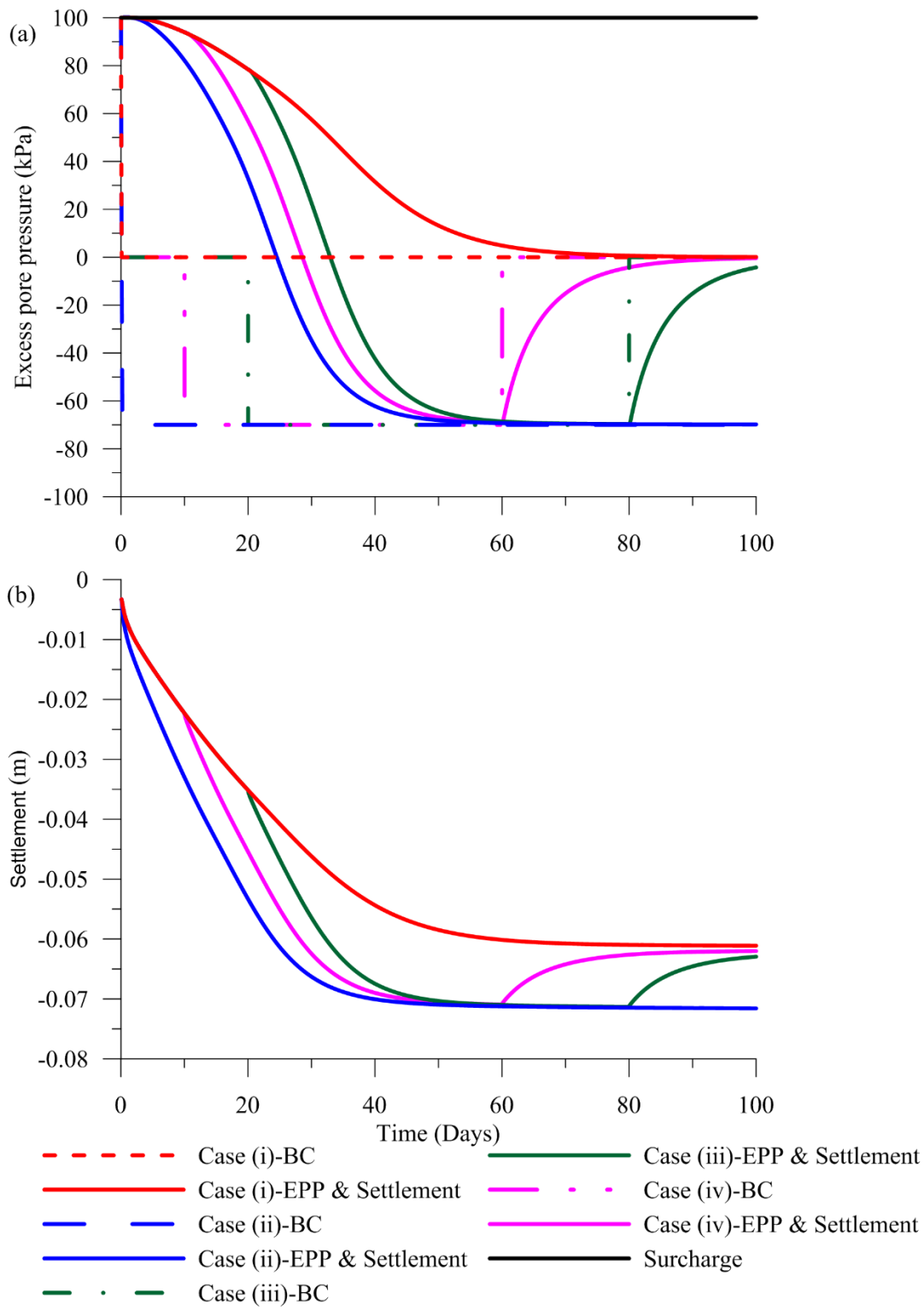

Figure 3-3: EPP and settlement with different boundary condition changes.

3.6.2 Verification against laboratory data

This section aims to compare the responses of the EVP model presented in this chapter against experimental results reported in Saowapakpiboon et al. (2011). It is not the aim of this section to back analyse and match the FEA predictions to the near perfection. Instead, this section primarily aims to illustrate basic behaviour of the model including its capability in practical application to vacuum consolidation and obtain a basic idea about what parameters chiefly influences the FEA results.

The soil samples used in this study has been obtained from site located at the Second Bangkok International Airport (SBIA) project in Thailand. The soft clay samples have been collected at 3.0 – 4.0 m depth. Salient properties of the clay are shown in Table 3-3. Evidently, some of the properties were adopted from Saowapakpiboon et al. (2011), and some were assumed and varied in the FEA.

Table 3-3: Summary of the clay properties from the SBIA project.

Property	Value	Property	Value
λ	0.569	p_c' (kPa)	50
κ	0.055	ν	0.3
M	0.80	γ_{sat} (kN/m^3)	14.70
e_0	2.29	k (m/day)	6.3E-05
[1]C_α	0.0393 to 0.0786	[2]k_h/k_s	1–3

[1,2] These values were assumed and varied in the FEA.

Saowapakpiboon et al. (2011) proposed to numerically simulate the system using a negative stress at the top of the soil sample. However, as discussed in Chapter 2, vacuum suction travels through the PVD, thus in this FE model, both the top and the PVD-soil

interface were kept as vacuum-applied boundaries. Both the FE mesh and the boundary conditions are presented in Figure 3-4.

Analysis was conducted looking into three key aspects. First is the vacuum intensity, which was varied from –40 kPa to –60 kPa since the experimental data revealed that the intended vacuum operates at –50 kPa. Second is the effect of the k_h/k_s ratio, for which values from 1 to 3 were adopted. Meanwhile, the third aspect concerned the effect of C_α. As no data were available to confirm the value of C_α, lowest and highest C_α/C_c ratios defined by Mesri and Godlewski (1977) were adopted.

Results of the numerical simulation are given in Figure 3-5. The input data were not fine-tuned to match the experimental results since such an attempt would jeopardise the intention of the analysis. However, it is clear that the FEA model with appropriate boundary modification gives results within an acceptable range.

The influence of each parameter mentioned above is illustrated in the Figure 3-5. In terms of permeability $k_h/k_s = 2$ seems the better option to match the settlement curve and simultaneously allow some under-prediction for EPP. For this set of curves $C_\alpha = 0.0655$ has been adopted (representing the $C_\alpha /C_c = 0.05$, the typical upper bound) since this is soft clay. When the k_h/k_s ratio is subsequently changed from 1 to 3, a maximum difference of ~12% for settlements and ~52% for EPP can be observed.

Although the experimental information states that –50 kPa vacuum intensity was used, p_{vac} values of –40 kPa and –60 kPa were simulated to observe the FEA numerical model's

sensitivity to vacuum intensity. As discovered the vacuum intensity is a variable with significant influence.

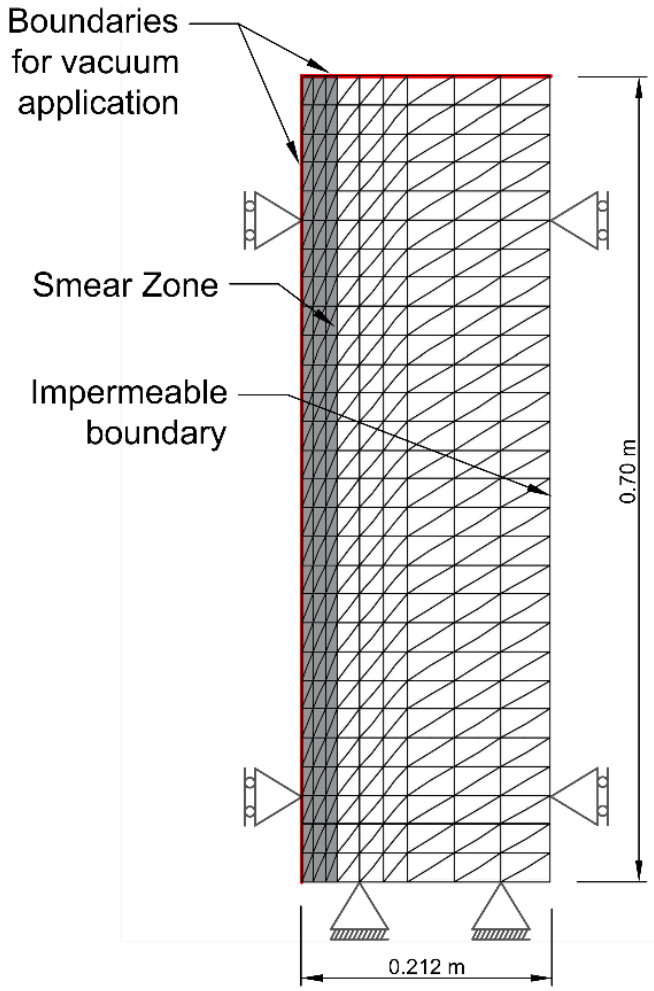

Figure 3-4: FE mesh with boundary conditions to simulate laboratory experiments of Saowapakpiboon et al. (2011).

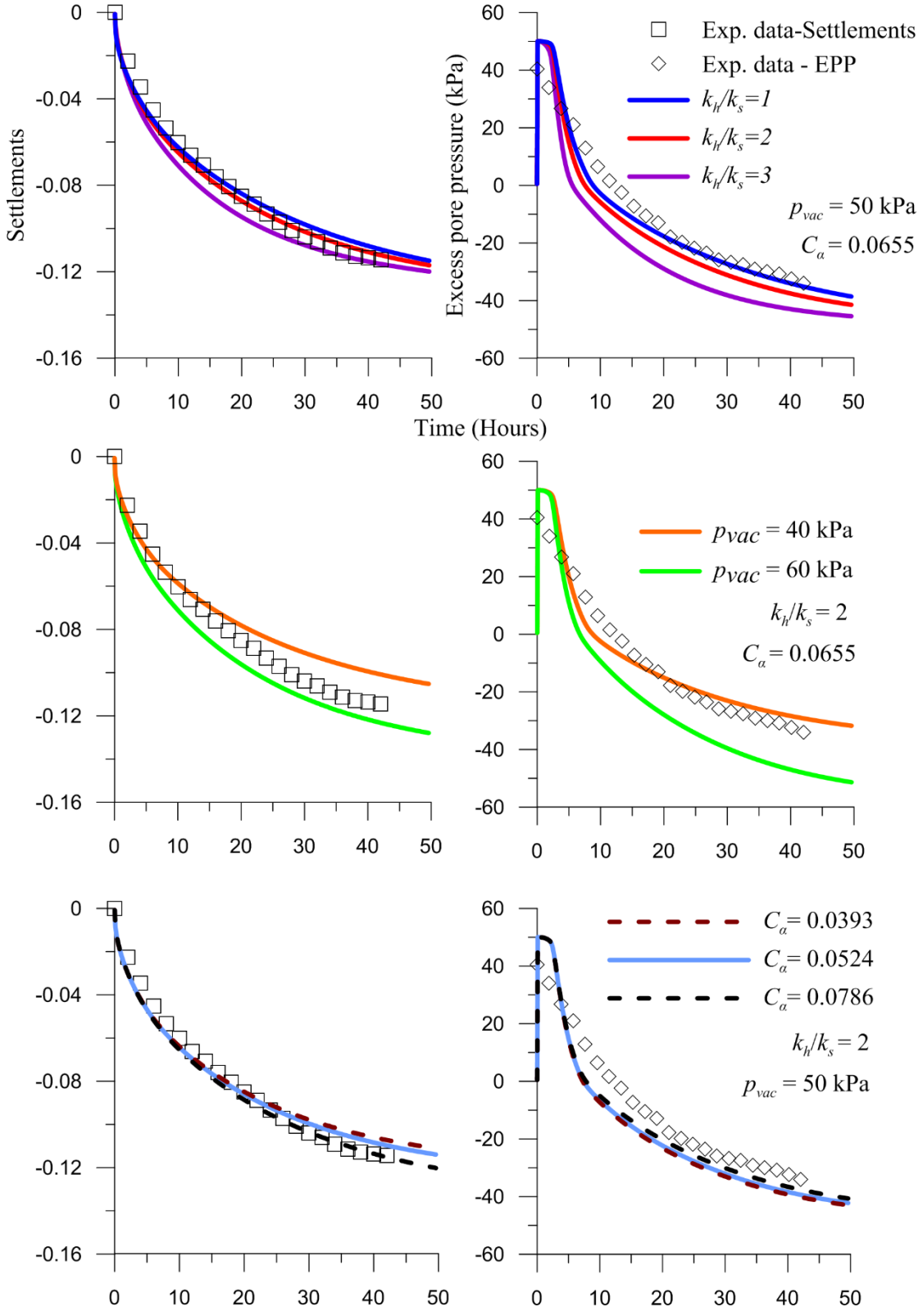

Figure 3-5: Settlement and EPP response against experimental data (experimental data obtained from Saowapakpiboon et al. 2011).

At this scale and time frame, C_α has negligible influence. As such using the approximation (Mesri and Godlewski 1977) values applicable to C_α/C_c = 0.03; 0.05 and 0.06 are plotted. It is understood that C_α/C_c = 0.06 is out of the range proposed by Mesri and Godlewski (1977). As seen from results, the best matching FEA results for settlements are obtained by C_α = 0.0786 (representing C_α/C_c = 0.06). This proposes a possibility of surpassing the typical C_α/C_c ratio. More detailed investigation on this matter is discussed in Chapter 4.

As discussed in the literature review (Chapter 2), to date limited data is available to model the reduction of C_α in the presence of vacuum. However, the formulation carried out in this thesis includes a variable C_α which is governed by the change in apparent creep inclusive pre-consolidation pressure. Hence, the formulation readily facilitates to model the reduction in C_α by fitting the characteristic curve to Eqn. 3.21. However, due to limited availability of field data a case study on this matter is not discussed.

In all of the above examples, care has been taken to converge the solution accurately by reducing the vacuum surcharge ratio (VSR) which will be defined in Chapter 6 as it was discovered when VSR $\geq$ 0.5, numerical instability can occur in application and removal of vacuum. This convergence problem is also discussed and addressed in Chapter 6 of the thesis.

There is a practical upper limit for the magnitude of the vacuum suction that can be applied in ground improvements. The atmospheric pressure is about 101.3 kPa. Hence, theoretically this value can be considered as the upper limit for vacuum application. As suction eventually surpasses 90 kPa, unsaturation can occur as detected in many field and

laboratory cases. With this upper level, ground-improvement project reaching VSR ≥ 0.5 condition at the time of removing vacuum is unlikely to occur. However, as will clarify in this thesis, numerical instabilities can occur in modelling laboratory experiments, hence this constitutes an essential element in effective geotechnical analysis.

3.7 Summary

This chapter introduced time-dependent boundary conditions to a creep-based EVP model. The said boundary conditions were intended to be applied to the third DOF of the nodes along the line representing the vacuum-assisted PVD. This enables the model to be used in the context of vacuum consolidation. Options available in incorporating C_α to the model was also discussed with a 3D illustration of a creep surface. FE formulation of the coupled analysis was also discussed. The basic EPP response due to time-dependent boundary conditions were demonstrated using HKMD clay as an example.

The model was then used to numerically simulate both EPP and settlement response with vacuum suction in the laboratory based environment reported by Saowapakpiboon et al. (2011). Analysis revealed a good agreement against laboratory experimental results, and vacuum intensity, k_h/k_s ratio were identified as significantly influencing factors.

With the FEA carried out in this chapter it can be concluded that time-dependent boundary conditions can be successfully implemented into an EVP model to simulate vacuum suction for soft soil stabilisation cases.

Overall, the cases discussed in this chapter are rather limited. The analysis time was relatively short and simple. Hence, the model and the corresponding techniques are

applied in a case study in the next chapter (Chapter 4) for an actual ground-improvement case history. The numerical instability and their treatments are subsequently addressed in Chapter 6.

Chapter 4: Unit cell analysis of Ballina embankment using EVP model[2]

4.1 General

The Ballina bypass was constructed as part of the Pacific Highway upgrade project to reduce the traffic congestion near Ballina, New South Wales. Along the Pacific Highway, several types of clay were found to contain varying properties, most of which were from river flood plains. The area of Ballina is in the flood plans of Richmond River, where the deepest and softest soil is available (Figure 4-1). In this sense, the project brought with it some unique challenges in constructing the bypass and likewise marks the reported first case in which vacuum consolidation has been applied for a ground-improvement project in Australia.

This chapter illustrates application of the EVP model described in Chapter 3 for an actual ground-improvement project. Time-dependent boundary conditions have been used to numerically simulate vacuum application, and the foundation soil has been modelled using said coupled EVP model. Considering the long-term analysis, creep behaviour has been awarded special attention. Both the large-strain option and nodal updating was enabled and its importance is demonstrated. To highlight the improvements made,

[2] Material discussed in this chapter form part of the following publications:

Kumarage, P.I., and Gnanendran, C.T. 2019b. Long-term performance predictions in ground improvements with vacuum assisted Prefabricated Vertical Drains. Geotextiles and Geomembranes, **47**(2): 95–103. Elsevier. doi:10.1016/j.geotexmem.2018.11.002.

Kumarage, P.I., and Gnanendran, C.T. 2017. Viscoplastic behaviour of soft soil in vacuum consolidation. *In* Proceedings of the 70th Canadian Geotechnical Conference. Canadian Geotechnical Society (CGS), Ottawa, Canada.

comparisons were drawn with previous research attempts. To illustrate the precision of the methodology applied, settlement behaviours have been compared in different locations along the centreline of the embankment.

An investigation of the site revealed that the area consists of soft soil layers of up to 25 m thickness, and the liquid limit and plastic limit varying between 60–80% and 30–40% respectively (Kelly and Wong 2009). Soil mixing, stone columns, displacement auger piles, piled embankment were some of the potential methods that could be used to improve the ground. However, it was assessed that those soil-improvement methods were too expensive to treat such deep clay layers. On the other hand, conventional wick drains would be too slow to consolidate the clay to an acceptable level within a reasonable construction period. Consequently, vacuum assisted PVD consolidation was identified as the most suitable method to improve the clay foundation.

Since this attempt marks the first time vacuum-assisted PVDs have been used in a ground-improvement project in Australia, an instrumented trial embankment was constructed to investigate its effectiveness. Figure 4-2 is a schematic illustration of the instrumented embankment, which was divided into two sections A and B. To compare the performance of the vacuum-assisted PVDs, Section B had the vacuum suction applied and Section A had conventional PVDs without vacuum.

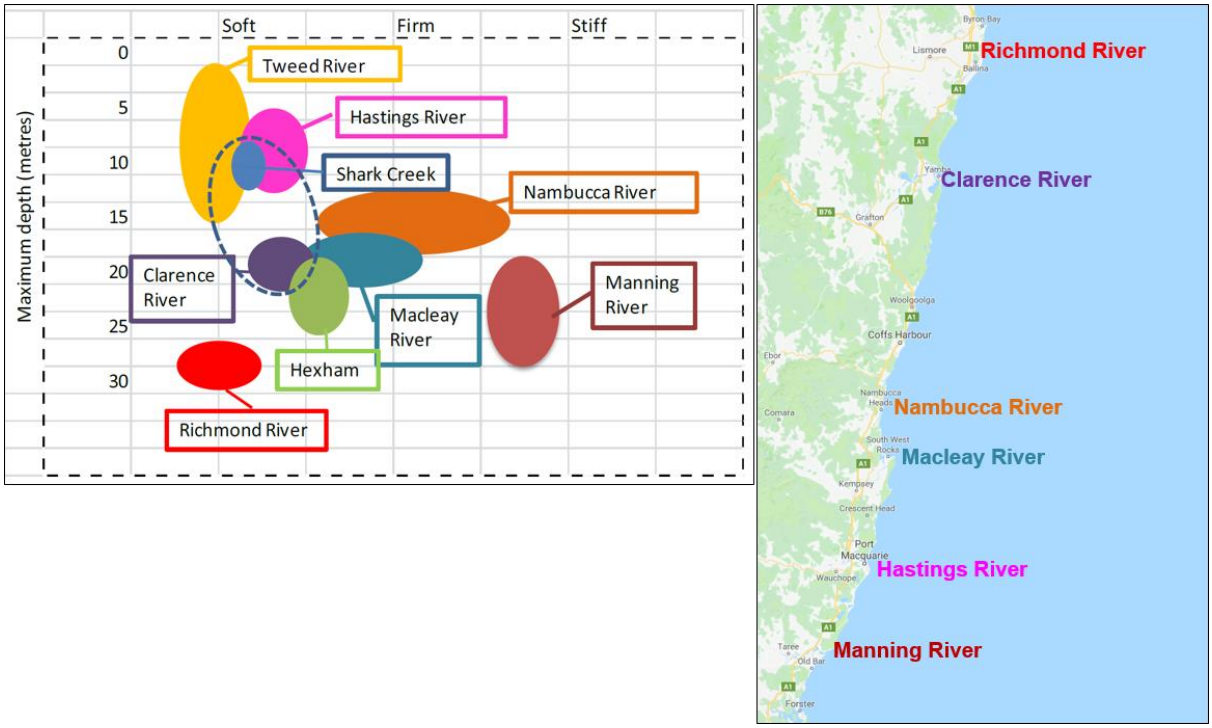

Figure 4-1: Clay types along the pacific highway (modified from Higgins 2016).

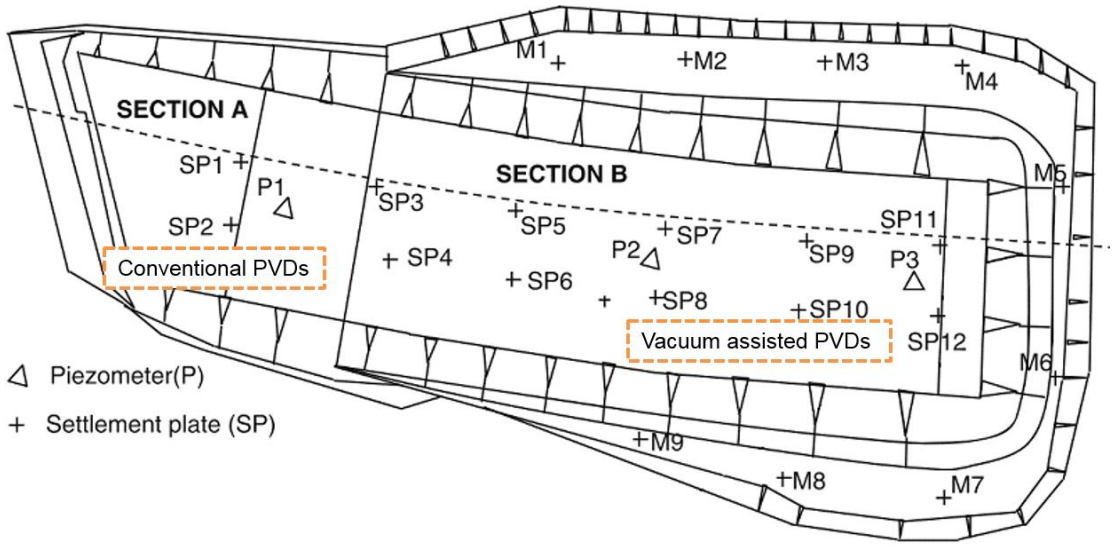

Figure 4-2: Instrumentation locations of the Ballina test embankment (modified from Parsa-Pajouh et al., 2014).

4.2 Challenges in understanding soil behaviour

Field data from piezometers in this project have reported sustained EPP despite the long duration vacuum application. Several other studies in ground-improvement projects have also reported this trend of EPP being sustained in deep clay layers (e.g. Kabbaj et al. 1988, Rowe and Li 2002). Secondary compression has often been highlighted as a possible reason, though with respect to vacuum consolidation, neither detailed investigations nor modelling attempts have been carried out with an EVP model. Notably, Kelly and Wong (2009) attempted to back-calculate the compression index (C_c) to match both settlement and EPP and reported it is not successful. Hence predicting both settlements and EPP for the entire 1,200 day project duration has been a significant challenge for researchers.

In the Newcastle symposium (Kelly et al. 2018) for the behaviour prediction of embankment on soft soil, some 20 research groups competed to predict and back-analyse the ground deformation in the Ballina embankment. However, the symposium mainly focused on Section A of the embankment where vacuum-assisted PVDs were not used. Few researchers who have attempted to predict the performance of Section B (e.g. Khan 2010, Indraratna et al. 2012b, Parsa-Pajouh et al. 2014), did not continue their predictions for the entire monitoring period of 1,200 days and failed to consider viscous behaviour of the soil, despite its evidence. As such, this chapter will address these challenges and create new knowledge to close the aforementioned gaps in the research.

4.3 Unit cell idealisation

The mechanism in consolidation with PVDs is essentially axisymmetric. Hence, unit cells can be considered as a viable option to model consolidation settlements. In this project, circular PVDs were installed in a square pattern. Hence, a making calculation to determine the well radius (r_w) is unnecessary (as reviewed in Chapter 2). It was reported

that r_w = 17 mm (Kelly and Wong 2009, Indraratna et al. 2012b, Mesri and Khan 2012, Parsa-Pajouh et al. 2014). Meanwhile the equivalent radius (r_e) can be calculated considering the area covered by each PVD as per Eqn. (4.1) and (4.2).

Given that S = 1 (Table 4-1), the calculated r_e was r_e = 0.5642 m. Table 4-1 summarises the properties of the PVD and unit cell adopted for the analysis.

Regarding the smear zone, since there is no promising way for estimation, a certain amount of trial and error was necessary. For this analysis r_s/r_w = 4 and k_h/k_s = 2 were adopted.

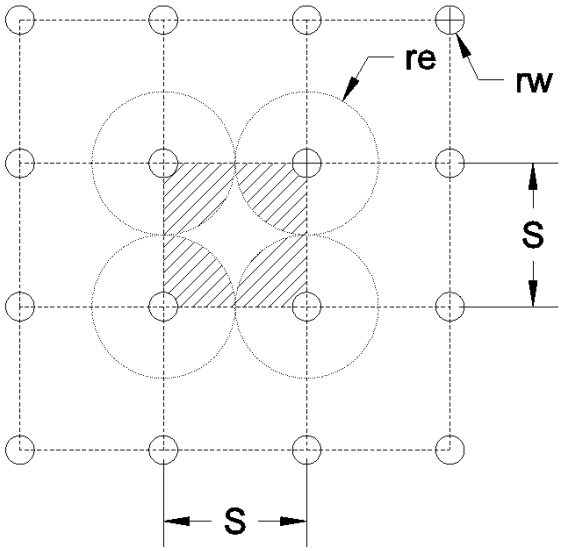

Figure 4-3: Calculation of equivalent radius (r_e) of the unit cell.

$$S^2 = \left(\frac{1}{4}\pi r_e^2\right) \times 4 \tag{4.1}$$

$$r_e = \frac{S}{\sqrt{\pi}} \tag{4.2}$$

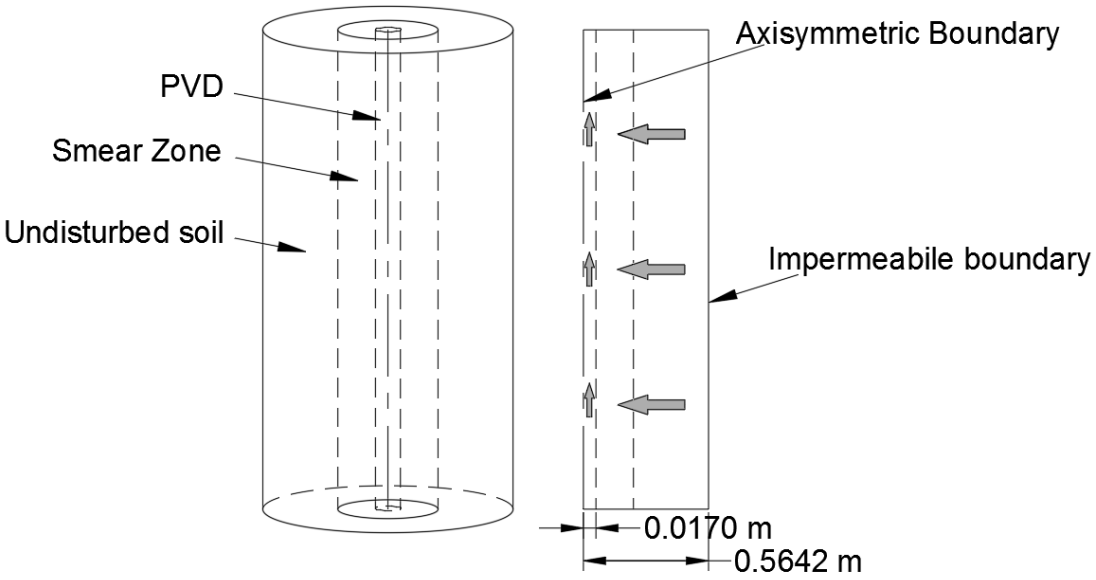

Figure 4-4 : Schematic diagram of the unit cell.

Table 4-1: Adopted PVD and unit cell properties for the case study.

Property	Value
Well radius (r_w)	0.0170 m
PVD spacing	1 m
PVD installation pattern	Square
PVD length	20 m
Equivalent radius (r_e)	0.5642 m
k_h/k_s	2
r_s/r_w	4

4.4 Embankment construction and vacuum application

There were several steps involved in the embankment construction near SP11. First was the placement of the 1.5 m thick sand layer which facilitated as a working platform for the remainder of construction. Next, PVDs were installed in a square pattern with a spacing of 1 m. Installation over the entire area took approximately one week. After placing the vacuum membrane, the embankment was constructed up to 2 m thickness. Approximately 115 days from construction commencement, the vacuum pump was started. A vacuum suction of –70 kPa was expected to be transferred along the PVDs to the soil foundation. In the first main embankment construction stage, a 6.5 m-thick filling was laid in 109 days while the vacuum pumps were running. This was followed by the consolidation stage with vacuum suction applied until the vacuum pump switched off after 400 days. The second construction stage ran from Day 750 to Day 1,050 during which the embankment was raised up to 14 m thickness, as illustrated in Figure 4-5. This phase was completed without vacuum suction. Field settlement data were available up to 1,200 days until which analysis was also done. Figure 4-5 illustrates the embankment construction history over time near SP11 and likewise the embankment construction history near SP7 is also plotted in the same figure. Following the determination of input parameters, FE results of the analysis on these locations are discussed in Section 4.7 and 4.8 subsequently.

4.5 Determination of input parameters

Figure 4-6 illustrates the basic soil parameters of the clay foundation. For the analysis in this chapter, the foundation soil was divided into four layers based on the yield profile with depth. The linear reduction of p_c' is a readily available option in AFENA which was used to model p_c' according to the reported values.

Determination of the secondary compression index (C_α), permeability and shape parameter are described in the following sections.

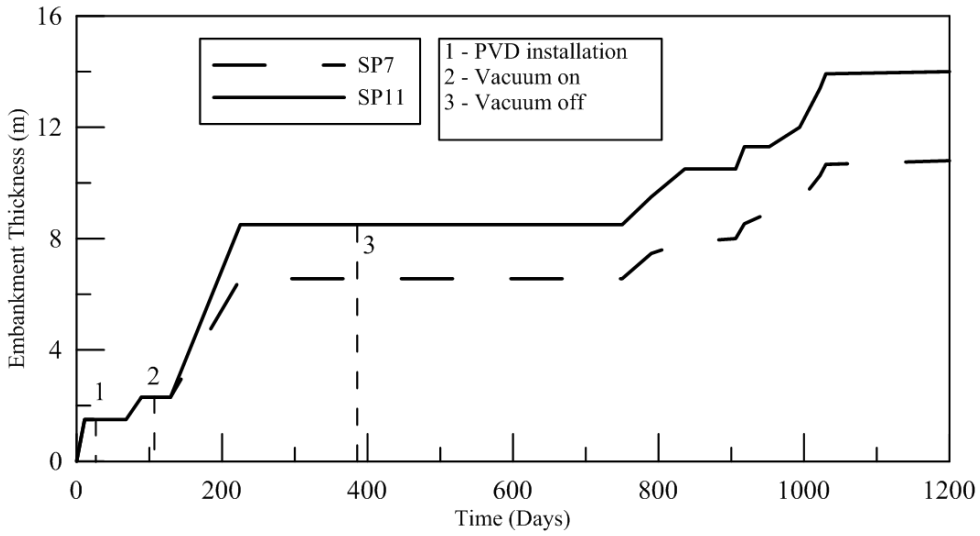

Figure 4-5 : Variation of embankment thickness at different times and settlement plate (SP) locations.

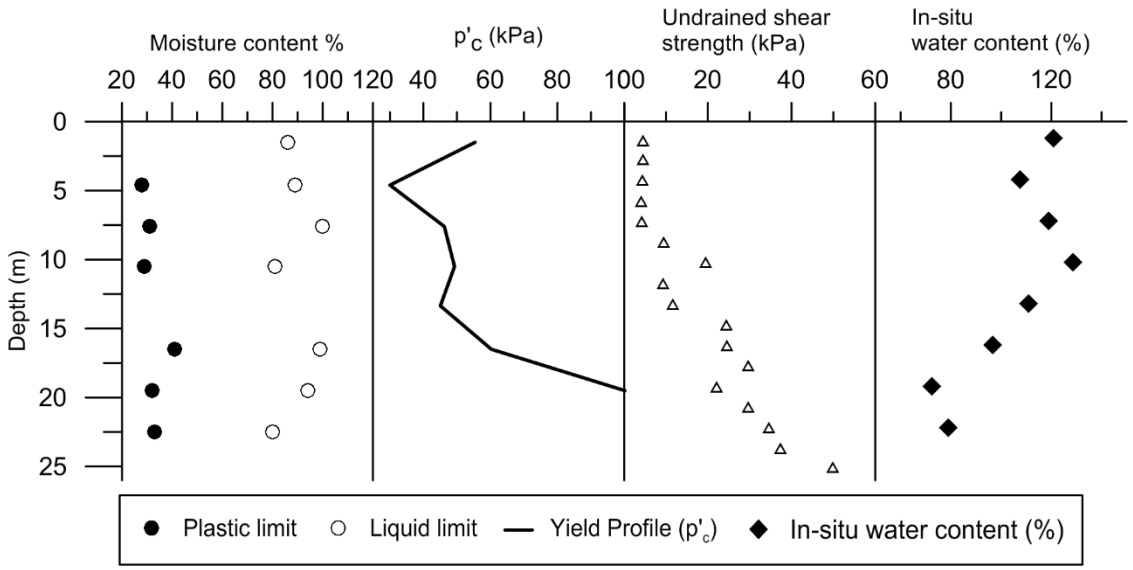

Figure 4-6: Foundation soil profile in Ballina bypass (modified from Indraratna et al., 2012).

4.5.1 Determination of secondary compression index (Cα)

The C_α/C_c ratio proposed by Mesri and Godlewski (1977) is one of the easiest approximations that can be adopted to determine the C_α. For most soft clays, this ratio falls within the range of 0.04 ± 0.01. Using this ratio, the calculated maximum and minimum values of C_α are 0.0656 and 0.0332, respectively. Another cross-check could be made since Kelly et al. (2008) reported the creep ratio, = $C_\alpha / (1+e_0)$, as 0.015 for the entire depth of the clay. Assuming $e_0 \approx 2.8$ it can be calculated that, C_α = 0.057; thus placing the value in between the previously calculated range of $0.0332 \leq C_\alpha \leq 0.0656$.

However, with the laboratory experiments carried out by Pineda et al. (2016), it is evident that C_α reached almost 0.09 as yielding begins (Figure 4-7). Although this maximum value is beyond the above calculated range of the C_α/C_c ratio, the minimum reported value of C_α was 0.04 which remains within the said range. This significant variation in C_α was not noticed by almost all researchers who worked with Ballina clay and attempted to model the embankment's deformations. For this analysis, the variability of C_α was modelled using the Eqn. (3.6) discussed in Chapter 3. $C_{\alpha\text{-}max}$ was set at 0.09, representing the maximum value for C_α as yielding starts (i.e. $p_0 - p_L = 0$).

Table 4-2 contains the values used for the creep function mentioned in Eqn. (3.6), and Figure 4-7 illustrates the creep function against the other approximations discussed. In modelling the embankment behaviour, three cases were considered. In Case A, the developed variable creep function was used, in Case B and Case C, constant creep values were set to represent the calculated upper and lower bounds of the creep values (i.e. C_α = 0.0656 and C_α = 0.0332).

Table 4-2 : Secondary compression values adopted for the simulation.

Soil Layer	C_α	$\alpha=C_\alpha/ln(10)$	$C_{\alpha\text{-}max}$	N
0.0 to 0.5 m	0.0563	0.02445	0.09	0.004
0.5 to 4.0 m	0.0563	0.02445		
4.0 to 15 m	0.0561	0.02436		
15 to 25 m	0.0464	0.02015		

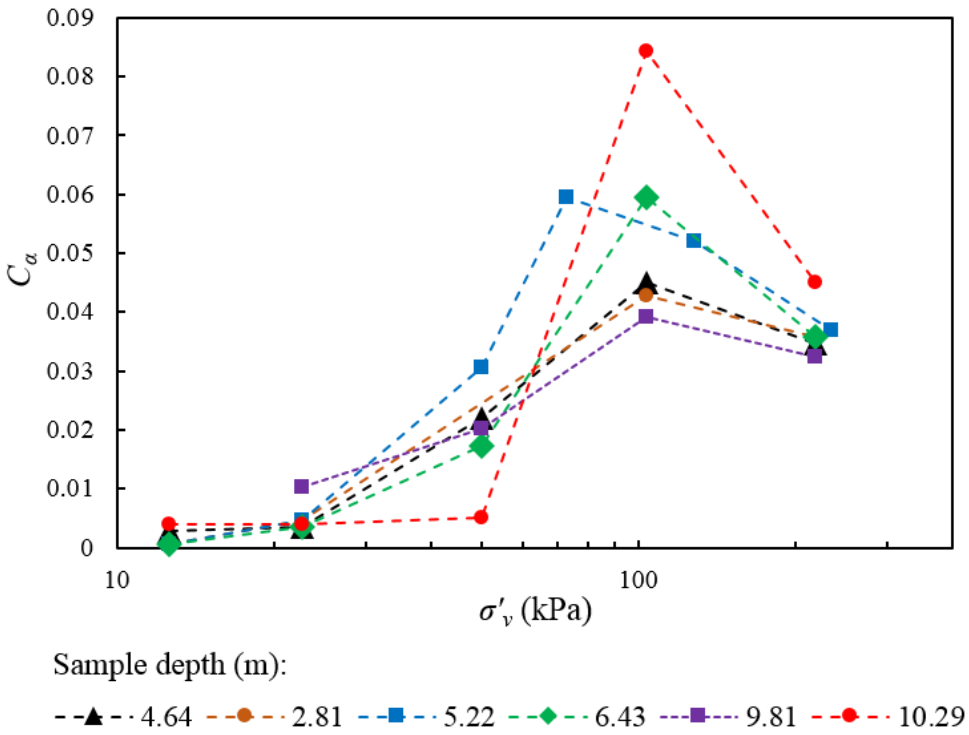

Figure 4-7 : Variation of C_α with effective vertical stress at different depths (after Pineda et al., 2016).

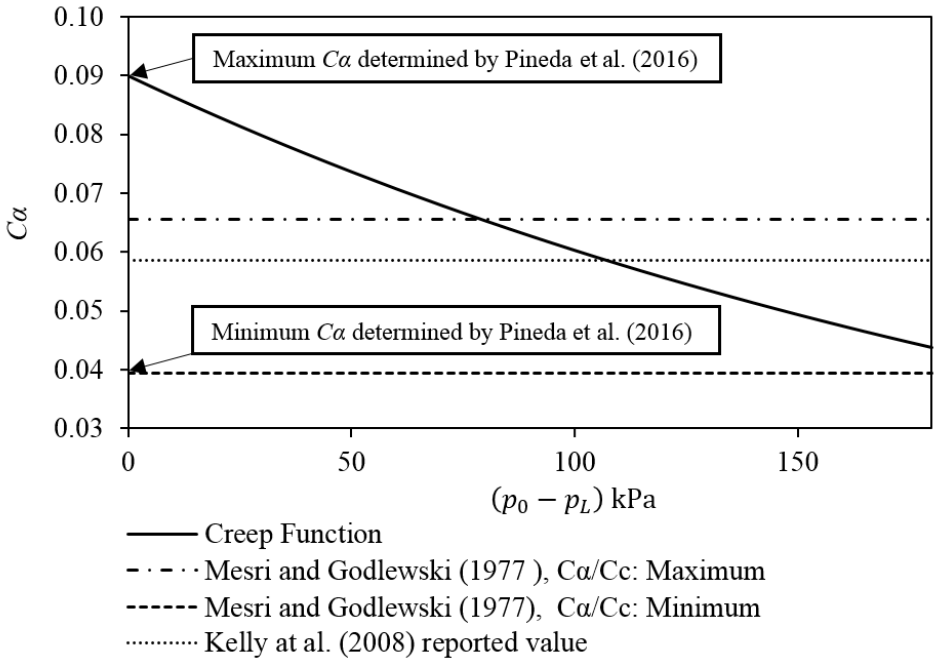

Figure 4-8 : Variation of C_α in accordance with the calibrated non-linear creep function (from Kumarage and Gnanendran 2019b).

4.5.2 Modelling permeability characteristics

Variation in permeability with void ratio can influence the rate of EPP dissipation. Particularly when the duration of an analysis is long-term, such variation for soft clays with high water content is not negligible. Figure 4-9 illustrates the variations in permeability with void ratio for the Ballina clay. The laboratory experiments conducted by Pineda et al. (2016) confirms that this variation is significant.

Permeability characteristics were subsequently modelled using the relationship proposed by Tavenas et al. (1983) as per Eqn. (4.3).

$$k = k_r EXP\left[\frac{e - e_r}{C_k / \ln(10)}\right] \tag{4.3}$$

where k_r is the permeability at the reference void ratio of e_r. The slope of the line indicated in Figure 4-9 was calculated as 1.125; hence, the value C_k = 1.125 was adopted for the analysis.

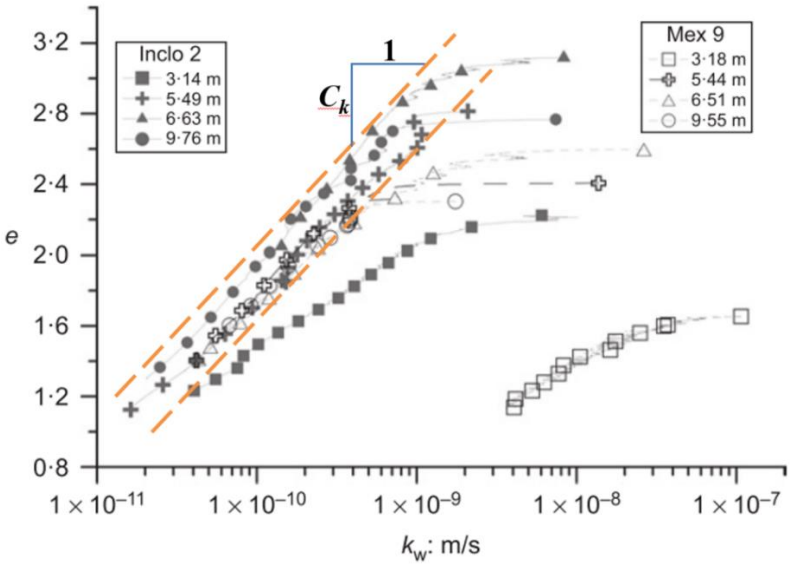

Figure 4-9 : Variation in permeability with void ratio (modified from Pineda et al. 2016).

4.5.3 Determining the shape parameter (R)

Implications of the shape parameter (R) and proposed methods for its determination were previously discussed by Dafalias and Herrmann (1986), Islam (2014) and Islam and Gnanendran (2017). Generally, the shape parameter can have a value close to two, with a higher value deeming the yield surface flatter, and vice versa. To determine R in this chapter, the undrained stress path from laboratory experiments by Pineda et al. (2016) on Ballina clay, from approximately 10 m depth was used. This was coupled with the expression in Eqn. (4.4), as proposed by Dafalias and Herrmann (1986) to calculate R.

$$\frac{|\bar{q}|}{\bar{p}_0} = \frac{M}{R-1}\left[\frac{2}{R}\left(\frac{\bar{p}}{\bar{p}_0}\right)^{\frac{\lambda-2\kappa}{\lambda-\kappa}} + \left(1-\frac{2}{R}\right)\left(\frac{\bar{p}}{\bar{p}_0}\right)^{\frac{-2\kappa}{\lambda-\kappa}} - \left(\frac{\bar{p}}{\bar{p}_0}\right)^{2}\right]^{1/2} \quad (4.4)$$

By following the undrained stress path, the average value of R was calculated as $R = 2.015$. The values determined at different points in the undrained stress path had deviations of no more than 10% of the average value. Hence, the value of $R = 2$ was adopted in the EVP model and the analysis reported in this chapter.

It is worth noting that, approximating the shape parameter to two (i.e. $R = 2$) greatly decreases the modelling complexity, as the yield surface reduces to a single ellipse. Also, it is justifiable to use a single ellipse when the soil is not predominantly behaving within the over-consolidated range.

4.6 Finite element implementation

4.6.1 Boundary conditions, FE mesh and material properties

As illustrated in Chapter 3, the UNSW, Canberra modified version (Islam and Gnanendran 2017) of the FE numerical algorithm AFENA (Carter and Balaam 1995) did not have the ability to simulate vacuum consolidation. Hence, the said algorithm was further modified (as described in Chapter 3) by introducing time-dependent boundary conditions to implement vacuum consolidation. This time-dependent boundary condition to represent the vacuum was applied to the 3rd DOF for the nodes along the symmetrical axis of the unit cell (Figure 4-10) for the entire PVD length (e.g. 20 m for SP11 location). The written subroutine was called to start, stop or to change the intensity of the vacuum

application during the consolidation period. Generally, boundary conditions can only be invoked at the start of an analysis in AFENA; however, the newly introduced subroutine eliminated this restriction by enabling the subroutine can be called at any time within the solution algorithm to change boundary conditions.

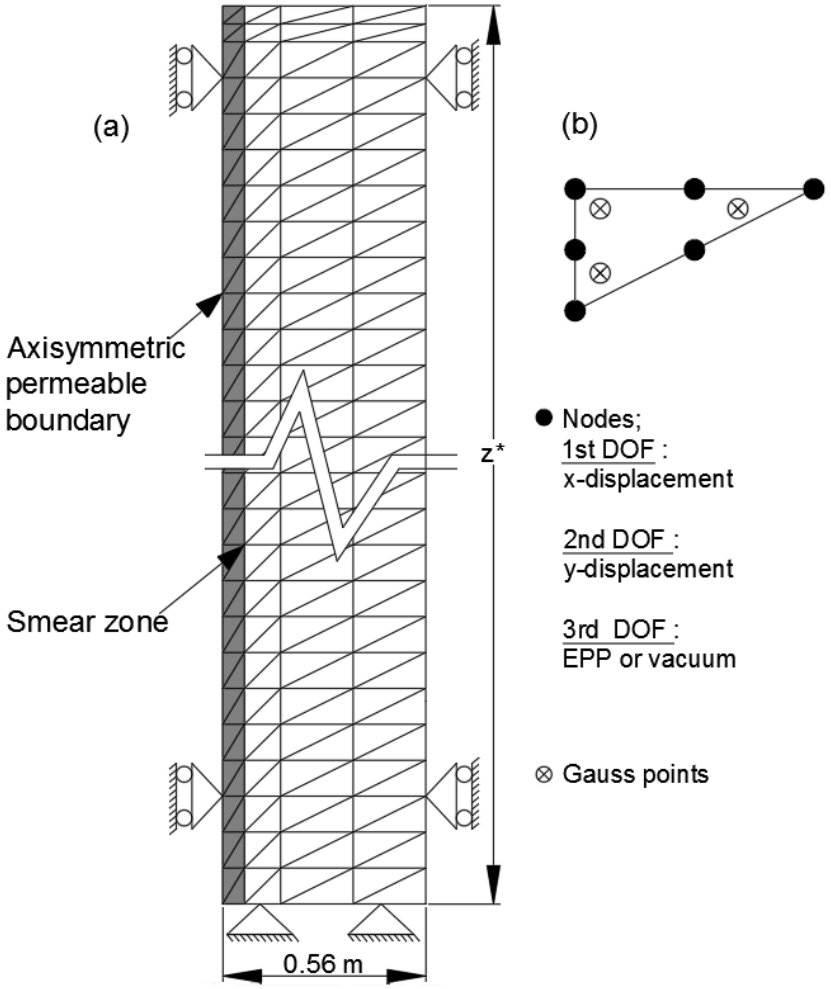

Figure 4-10 : (a) FE mesh for the unit cell analysis, (b) six-node element and respective DOFs (modified from Kumarage and Gnanendran 2017).

*z is the height of the unit cell depending on the embankment location.

Embankment construction was simulated by means of an equivalent vertical stress in the unit cell (Figure 4-10). In calculating the equivalent vertical stress, the average density

of the fill material was taken as 20 kN/m^3. A vacuum suction of –70 kPa was also applied at the axisymmetric PVD boundary only for the corresponding vacuum-application period. When the vacuum is switched 'off', unit cell represents a conventional PVD while the vacuum is switched on, the boundary condition is altered as necessary.

Unit cell analysis was performed for the location with the highest clay thickness (i.e. SP11 in Figure 4-2) using the presented numerical approach to predict the surface settlement and EPPs beneath the mid-section of the embankment. The entire soil column (e.g. 25m in SP11) was analysed although the PVD was assumed to be 20 m of length. These results were compared with the field monitoring data. It is worth noting that, unlike previous numerical studies (e.g. Khan 2010, Indraratna et al. 2012b, Parsa-Pajouh et al. 2014), special attention has been given to the viscous behaviour of soft clay by incorporating the secondary compression in the clay using the EVP model. Moreover, predictions and comparisons against field were made up to 1,200 days, which allows validation of the model for predicting both short-term and long-term behaviour.

The layout of the instruments to monitor the settlements and pore water pressures in the Ballina embankment project is shown in Figure 4-2. The Cam-clay equivalent properties of the soil layers adopted for the analysis are presented in Table 4-3.These parameters along with the variation of permeability and developed creep function as discussed in the previous sections were used as input parameters for numerical modelling to predict the settlement of the embankment and the EPP that developed in the soft clay foundation.

Table 4-3 : Soil Profile for FE modelling[1] (modified from Indraratna et al., 2012).

Depth (m)	λ	κ	e_0	γ_{sat} (kN/m^3)	k_h (10^{-10} m/s)	OCR
0.0 - 0.5	0.57	0.057	2.75	14.0	10.0	2.0
0.5 - 4.0	0.57	0.057	2.75	14.0	10.0	1.8
4.0 - 15.0	0.57	0.057	2.74	14.5	10.0	1.7
15.0 - 25.0	0.48	0.048	2.09	15.0	3.3	1.1

[1]PVD length was assumed to be 20 m for the SP11 location, but the consolidation of the entire 25 m depth was modelled and analysed.

4.6.2 Large-strain option and nodal position updates

Since this analysis was carried out for a duration of more than three years on a foundation composed of soft soil, significantly large settlements could be expected. Analysis on non-vacuumed section (Section A) from different research groups (e.g. Amavasai et al. 2018, Chan et al. 2018, Indraratna et al. 2018a, Chai et al. 2018, Gong and Chok 2018) have revealed the development of a 1.5 m settlement by the first year of the project. Assuming a total clay thickness of 25 m (conservatively), this is a 6% vertical strain. Previous research on large-strain vs. small strain FEA (e.g. Hu et al. 2014) have shown deviations in predictions when the total strain percentage becomes larger than ~5–10%. With vacuum application, higher embankment thickness and long-term analysis, strain percentage is expected to significantly exceed Section A. Hence the large-strain option in AFENA was decidedly activated.

When settlements are large in nature, it is often necessary to carryout corrections for hydrostatic pressure and EPP calculations. By updating the nodal positions, these manual corrections can be avoided. Hence after each time increment, nodal positions were updated for the entire analysis period. However, to illustrate the implications that follow

from this option, a separate case (Case D) was run with variable creep index without the large-strain option. Table 4-4 provides a summary of the all the cases analysed and their descriptions.

Table 4-4: Summary of cases analysed.

Case	Description
Case A	Developed variable creep function is used.
Case B	A constant creep value to represent the calculated upper bound is used (i.e. C_α = 0.0656).
Case C	A constant creep value to represent the calculated lower bound is used (i.e. C_α = 0.0332).
Case D	Similar to Case A except the large-strain option is switched 'off'.

4.7 Synthesis of finite element simulation results

Figure 4-11(a) illustrates the FE numerical predictions against the field measured settlement data at location SP11. Evidently, the predictions with a variable creep function (Case A) have strong agreement with the measured field settlement data. Further, all four cases have reasonably good predictions up to 200 days, but this changes around 400 days when Case A and Case B still correspond with the measured values while Case C underestimates the settlements by 9.86%. By this time, Case D shows gross overestimation of the settlements, which continues throughout the analysis period. As such differences between each case are largely visible when the analysis period exceeds 400 days. At 1,200 days, Case A still shows strong agreement with the field settlement data with a marginal error of 0.79%. Meanwhile, Case B overestimates the total

settlement approximately by 5.41% while Case C, does so by 7.15%. Previous settlement predictions, (e.g. Parsa-Pajouh et al. 2014), also corresponds well with the field settlement data measurements but the prediction has been carried out only up to about 400 days.

The following observations can be made upon comparing the EPP predictions with the field data in Figure 4-11(b). Throughout the 100 to 200-day period, the analysis predictions from Case A and Case B follow the field data closely. From 200–300 days, all three cases over estimated the EPP up to 18%. Conversely, predictions made by previous researchers showed much larger over prediction (e.g. difference as high as ~ 400% reported in Parsa-Pajouh et al., 2014) compared to the field measurements. After the end of the second construction phase (i.e. after 1,050 days), dissipation of EPP in the field was slower than the analysis predictions. Notably, Case A, with the variable creep function, predicted almost similar results as Case B in the initial phase and very close results to that of Case C towards the end (i.e. ~ 1200 days). This indicates that the variable creep function was reaching its upper and lower bounds respectively. However, differences in overall predictions made with each case were generally in the range of 15% to 18%. Interestingly, the EPP predictions from Case D are far more noteworthy than expected. In the first 200 days, the predictions generally match the field data, as expected due to limited strain. However, after 200 days the peak EPP value is significantly overestimated by Case D. This trend continues in the vacuum-consolidation period and even after the vacuum pump is switched ‘off’ around 400 days. Yet as the time elapsed the amount of overestimation begins to reduce and the EPP predictions tally the field data around 800 days and provides reasonably good predictions up to 1,200 days.

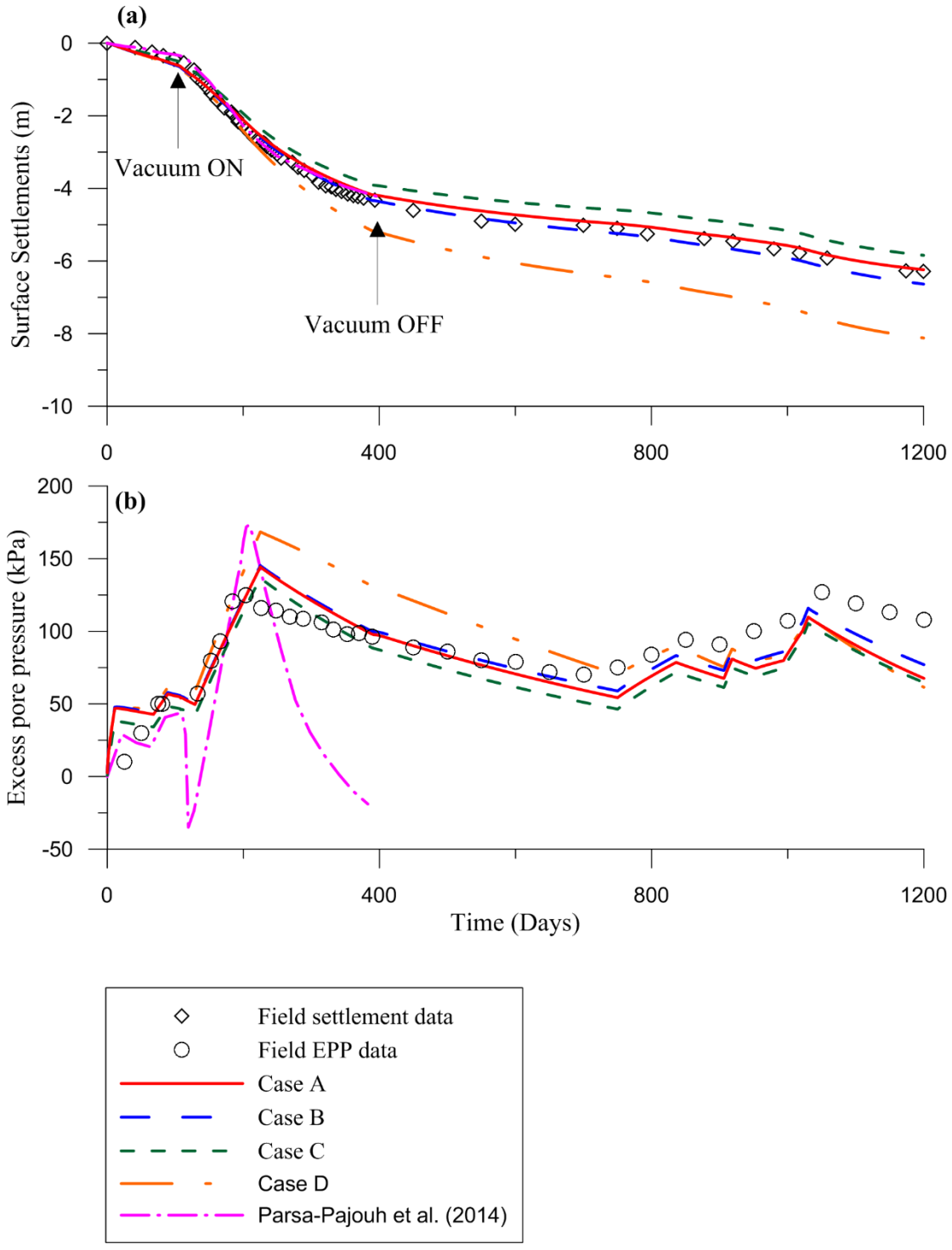

Figure 4-11 : Field measurements vs. FEM simulations; (a) Settlements at SP11; (b) EPP at P3-C (at 4.8 m depth).

Meanwhile, the highest EPP values were recorded at the end of each embankment construction phase. In the first phase, 6.5 m-thick fill was added in 109 days, which is equivalent to 130 kPa; on top of that, there was prevailing EPP of approximately 50 kPa just prior to commencement of this phase. However, due to the vacuum application, the maximum EPP did not exceed 130 kPa. This can be identified as a characteristic in vacuum consolidation where the total stress of soil can be increased without elevating the EPP by the same magnitude. The extended EVP model with modified boundary conditions, proposed in this thesis appears to capture this phenomenon well. Overall, it appears that significant improvement has been achieved in the predictions of settlement and EPP behaviour in contrast to previous modelling attempts.

4.8 Comparison of settlements at different locations

Since Case A provides better predictions than Cases B and C, the approach used for the former was used to predict the settlements at SP1 and SP7 locations in the embankment. This was mainly to provide a better understanding of settlement behaviour at other locations where the thickness of the soft clay foundation was different.

Just like SP11, SP7 was also in the vacuum applied area (i.e. Section B). However, the thickness of the soft clay foundation soil near the latter was about 15 m (Table 4-5). History of embankment construction in each of these locations are illustrated in Figure 4-5. In predicting the settlement at SP7 location, only the first three soil layers illustrated in Table 4-3 were applicable due to low clay thickness. Nonetheless the same soil parameters of SP11 (presented in Table 4-3) including permeability provided satisfactory results for SP7.

Meanwhile, SP1 location was situated in the Section A of the embankment where conventional PVDs (no vacuum applied) were used and the clay thickness was approximately 7 m (Table 4-5). Simulation of conventional PVDs is relatively simple. Nodes in the FE mesh, which represent the PVDs should be fixed with a boundary condition for the respective DOF. Unlike in vacuum consolidation, this boundary remains constant throughout the analysis.

Table 4-5: Bottom level of the soft clay layer at each settlement plate location.

Settlement plate	SP1/SP2	SP7/SP8	SP11/SP12
Bottom level of the soft clay layer	6.7	14.7	24.7

As illustrated in Figure 4-12(a), settlement in SP7 is significantly different from SP11. The main reason for this disparity could be from the dissimilar thickness of the soft clay foundation in these two locations and the difference in embankment height (see Figure 4-5). It also appears that in SP1 and SP7 locations, the settlements have almost ceased. However, in SP11 it is interesting to note that, despite long-duration vacuum application, settlements appear to continue even after 1,200 days and the proposed analysis method seems capturing this behaviour well.

4.9 Influence of vacuum intensity

As reviewed in Chapter 2, vacuum intensity can vary widely. To gain insight into its influence a sensitivity analysis was carried out. Details of the variation in vacuum intensity are presented are presented in Table 4-6.

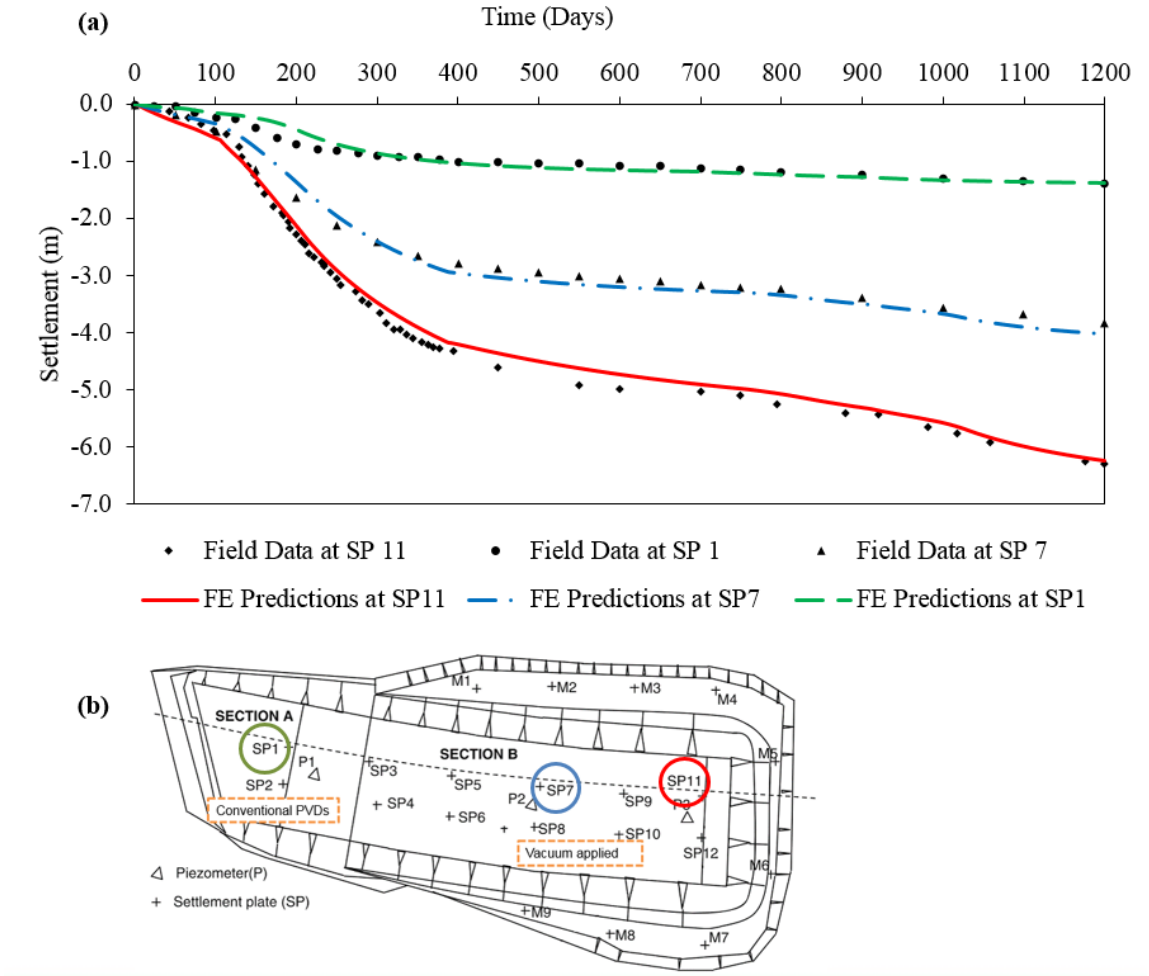

Figure 4-12 : (a) Comparison of settlements at different locations with the creep function, (b) SP locations of SP1, SP7 and SP11.

Table 4-6: Cases and their descriptions for variation in vacuum intensity.

Case	Description
Case E	20% higher vacuum intensity (~84 kPa)
Case F	20% lower vacuum intensity (~56 kPa)
Case G	50% lower vacuum intensity (~35 kPa)
Case H	No vacuum

It is important to clarify why cases with 50% greater or even more vacuum intensities were not considered. Basically, such an increment from 70 kPa (which is the original designed vacuum intensity) would result a vacuum intensity of 105 kPa, which exceeds the atmospheric pressure (~101 kPa). No ground-improvement project would use such high vacuum intensity for the reasons discussed in Chapter 2. However, there is no problem in using lower vacuum suctions, in fact it is worth considering such cases since air leaks are common in vacuum projects. In Case I, a non-vacuum case is also considered to represent conventional wick drains.

Figure 4-13 presents the results of the analysis. For this field case it can be observed from the figure that vacuum intensity has the greatest effect for mid-term, rather than for long-term prospects. This trend is especially applicable to settlements (Figure 4-13(a)) where it appears that settlements with different vacuum intensities eventually converged to reach almost equal values around 1,200 days. However, during the vacuum-application period, a significant difference in settlements can be observed. Around 300 days, vacuum application has achieved almost 25% more settlement than the non-vacuum case (Case H). The main reason for the settlement around 1,200 days to be similar is due the termination of vacuum pump around 400 days. For economic reasons, it is not practical to operate vacuum pumps for several years. However, as observed in the FE results, while the vacuum pump is in operation (say around 300 days), vacuum intensity has major influence (up to 25% more settlement than no vacuum case) towards achieving faster consolidation in short duration.

In terms of EPP (Figure 4-13(b)), Case H (with no vacuum) always had higher values than all other cases. Unlike in the settlements, EPP values presents noticeable differences between each case (E, F, G and H) even at 1,200 days.

The designed vacuum intensity of –70 kPa for this field case appears to be the optimum choice, as a 20% increase did not yield significantly better results, and any vacuum value higher than that appears practically impossible. Conversely, smaller vacuum intensities such as Case G are less effective. This analysis confirms the observations made in Chapter 2, Appendix A), that is in past ground-improvement projects the recommended vacuum intensity lies within the range of 60–80 kPa. However, a proper sensitive analysis is still required to find the optimum vacuum intensity depending on the respective soil foundation in each individual condition.

4.10 Summary

The creep-based EVP model with the time-dependent boundary conditions described in Chapter 3 was applied in this chapter to numerically simulate vacuum assisted PVD consolidation in the Ballina test embankment. The model was first validated by comparing the settlements and EPP at the SP11 location where 25 m thick soft clay layer was available. Second, the settlement predictions were compared at two other locations, with different foundation soft clay thickness.

It can be concluded that the analysis method involving an EVP model with the presented time-dependent boundary conditions presented is capable of predicting both short-term and long-term deformational behaviours under vacuum application. Creep characteristics of Ballina clay were captured by an exponential creep function rather than a constant C_α

value which led to improved predictions. This chapter both illustrated and emphasised the importance of utilising such variable creep function in modelling long-term vacuum-consolidation projects.

Ground settlements were also significantly different at the three locations considered in the embankment, primarily due to differences in initial clay thickness. At SP11, despite long-duration vacuum application, the settlements seemingly persist even after 1,200 days. The rate of settlement at 1200 days is still high which demands better and faster methods of ground-improvement in such cases where the thickness soft clay is high. Predictions regarding both settlement and EPP in this location appear reasonable, thus confirming the applicability of the model and proper selection of input parameters.

This chapter also illustrated the large-strain option is a vital choice in analysis similar cases with large settlements. In this case both settlements and EPP predictions without the large-strain option were acceptable before 200 days, but the former was grossly overestimated thereafter. EPP values were initially overvalued throughout the 200–800-day period but eventually became close to field data as time passes. Hence the most error occurred for settlement predictions rather than for EPP relative to deciding on the large-strain option.

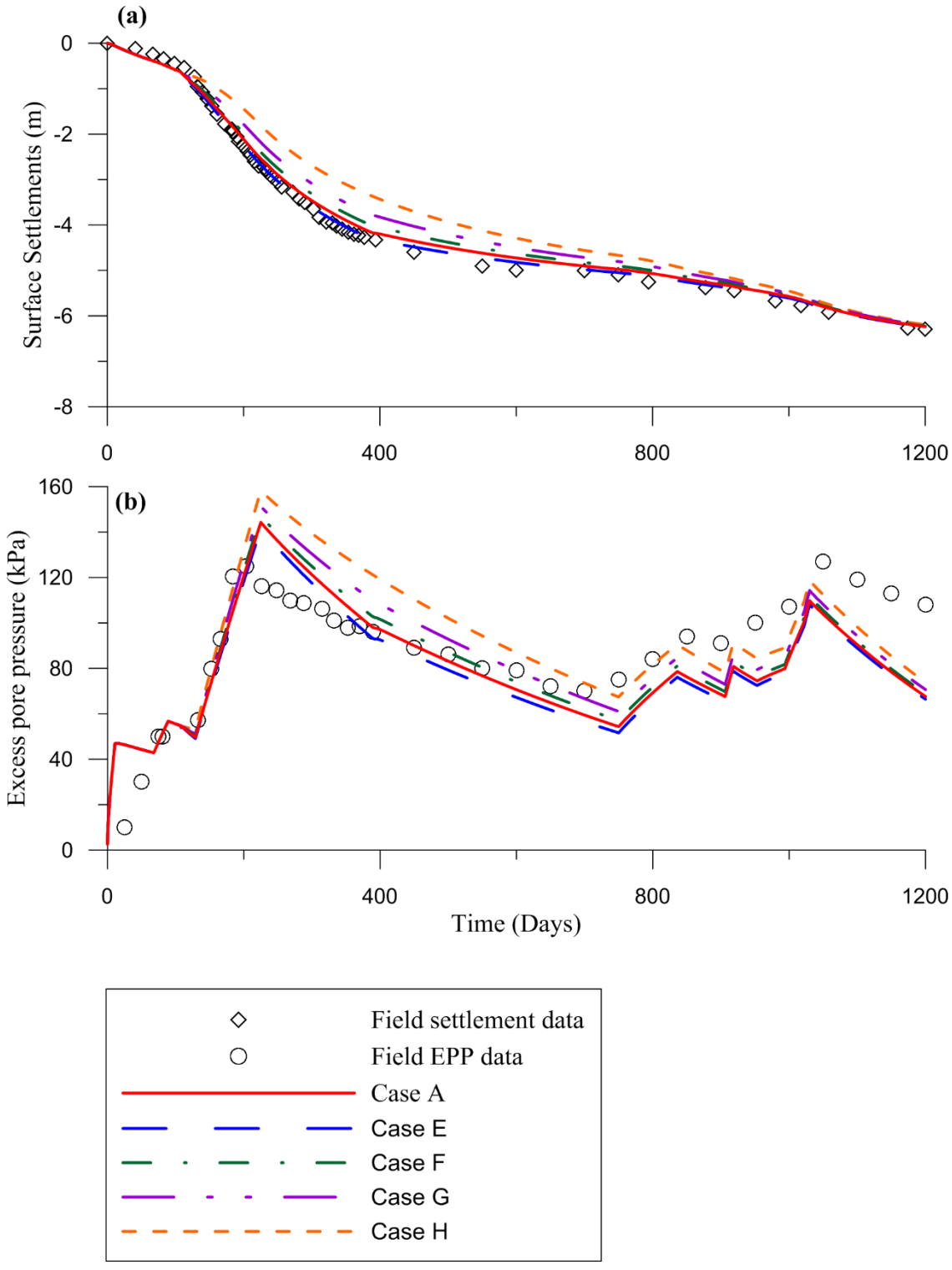

Figure 4-13: Influence of vacuum intensity towards settlements and EPP.

Influence of vacuum intensity for a long-term project was also outlined in this chapter. As discovered the optimum value of vacuum intensity for a ground-improvement project largely depends on a given foundation soil properties. For the conditions prevailed in the Ballina case study, –70 kPa appears to be an optimum choice. With the comparison to conventional drains with no vacuum applied, acceleration of the consolidation process with vacuum is made clear with a maximum difference of 25% noted in terms of the settlements.

Finally, as this chapter explored only the unit cell analysis, which carries some inherit limitations in terms of the scope of the analysis. For example, lateral displacements and total settlement profile across the embankment cannot be evaluated. As such, the next chapter (Chapter 5) addresses these limitations by converting the unit cell model to a plane-strain model that enables a full-scale embankment analysis.

Chapter 5 : Plane strain modelling of Ballina embankment[3]

5.1 General

In this chapter the axisymmetric unit cell idealisation is converted to a plane strain (PS) model to analyse the Ballina vacuum consolidation project introduced in Chapter 4. Axisymmetric unit cell would be more representative model to idealise the physical phenomena occurring around a PVD. The size of the FE mesh associated with such a model is rather small ensuring the computational productivity. However, this convenience in unit cell modelling comes with a significant cost to a researcher or a design engineer due to its' inherit limitations. Unit cell analysis only permits to analyse settlements and EPP, but provides no idea about lateral deformations, embankment stability. Thus, unit cell analysis is often used to predict the behaviour near the centreline of the embankment where lateral displacements are small or nil. Also, the analysis limits to one PVD location at a time which would not provide a broadscale understanding about the deformational behaviour of the whole embankment. Due to these limitations, some researchers have used 3D models to predict and back analyse embankments (e.g. Indraratna et al. 2018b, Müthing et al. 2018, Tschuchnigg and Schweiger 2018). This is a very expensive option in terms of computational resources and time, since such analysis requires excessive amount of cubic elements, which intern demands significant computational power and

[3] Material discussed in this chapter form part of the following publications:

Kumarage, P.I., and Gnanendran, C.T. 2019c. Plane strain analysis of an embankment with vacuum-assisted PVDs using an elasto-viscoplastic model. Submitted for the Computers and Geotechnics Journal. Manuscript No. COGE-D-19-01019.

Kumarage, P.I., and Gnanendran, C.T. 2019a. Plane strain viscoplastic modelling in vacuum consolidation. *In* Proceedings of the 17th African Regional Conference on Soil Mechanics and Geotechnical Engineering. Cape Town, South Africa.

analysis time. At the same time, literature has shown that without some extensive set of foundation soil data, 3D modelling of structures like embankments will not yield significantly accurate results (Indraratna et al. 2012a, Kelly et al. 2018). Even though some benefits can be achieved, they generally out-weighs the computationally intensive effort and cost. Thus, 2D PS model can be considered as a proper balance between the computational costs and benefits.

PS unit cell width is a main uncertainty in the axisymmetric to PS conversion process. In this chapter the cross section of the Ballina embankment at SP11 location (discussed in Chapter 4) is modelled using the converted EVP PS model. Then the FE results of the PS model is compared with its axisymmetric case. Settlement profile across the embankment and lateral displacements are also discussed taking the advantage of the full-scale embankment model.

5.2 PS conversion of the EVP model

There are several methods to convert an axisymmetric unit cell to an equivalent PS model. These are commonly known as matching procedures. Hird et al. (1992) proposed three matching techniques called permeability matching, geometry matching and combined matching. These methods require the PVD and the surrounding soil to be modelled as a PS unit cell. Either the permeability of the unit cell, the spacing between each PVD (i.e. the spacing between unit cells) or both should be varied. Conversely, Lin et al. (2000) proposed a simpler method to convert the axisymmetric condition to PS. Rezania et al. (2017) showed the Lin et al. (2000) method has a significant limitation since the method requires the actual drain spacing (in the field) to be close to the equivalent PS drain spacing (in the FE mesh) for the results to be accurate. When PS drain spacing becomes

larger than the actual spacing in the field, settlements are highly overestimated. Chai et al.(2001) proposed an even simpler method to approximate the settlements by calculating an equivalent permeability for the entire soil mass considering the effect of PVDs as well. In this approach, explicit modelling of each PVD was not necessary.

Extremely limited analysis have been reported in the literature concerning the long-term deformational behaviour of vacuum consolidation using PS models. As pointed out, the main uncertainty in the matching technique proposed by Hird et al. (1992) is the unit cell width. In the presence of vacuum suction, the effect of changing unit cell width on settlements, EPP and lateral displacements in PS compared to axisymmetric cases is not well understood and has not been investigated.

In this chapter, the matching technique proposed by Hird et al. (1992) is used along with the EVP model (discussed in Chapters 3 and 4) in the context of vacuum consolidation. Ballina test embankment (Kelly and Wong 2009), Australia is back analysed using the EVP PS model and the settlements, EPP, lateral deformations and embankment stability is discussed for a period of over three years with varying unit cell widths. Although FEA for the embankment for the same duration was carried out in Chapter 4, it discussed only the axisymmetric unit cell analysis and did not comment on lateral displacements and embankment stability in PS conditions. Several other research groups also have carried out FEA to understand the soft soil behaviour in this particular case history (e.g. Amavasai et al. 2018, Gong and Chok 2018, Indraratna et al. 2018b). However, they all considered only Section A, the non-vacuum section of the embankment (Figure 5-1). Even then, the back analysed FEA results of Indraratna et al.(2018b) had significant overestimation in settlements. To the best of the knowledge, PS modelling of Section B

for a total duration of 1,200 days period has not been carried out before. Hence this case history was chosen as an ideal candidate to study the PS conversion procedure in the presence of vacuum-assisted PVDs. PS FEA results were compared with the equivalent axisymmetric results obtained from Chapter 4 and field data. Lateral displacement profile was compared with field data and verified. It is also illustrated that maximum lateral displacements can be predicted approximately using an empirical method. Based on the horizontal and vertical displacements at two critical inclinometer locations, the embankment stability is also discussed.

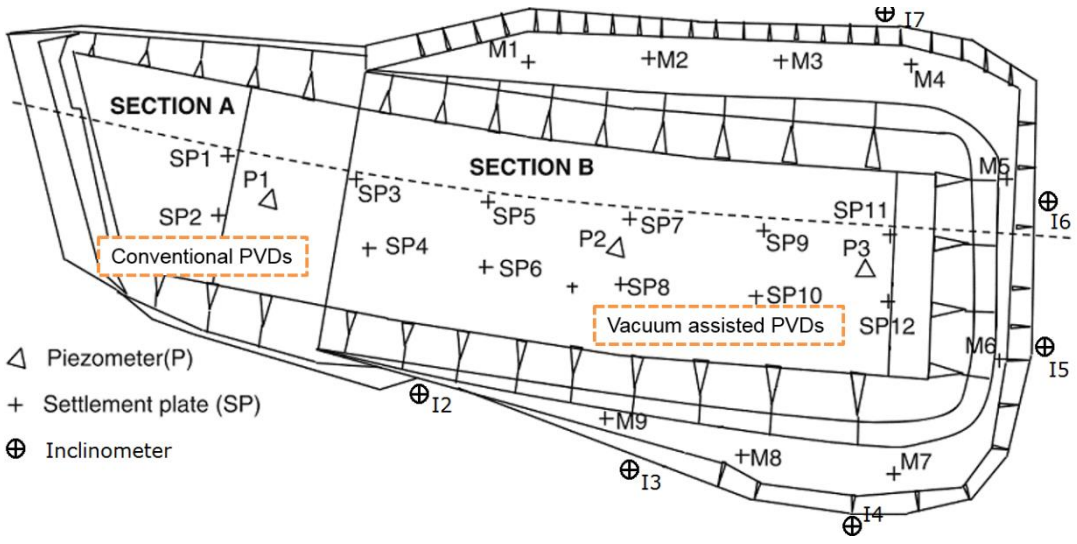

Figure 5-1: Layout of instrumentation (modified from Kelly and Wong, 2009).

5.3 PS matching procedure

Out of the three matching approaches proposed by Hird et al. (1992), combined matching permits to change the PS unit cell width with appropriate changes to the permeability of

the foundation soil. Thus in this chapter, combined matching was selected to gain insight into the influence of the FE mesh.

According to Hird et al. (1992), the combined matching approach can be summarised as follows: Neglecting the well resistance, for the average degree of consolidation ($\bar{U}$) to be matched at every time and every depth it requires,

$$\bar{U}_{pl} = \bar{U}_{ax} \tag{5.1}$$

where, subscript *pl* and *ax* denote PS and axisymmetric conditions respectively. From Hansbo (1981),

$$\bar{U} = 1 - \exp\left(-8T_h/\mu\right) \tag{5.2}$$

where, T_h is the time factor for radial drainage such that, $T_h = C_h/4r_e^2$; C_h is the coefficient of consolidation and r_e is the equivalent radius of the unit cell. Neglecting well resistance, $\mu = \ln\left(n/s\right) + (k/k_s)\ln(s) - 3/4$, where $n = r_e/r_w$ and $s = r_s / r_w$; r_w and r_s are the radii of the well and the smear zone respectively, k is the permeability of the intact (undisturbed) zone in the unit cell, k_s is the permeability of the smear zone. Hird et al. (1992) proposed the following equation for combined matching:

$$\frac{k_{pl}}{k_{ax}} = \frac{2B^2}{3R^2\left[\ln\left(\frac{n}{s}\right) + \left(\frac{k}{k_s}\right)\ln\left(s\right) - \left(\frac{3}{4}\right)\right]} \tag{5.3}$$

where, 2*B* is the drain spacing or unit cell width in PS condition (hence *B* is the half unit cell width), k_{pl} and k_{ax} are the permeability in the axisymmetric and PS conditions respectively. From Eqn. (5.3), geometric matching can be obtained by substituting $k_{pl} = k_{ax}$, whereas permeability matching can be obtained by substituting $B = R$.

In combined matching, once *B* is decided using Eqn. (5.3), and other parameters are determined, a ratio between k_{pl} and k_{ax} can be determined as in Eqn. (5.4),

$$k_{pl} = \eta\, k_{ax} \tag{5.4}$$

where, η is the conversion ratio of permeability from axisymmetric to PS.

5.4 Modelling the smear zone

There are few options to model the smear zone in PS condition. First and the most obvious method would be to explicitly dedicate elements with reduced permeability to represent the smear zone (e.g. Indraratna and Redana 2000, Parsa-Pajouh et al. 2014). In this approach, to represent the smear zone it requires to introduce small elements in the FE mesh adjacent to the PVD centreline, which in-tern make the FE mesh denser. Defining new material types for these elements would also be required. Hence explicit modelling of smear zone would result in long analysis time and less computational efficiency. Conversely, a simple and conveniently applicable equivalent-permeability is calculated in this chapter, considering both smear and intact zone parameters, such that:

$$k^* = \left(\frac{\mu_0}{\mu}\right) k \tag{5.5}$$

where, k^* is equivalent permeability of the soil with the effect of smear zone and μ_0 is without the effect of smear zone and it can be written as,

$$\mu_0 = \ln\left(\frac{R}{r_w}\right) - \frac{3}{4} \tag{5.6}$$

combining Eqn. (5.4) and (5.5), the following can be obtained,

$$k_{pl}^* = \left(\frac{\mu_0}{\mu}\right) \eta k_{ax} \tag{5.7}$$

where, k_{pl}^* is the equivalent PS permeability with the effect of smear zone.

5.5 Effect of changing the PS unit width

The ratio η in Eqn. (5.4) changes with the defined PS unit cell width ($2B$) and other parameters in Eqn. (5.3). With respect to vacuum consolidation, extremely limited discussion is available in the literature regarding the effect of $2B$ towards the FE results. In this chapter $B = 1$, $B = 2$ and $B = 4$ values were adopted, and k_{pl}^* / k_{ax} ratios are calculated for each half unit cell width (B) values. These values were chosen to represent the most commonly adopted values reported in literature by the research community in PS modelling. After determining input parameters, a graph was produced in a later section

(Section 5.8) to illustrate the variability of k_{pl}^{*} / k_{ax} vs 2*B*. These ratios were then used in the PS model to determine the equivalent PS permeability.

5.6 Predicting and verifying lateral deformations

After analysing several case studies, Chai et al. (2013) proposed the following Eqn. (5.8) to predict the likely range of the lateral deformations in vacuum consolidation projects.

$$NLD = 0.05 + 0.168RLS \tag{5.8}$$

where, *NLD* and *RLS* are defined as in Eqn. (5.9) and (5.10) respectively,

$$NLD = \frac{\delta_{nm}}{S_f} \tag{5.9}$$

$$RLS = \frac{p_n}{s_u} \tag{5.10}$$

where, S_f is the ground surface settlement under the centre of the embankment and s_u is the representative undrained shear strength of the subsoil. δ_{nm} in Eqn. (5.9) and p_n in Eqn. (5.10) are defined in Eqn. (5.11) and (5.12),

$$\delta_{nm} = \delta_{mo} - |\delta_{mi}| \tag{5.11}$$

$$p_n = p_{em} - (|p_{vac}| + p_{em})U \tag{5.12}$$

where, δ_{mo} and δ_{mi} are the maximum outward and inward lateral displacements respectively. p_{em} and p_{vac} are the stress induced by the embankment construction and vacuum application respectively. U is the average degree of consolidation of the PVD-improved zone at the end of the embankment construction period.

After the FE mesh deforms with time, horizontal deformations were plotted with depth. *NLD* and *RLS* values were also calculated from Eqns. (5.9) – (5.12) and plotted against the range calculated by the above empirical method. It is important to note that Chai et al. (2013) used field measurements to validate the proposed method. Conversely, in this chapter, readings such as S_f were obtained using the FEA results with the EVP model and both fled data and FEA results were plotted in the *NLD–RLS* space.

Importantly, to investigate the accuracy of the FEA predictions further, the complete lateral displacement profile was plotted and compared against field data. Furthermore, the influence of 2B towards the lateral displacements are also illustrated using the lateral displacement profiles.

5.7 Assessing the stability of the embankment

Plotting maximum lateral displacements against vertical settlement vs time is one way of assessing the stability of an embankment. A function can be suggested to represent such curve as in Eqn. (5.13),

$$y_h = f\left(S_v\right) \tag{5.13}$$

where, y_h is the maximum lateral displacement and S_v is the vertical settlement at the embankment centreline. If the above curve is approximated to a straight line with a slope of m_1 such that,

$$m_1 = \frac{\Delta y_h}{\Delta S_v} \tag{5.14}$$

Tavenas and Leroueil (1980) suggested that when m_1 reaches 1.0 it would reflect undrained distortion of the clay foundation, while ratio of 0.15 to 0.2 indicates a low risk of instability.

Maximum lateral displacements of two inclinometer locations (I6 and I4 in Figure 5-1) was plotted as per the above approach to assess the stability of the embankment.

5.8 Parameters for PS conversion

The project used circular PVDs with a diameter of 34 mm and was installed at a spacing of 1.0 m (Kelly and Wong 2009, Indraratna et al. 2012b). With this information, r_e was calculated approximately as 0.56 m (Table 5-1). B = 1 was chosen as a starting point to achieve a balance between computational efficiency and accuracy.

Data in Table 5-1 refers to the characteristics of the PVD in the project. From the values in Table 5-1, the value of μ_0/μ was calculated as 0.67. Using Eqn.(5.3) for B = 1, η = 0.506 can be calculated. Then the k_{pl}^*/k_{ax} ratio was calculated as per the Eqn.(5.7). Thus, the correlation of k_{pl}^* to k_{ax} (including the effect of smear zone) was determined

as k_{pl}^{*} = 0.34 k_{ax} which was used for the analysis. This procedure can be repeated for each desired 2*B* value and the appropriate k_{pl}^{*}/k_{ax} ratio can be calculated. Figure 5-2 presents results of such repetitive calculations in the plot of η and k_{pl}^{*}/k_{ax} vs 2*B*; the shaded area in the figure is the reduction of PS permeability due to the effect of the smear zone. Additionally, Table 5-2 presents the results of permeability matching and geometric matching and combined matching when *B* = 1.

Table 5-1: Input values for PS matching.

Parameter	Value
r_e	0.56 m
n	33.19
s	4
k/k_s	2

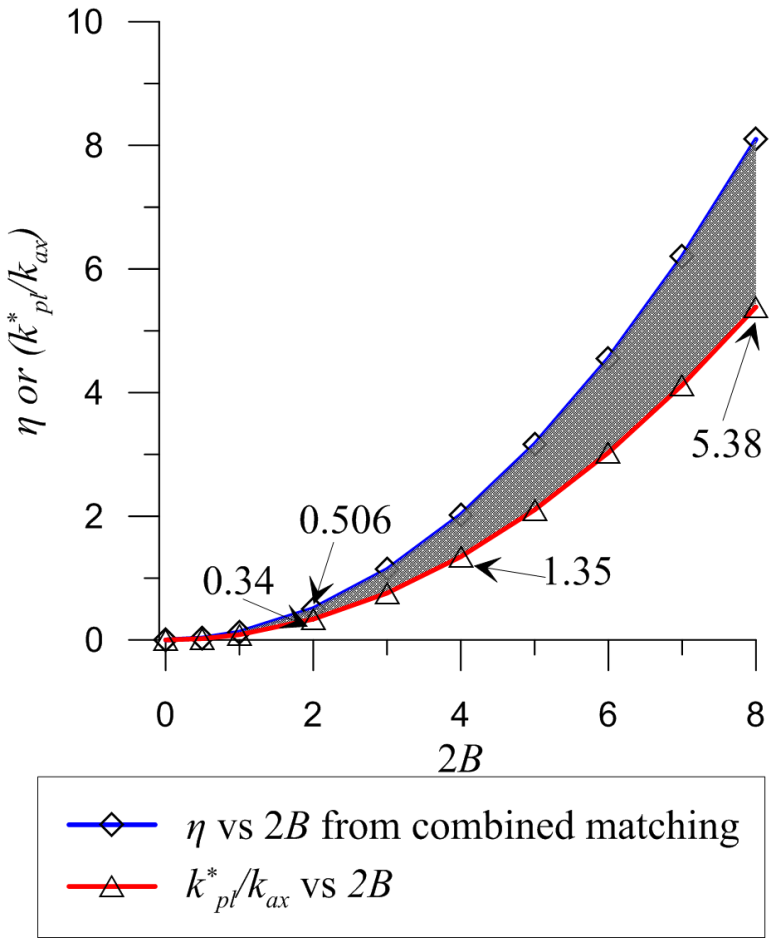

Figure 5-2: η and k^*_{pl}/k_{ax} vs the Unit cell width (2*B*).

Table 5-2: Comparison of matching methods.

Matching method	Resultant Ratio	Value
Geometry Matching	*B/R*	B/R = 2.495
Permeability Matching	k_{pl}/k_{ax}	k_{pl}/k_{ax} = 0.161
Combined Matching	k_{pl}/k_{ax} (for a given Let B/R value)	When B=1; k_{pl}/k_{ax} = 0.506

5.9 Foundation and fill material parameters

Foundation soil was modelled with the PS equivalent EVP model mentioned in Chapter 3. Determination of critical state soil parameters and creep characteristics were well described in Chapter 4 is not repeated here. Summary of material properties are presented in Table 5-3. Permeability values of the foundation soil layers in Table 5-3 were converted to respective PS permeability by the previously discussed conversion method.

Fill materials were modelled as an elasto-plastic Mohr-Coulomb continuum. This was done intentionally to reduce the modelling complexity. With the previous experiences in modelling vacuum consolidation, modelling fill material as Biot type coupled Cam-clay or equivalent model can lead to numerical instability in vacuum consolidation. This happens primarily in the layers adjacent to the ground surface where the vertical effective stress is lesser than the vacuum suction. Since elasto-plastic Mohr-Coulomb type model has only two DOFs per node in the mesh, analysis becomes simpler without any significant effect on the accuracy of the results.

Table 5-3: Material properties for the PS analysis.

	Depth (m)	λ	κ	e_0	γ_{sat} (kN/m^3)	k_h (10^{-10} m/s)	OCR
Fill material c = 5.0 kPa, ϕ = *35.0*, γ= *19.0* kN/m^3, ν = 0.3, K = 750, β = 0.5							
Soft Soil	0.0–0.5	0.57	0.057	2.75	14.0	10.0	2.0
	0.5–4.0	0.57	0.057	2.75	14.0	10.0	1.8
	4.0–15.0	0.57	0.057	2.74	14.5	10.0	1.7
	15.0–25.0	0.48	0.048	2.09	15.0	3.3	1.1

*K and β are material data for stress-dependent stiffness characterisation (Janbu 1963).

5.10 FE implementation, mesh and boundary conditions

Six-noded triangular elements were used for the FE mesh, each node having three DOFs in the foundation soil. For the fill materials, six-noded triangular elements with two DOFs were used. Figure 5-3 is a sample of the FE mesh adopted while B = 1. In this PS analysis, the location for EPP monitoring was chosen to represent the field location. Field data were captured from the P3-C location at -4.8 m depth (Kelly and Wong 2009), thus a node at the same depth and at the mid location between two consecutive drains was selected and the same rational was adopted when changing the unit cell width.

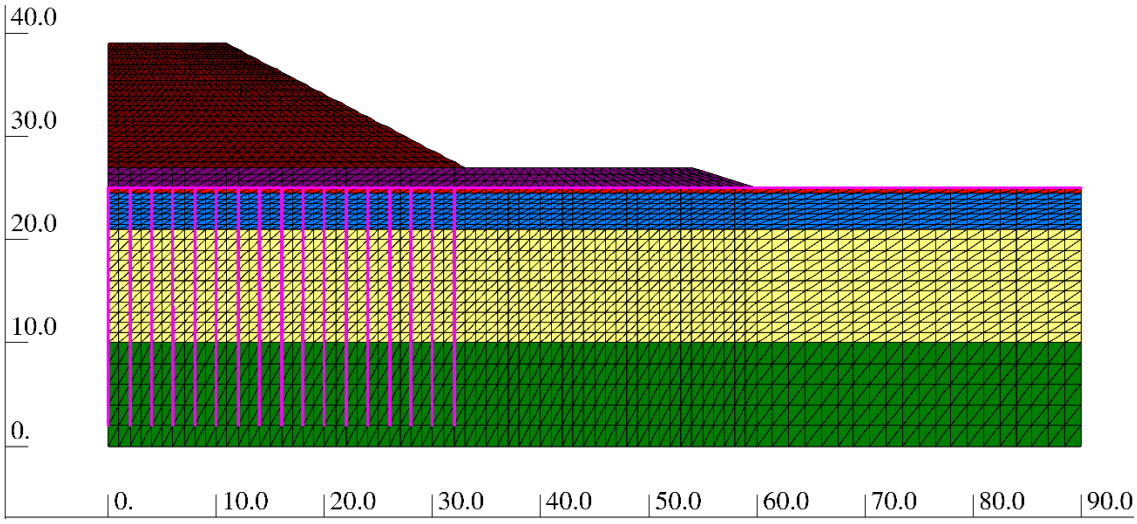

Figure 5-3: Sample FE mesh used for the analysis when B = 1 (Kumarage and Gnanendran 2019a).

As discussed Chapter 4, in the unit cell analysis, stress on the foundation soil was modelled as a traction. However, in the PS model, the actual filling was done by generating the FE mesh with the embankment fill. The embankment fill material at the start of the analysis is disabled (i.e. excavated or removed) and re-enabled (i.e. turned on

or filled) gradually in the correct sequence to represent the embankment construction. The FEA numerical algorithm AFENA (Carter and Balaam 1995) used for this analysis has readily implementable functions to perform these operations.

In general, FEA with the EVP models needs smaller time steps compared to Cam-Clay equivalent models (Gnanendran et al. 2006). In vacuum consolidation, this requirement was very particular. For example, in this Ballina embankment PS analysis, a time step of 0.1 day made the solution diverge, while 0.01 day time increment was sufficient for the convergence with an error less than 10^{-8}.

5.11 Results and synthesis

5.11.1 Settlements and EPP

Figure 5-4 presents the comparison between axisymmetric unit cell and PS FEA predictions of settlement (Figure 5-4-a) and EPP (Figure 5-4-b) against field data. Axisymmetric FEA results were adopted from Chapter 4. According to literature, when Hird et al. (1992) matching techniques are used, the average EPP in PS FEA is generally less than that of the corresponding axisymmetric case. From Figure 5-4-b, it is clear that the above result holds true for vacuum consolidation as well. The deviations reported by Hird et al. (1992) without vacuum are around 7–10% of the axisymmetric case. In this PS analysis with vacuum suction, the maximum differences are around 20%. Hence, it can be observed that the magnitude of the deviation, in EPP predicted by FEA is higher in vacuum consolidation. However, when vacuum is switched off, the axisymmetric and PS EPP predictions get closer as time passes. When PS unit cell width is increased, EPP values are reduced. This can be specifically observed at the peak EPP values around 200

days. Highest value can be observed from the axisymmetric analysis result and observed peak value is reduced with increasing unit cell width. This may not be intuitive since larger *B* value increases the drainage length which retards the EPP being dissipated. However, as per Figure 5-2, due to the non-linear correlation between k_{pl}^{*}/k_{ax} and 2*B*, higher *B* values quadratically increase the k_{pl}^{*}/k_{ax} ratio facilitating faster EPP dissipation. Thus, larger *B* values result faster EPP dissipation and consequently result smaller EPP values.

From Figure 5-4(a), it can be observed that PS FEA underpredicts settlements than the axisymmetric unit cell FEA during the 150–250 days period. From 250–900 days predictions from both FEA are almost equal. From 1000 days onwards, PS FEA overpredicts settlements. This could be due to the faster EPP dissipation in the PS FEA resulting more effective stress being transferred to the foundation soil. Also, it is interesting to note that settlements are almost not affected by the change of PS unit cell width. For practical purposes, predictions of settlements from all $B = 1$, $B = 2$ and $B = 4$ can be considered as equal.

In overall, the axisymmetric unit cell FEA is more accurate than the PS FEA solution for EPP. The main reason for this can be the natural phenomena in dissipating EPP occurring around a PVD is closer to axisymmetric than PS, and the unit cell is better representation in FE numerical modelling of EPP dissipation.

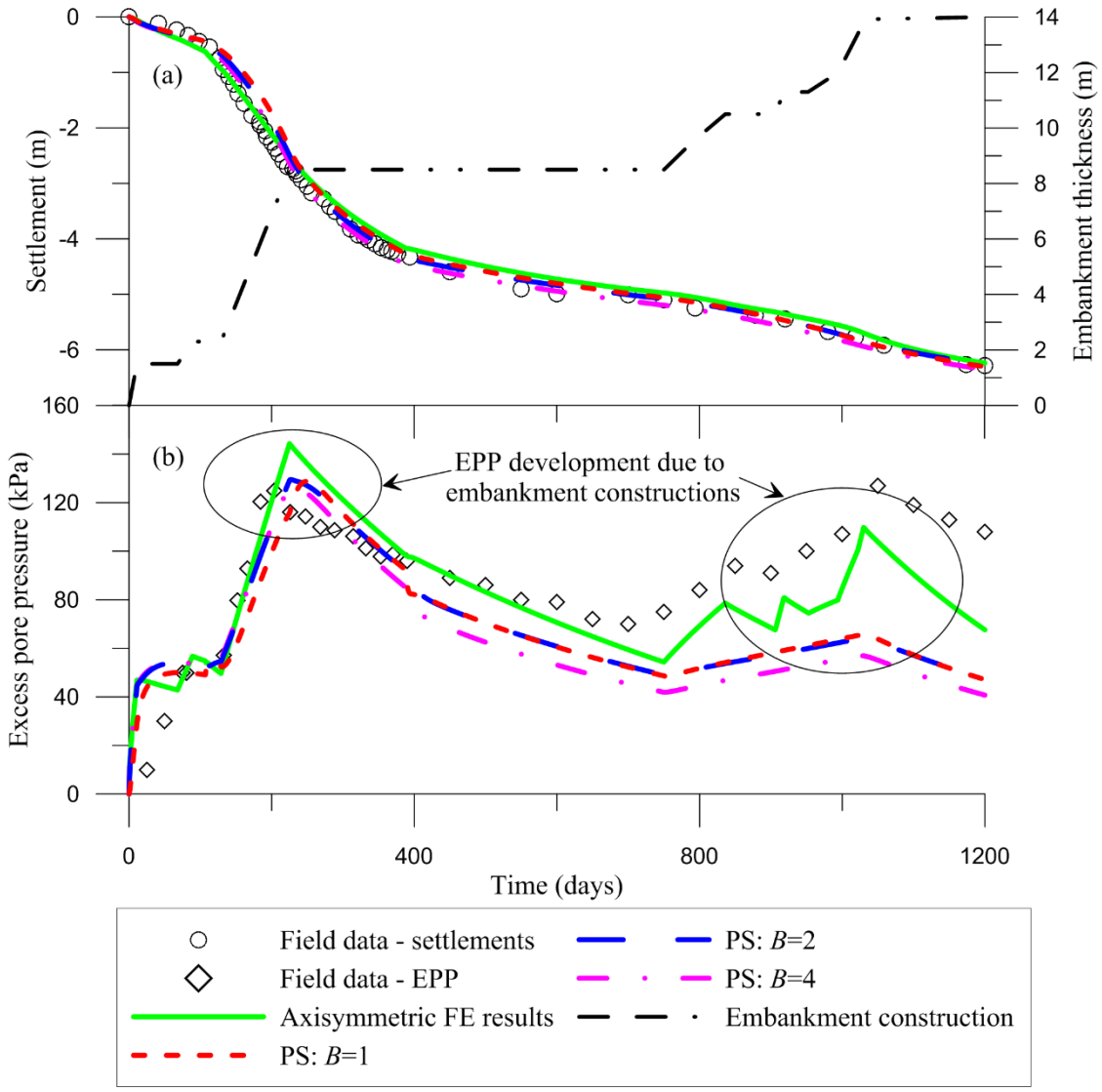

Figure 5-4: Comparison of axisymmetric vs PS FEA.

Figure 5-5 shows the settlement profile across the embankment. Although no comprehensive set of field data was available to validate FEA results, still the Figure 5-5 provides valuable insight about the deformation behaviour of the embankment. As expected, maximum settlement is observed at the embankment centreline. Settlements are reduced as moving away from the centreline and becomes near zero at approximately 35–40 m away from the centreline. As time passes some heaving can be observed beyond the embankment toe. This heave is highest at 65 m from the embankment centreline and is around 1 m. About half of the total settlement observed at 1,200 days occurred by the first 300 days. This is due to the embankment construction and vacuum application. The next 50% of the total settlement occur in a span of 900 days.

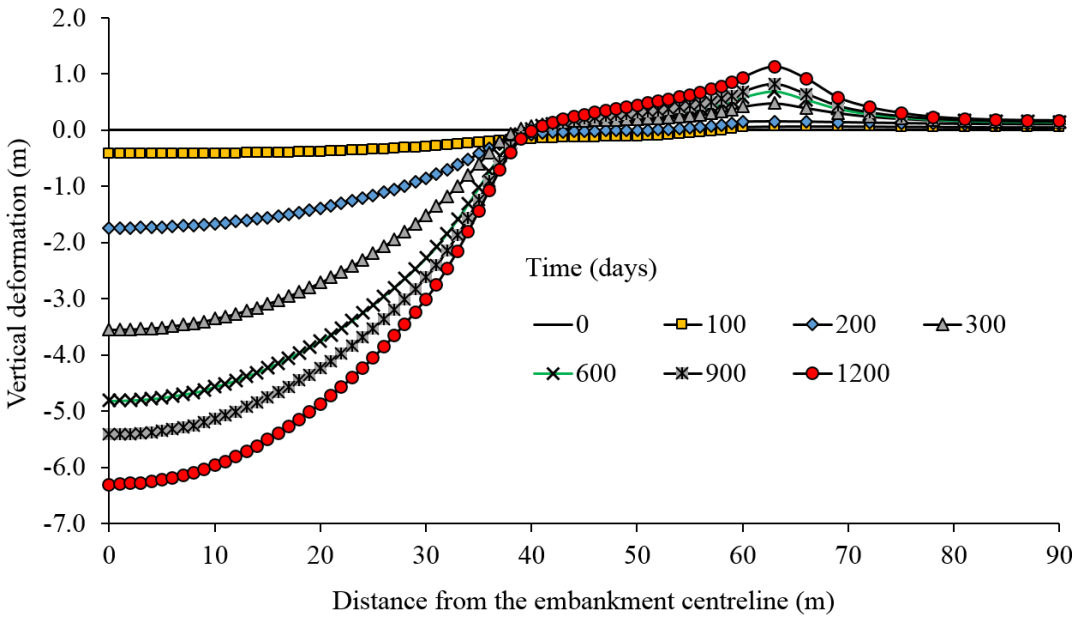

Figure 5-5: Settlement profile with the distance from the embankment centreline.

5.11.2 Lateral deformations with varying unit cell width

Figure 5-6(a) compares the lateral displacements at I6 location against field data. Predictions are plotted for $B = 1$ and $B = 2$ cases at 750 days. For the deeper soil layers (i.e. 15 – 25 m), predictions with both $B = 1$ and $B = 2$ match well with the field data. For 5 – 15 m depth range, results with $B = 1$ are more accurate than of $B = 2$. FEA results from both $B = 1$ and $B = 2$ indicate maximum lateral displacements in the 0–5 m depth where field data indicate the same in 5–10 m depth.

The field data in Figure 5-6(a) shows a shear plane developing between 10 – 15 m of depth of the foundation soil. Kelly and Wong (2009) have also confirmed this observation. It is interesting to observe a significant reduction in lateral displacement occurs across this depth according to FEA prediction as well (especially when $B = 1$). This significant change in lateral displacement can be inferred as a possible development of a shear plane. However, according to FEA results, the reduction is not as rapid as field data indicate.

Figure 5-6(b) illustrates the effect of B towards lateral displacements at different time durations. The plots have been made at 300, 750 and 1,200 days. From all three plots it can be seen that, as the B value is increased from 1 to 2, FEA predict lesser lateral displacements.

5.11.3 Empirical method in predicting maximum lateral displacements

The method is applied for the case history being discussed in this chapter to gain further insight towards lateral displacements. As the horizontal deformations in the Ballina

embankment foundation soil predicted from PS FEA at different times were already plotted with depth, they are compared against the method proposed by Chai et al. (2013).

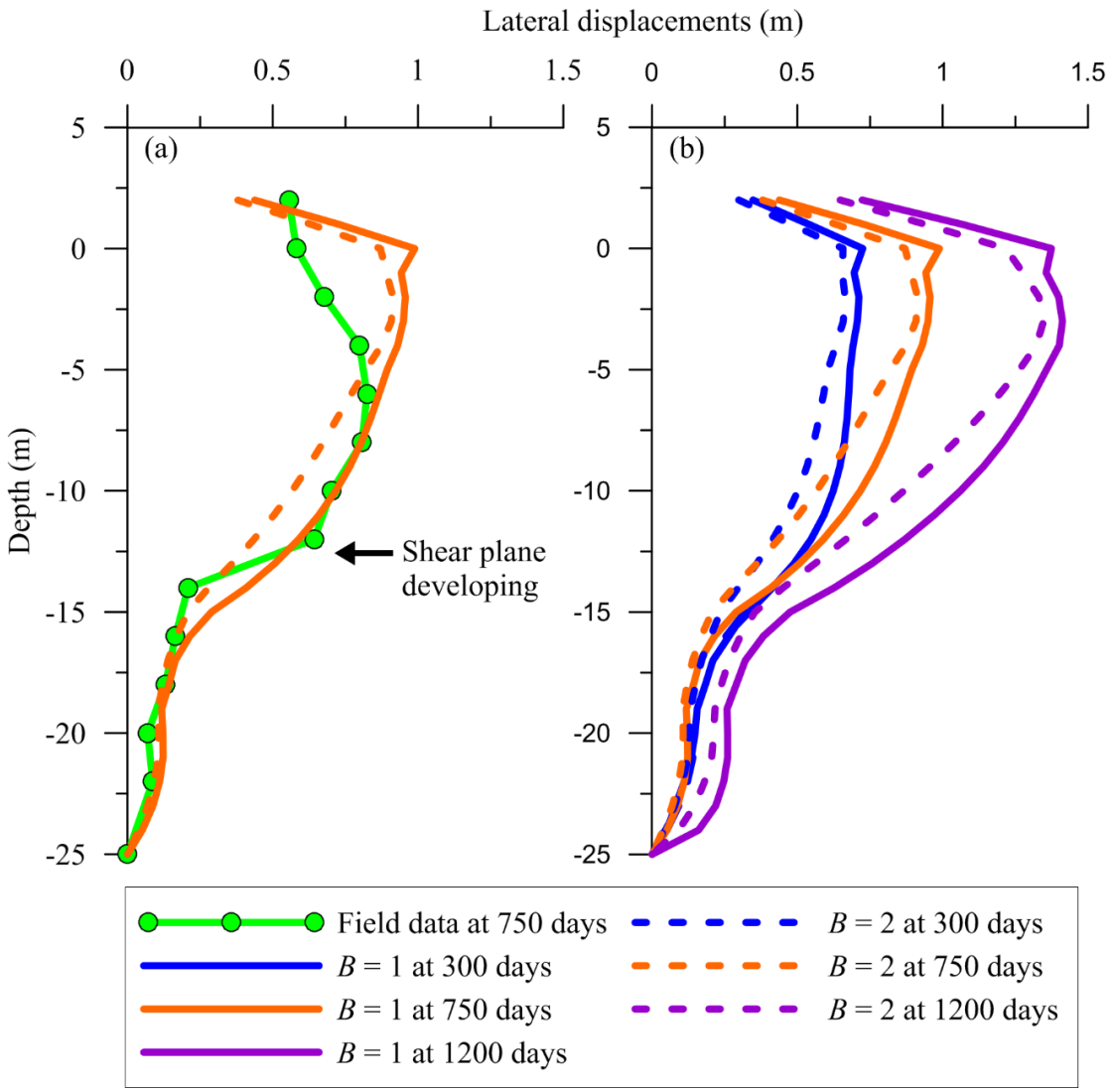

Figure 5-6: Lateral displacements at I6 location; (a)-Comparison with field data; (b) - Effect of *B* for lateral displacement predictions.

NLD and *RLS* values were calculated from Eqns. (5.9) – (5.12) and plotted against the range calculated by the above empirical method. Figure 5-7 illustrates the likely range of maximum lateral displacements. The continuous line in the middle is the Eqn. (5.8), which was proposed by Chai et al. (2013). Other two lines are its mirror images with an offset of 0.05 on the y-axis. I2 and I3 locations of the same embankment were studied by Chai et al. (2013) and their plots have been made in the same figure. In this chapter, both FEA predicted values and field data of I4 and I6 locations are plotted in Figure 5-7 against $x = RLS$ vs $y = NLD$ axes. This was done to position the maximum lateral displacement simulated by FEA for the I4 and I6 locations in the *RLS*, *NLD* space and cross-check the same against field data.

Generally, both field data and FEA results fall to a close range in Figure 5-7. Mirror lines with the 0.05 offset seem to sandwich all data, with the exception of field data and FEA results in the I4 location are marginally less than the proposed range. It appears that as increasing *RLS* (increasing vacuum suction compared to undrained material strength) the net lateral displacement (*NLD*) tends to reduce. This is a well-known benefit of vacuum application as vacuum tends to reduce outward lateral displacement caused by embankment construction and result low net lateral displacement.

Figure 5-6(b) carries the lateral displacement plot against time when $B = 1$ and $B = 2$. However, the benefit of vacuum application can be more clearly seen in Figure 5-7, where net lateral displacements are plotted in several inclinometer locations. In the presence of vacuum, despite of the soil foundation thickness, the net lateral displacements are constrained to a narrow region in the *LND–RLS* space. Specially provided the clay thickness of corresponding to I6 location is almost twice of I3 (i.e. 24.7 m and 14.7 m

respectively; please refer to the Table 4-5 in Chapter 4) only marginal increment in *NLD*s are measured and the same was confirmed in FEA results.

Although the *RLS*, *NLD* space provides a convenient way of approximating maximum lateral displacement, there are few limitations in this method which are worth to note. The lateral deformations can only be analysed in certain points in time during the project. For example, S_f should be determined after the embankment construction and p_{em} should be determined at the end of the vacuum application.

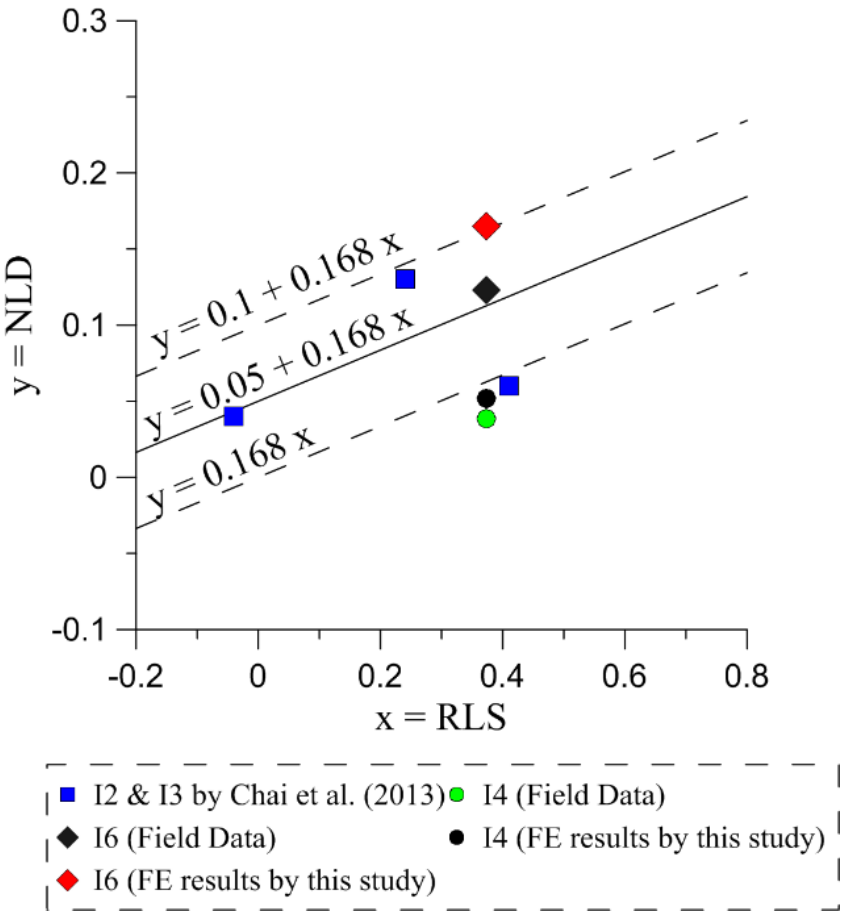

Figure 5-7: Predicted maximum lateral displacements.

In this Ballina embankment project, the first stage of embankment construction finished in 225 days where S_f was measured, and vacuum application ceased around 400 days where p_{em} was measured. In determining s_u, it was approximated as Ladd (1991) proposed;

$$s_u = \sigma'_v S_1 (OCR)^n \tag{5.15}$$

where S_1 and n are material constants. Ladd (1991) proposed the appropriate range for S_1 and n as, $0.162 < S < 0.25$ and $0.75 < n < 1$, also described the procedure to obtain the same. In this chapter, by the end of vacuum application, it was assumed $OCR = 1$ and in such context, the value n is not significant and was assumed as $n = 1$ as well. Since there was no data to confirm the value of S_1, an average value of $S_1 = 0.206$ was chosen.

5.11.4 Results of the stability analysis

Figure 5-8 presents the plot of maximum lateral displacement against the embankment centreline settlement in two locations (I6 and I4). For I6 location, a straight line is drawn according to the field data (L-1 in Figure 5-8). As per the straight line drawn, $m_1 = 0.18$ was obtained. However, since FEA results have overestimated the lateral displacements, $m_1 = 0.22$ was observed for the trend line drawn for FEA results at I6. Both field data and FEA results have not indicated a potential embankment failure. For the I4 location, 0.07 and 0.05 values were obtained for m_1 in FEA results and field data respectively. This was a better agreement between the field and FEA data than the I6 location. As per the value of m_1 obtained, both I4 and I6 locations are stable. Field reports and related literature also did not report any embankment instability; hence the results obtained from FEA seems acceptable.

It is important to understand the difference between Figure 5-7 and Figure 5-8. Although they apparently looking at lateral deformations against vertical (or some invariants of it), the calculations are significantly different, and two figures serve for two different purposes. Figure 5-7 compares the FEA predictions against the likely range of maximum lateral displacements and has been used as an empirical method to confirm the FEA predictions made in this chapter. The vertical deformation and lateral deformation measurements are not necessarily measured at the same time. Figure 5-8 is used to assess the stability of the embankment where lateral deformations are plotted against the vertical deformations at a given instant.

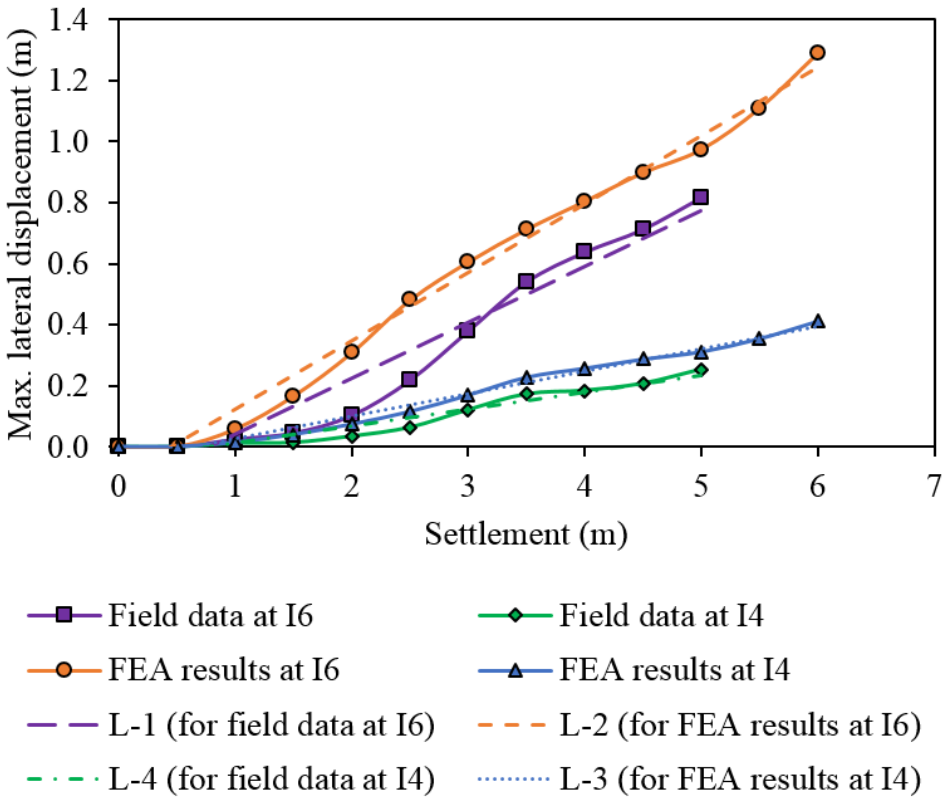

Figure 5-8: Plot of y_h against S_f.

5.12 Summary

In this chapter, the axisymmetric unit cell was converted to an equivalent PS model in the context of a ground improvement project with vacuum-assisted PVDs. Foundation soil was modelled using an EVP model with time-dependent boundary conditions to represent the start and termination of vacuum application. Smear zone was captured by an equivalent mass permeability calculation in the model. Using the Hird et al. (1992) combined matching approach, unit cell width was changed to investigate its effects.

It was observed that changing the unit cell width has a negligible effect on settlement predictions for either short or long-term. There is a slight increase in the rate of EPP dissipation with increased *B* value which results in lesser EPP values, especially at its peaks.

In terms of lateral displacements, it was illustrated that the unit cell width has a direct influence on lateral displacements. Increasing unit cell width in the FE mesh reduces the overall lateral displacement predictions. Comparison of lateral displacement profile revealed that predictions at deeper (15 – 25 m) levels had good agreement with field data. Generally, FEA predictions over predicted the lateral displacements at shallow depths. Foundation soil had an identifiable shear plane according to the field data. Although it was not obvious in FEA results, there were some supporting evidence for this shear plane development from the changes (reduction) in lateral displacements closer to this depth. Maximum lateral displacements were reasonably well predicted and they compared well against field data. Although the empirical method proposed by Chai et al. (2013), to predict the maximum lateral displacement has few limitations, yet it was confirmed that the method could be a useful tool in predicting lateral displacements.

Embankment stability was analysed at two inclinometer locations and determined to be high according to Tavenas and Leroueil (1980) method.

Chapter 6: Application and removal of vacuum[4]

6.1 General

The duration of the vacuum application is a common problem encountered by geotechnical engineers in vacuum consolidation projects. It is generally considered that a vacuum application with a longer duration can reduce the post-construction settlements. Kosaka et al.'s (2016) field observations on applying vacuum to reduce secondary compression confirm this idea. However, the duration of the vacuum application is often bounded by economic factors such as the costs of running the vacuum pump and labour costs. Additionally, technical problems (e.g. accidental termination of the vacuum pump) and administration problems (e.g. long holidays) may disturb the vacuum application process. These practical problems not only limit the duration of the vacuum application but also require that vacuum be stopped and re-applied. Thus, it is crucial that the implications of repetitive vacuum application and removal be investigated.

The main aims of this chapter are to:

(i) Illustrate the effects of the duration of vacuum application on long-term consolidation and creep;

(ii) Examine the effects of the application and subsequent removal of vacuum;

[4] Material discussed in this chapter form part of the following publications:

Kumarage, P.I., and Gnanendran, C.T. 2018a. Creep based viscoplastic numerical modelling of soil deformations in vacuum application and removal. *In* Proceedings of the 71st Canadian Geotechnical Conference. Edmonton, AB, Canada.

Kumarage, P.I., and Gnanendran, C.T. 2019d. Predicting deformations in vacuum assisted ground improvements using an elasto-viscoplastic numerical model. Accepted for the Proceedings of the XVI Panamerican Conference on Soil Mechanics and Geotechnical Engineering. Cancún, México.

(iii) Highlight and find possible solutions for numerical instabilities in modelling such activities;

(iv) Discuss the practical applications such as accidental termination and recovery of vacuum pumps, using a relevant case history.

6.2 Implications of the duration of vacuum application

This section discusses the results of a sensitivity analysis that was numerically simulated to examine the implications of vacuum duration. In the sensitivity analysis, the duration of the vacuum application was varied and the EVP response of soft soil was simulated. A FEA was undertaken using the unit cell idealisation and the soft soil properties of Ballina clay (see discussion in Chapter 4) were used. Five scenarios were simulated with varying vacuum durations (see Table 6-1). A no-vacuum case (Test -1) was considered to enable comparisons to be drawn. At the end of each respective vacuum application period, vacuum was terminated, and the soil was expected to respond as it would with a conventional PVD.

Table 6-2 sets out the soil parameters used in the analysis. These parameters reflect the attributes of Ballina clay, at approximately at 10 m in depth and were adopted from Pineda et al. (2016). A unit cell (with a height of 10 m and a radius of 0.5 m) was discretised with six-noded triangular elements for the FE mesh. Smear zone was not

considered since the primary objective of the analysis is to illustrate the implication of the vacuum duration and not to back analyse field data.

The axisymmetric FE mesh adopted for the sensitivity analysis is illustrated in Figure 6-1. A vertical stress of 70 kPa was applied to the topmost elements of the mesh and a vacuum intensity of the same magnitude was applied to the axisymmetric boundary as discussed in Chapter 3 and Chapter 4. This vertical stress was chosen to exceed the p_c' reported for the clay sample to allow the material to undergo plastic deformations. A vacuum intensity of the same magnitude was used ensure the vacuum surcharge ratio (VSR) would satisfy the condition VSR $= 0.5$ so that numerical instabilities can be minimised (more details about the VSR ratio and numerical instabilities are discussed later in this chapter). Settlements over the time were monitored at the surface of the mesh and the EPP was monitored at the outer most element at the mid-depth (i.e. 5 m). This location was chosen as it indicates the halfway point between the drains in the field and thus shows the maximum change in EPP.

Table 6-1: Test details for the sensitivity analysis.

Test No.	Vacuum duration (Days)
1	No Vacuum
2	50
3	100
4	150
5	200

Table 6-2: Soil parameters adopted for the sensitivity analysis.

Parameter	Value
M	1.5148
λ	0.525
κ	0.0525
e_0	2.80
C_α	0.057
k_h(m/s)*10^{-10}	9.38
p'_c (kPa)	60

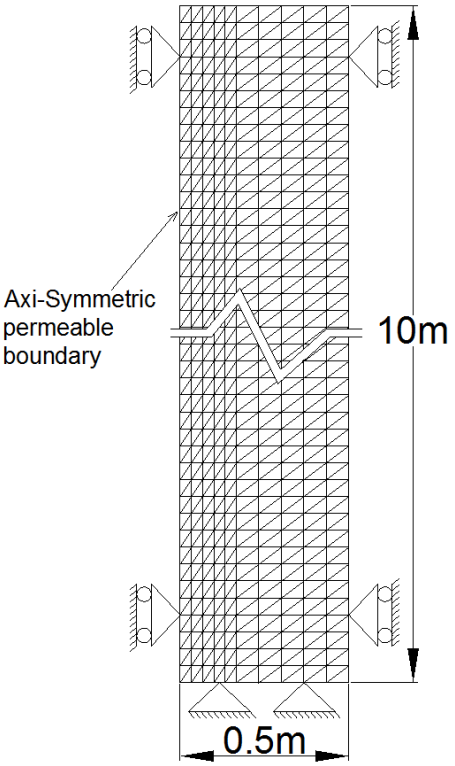

Figure 6-1: FE mesh for the sensitivity analysis.

Figure 6-2(a) and (b) present the FEA results of the respective settlement and EPP responses with varying vacuum durations. Figure 6-2(a) shows that by 800 days, EPP had almost dissipated in all five tests. In relation to Test-1 (i.e. the no-vacuum test), it took approximately 800 days to dissipate EPP completely. Conversely, other tests (with vacuum) achieved the same result much more quickly; for example, in Test-5, the application of vacuum accelerated the process and reduced the EPP to zero in approximately 100 days. After approximately 800 days, at which time there was no significant EPP, and vacuum was switched off, the settlements were primarily governed by secondary compression.

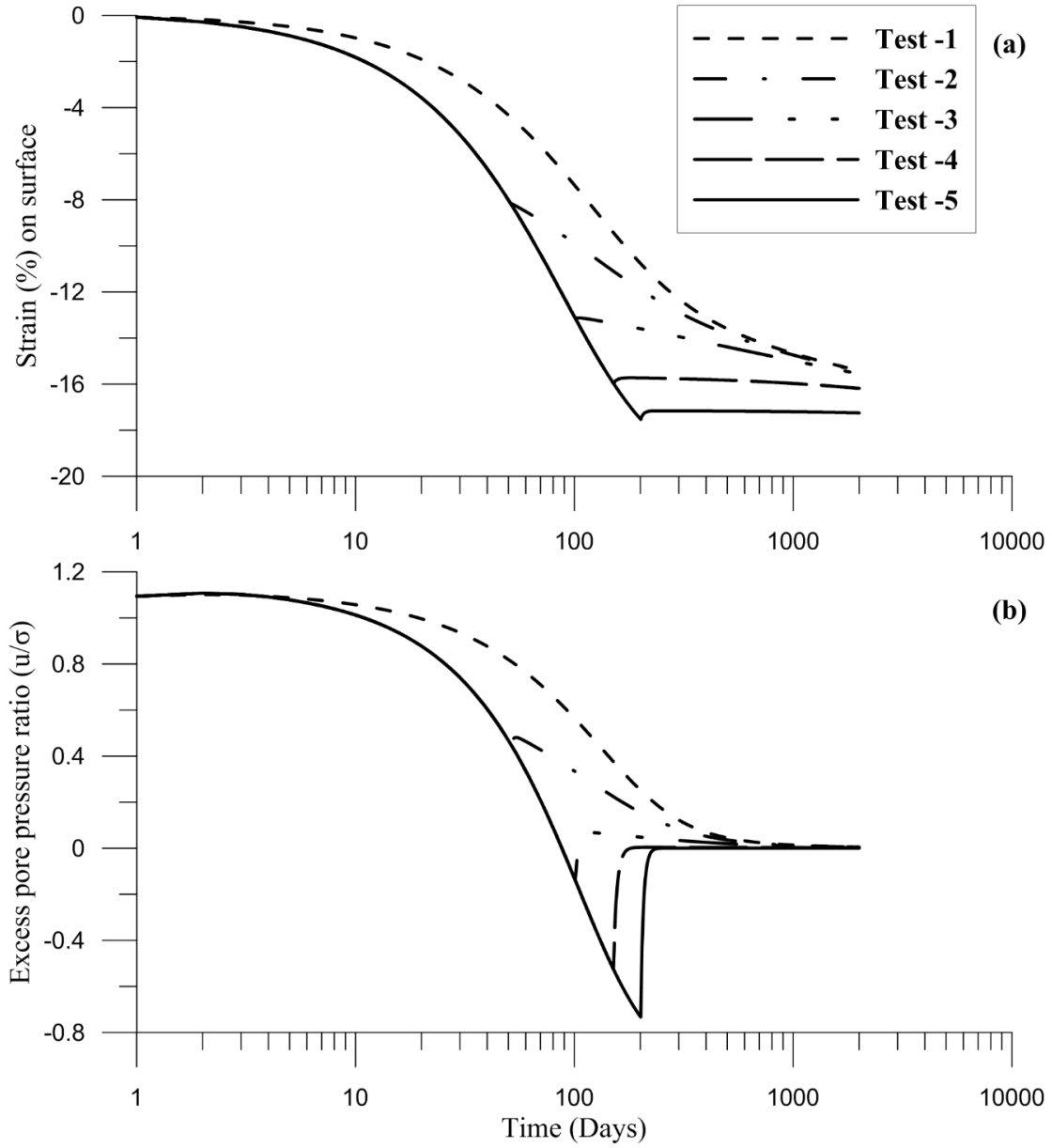

Figure 6-2: Effect on vacuum duration: (a) Vertical Strain %; (b) Excess pore pressure.

The slope of the time-strain curve after 800 days provides insight into the secondary compression that occurs in this duration. It is clear that by applying vacuum for an extended period, the slope of the time-strain curve reduces significantly. The reduction in the secondary compression is significant when vacuum continues to be applied until EPP becomes negative. Soil swelling can also be observed at this stage. The application of vacuum for a sufficient duration can bring the soil to an over-consolidated state and thus

reduce the coefficient of secondary compression. Fukazawa et al. (1994) also discussed the reduction of the coefficient of secondary compression with the over-consolidation ratio (OCR), however their discussion was limited to conventional soil improvements. Conversely, the soil rebound observed in Test-4 and 5 in Figure 6-2(a) is an indication that the over-consolidated soil swelling upon vacuum being removed.

Generally, it is convenient to first monitor the EPP and then the settlements, as the engineer can identify the time at which EPP becomes zero. The sensitivity analysis showed that running the vacuum pump after EPP becomes zero causes the soil to swell when vacuum suction is removed. Thus, it is vital to observe the EPP and run the vacuum pump until the desired degree of consolidation (based on EPP) or OCR is achieved, to reduce long-term post-construction settlements. As sensitivity analysis also showed, bringing the soil to an over-consolidated state by applying vacuum can significantly reduce the creep deformations.

Figure 6-3 presents the mean effective stress inside the unit cell at different times for Test – 3. Since all tests were conducted using the same surcharge (70kPa) and same vacuum (–70 kPa) there was no preference in selecting a particular test to this illustration. Figure 6-3(a), at one day shows the stress just before vacuum application. Figure 6-3(b) to (e) is while the vacuum is applied. These figures show the significant increment in effective stress during vacuum application. The stress distribution pattern is largely vertical (could be seen from the colour pattern) and increase towards the drain, ensuring the vacuum is applied at the axisymmetric boundary. OCR calculated at the end of each test (i.e. 2000 days) are 1.70, 1.78, 1.84, 1.95, 2.04. This confirms that longer vacuum duration results in higher OCR.

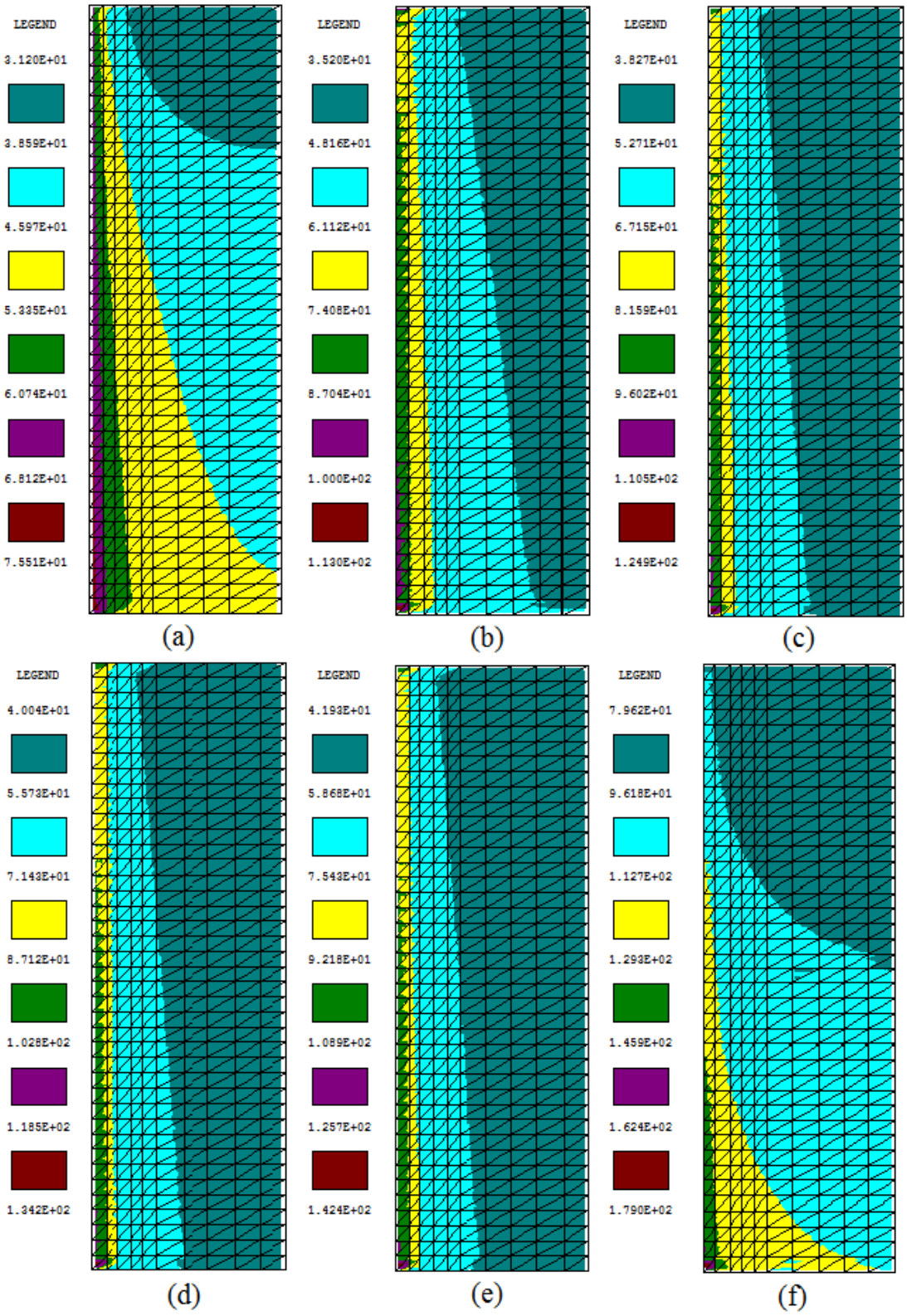

Figure 6-3: Mean effective stress inside the unit cell (a) after one day; (b) after 25 days; (c) after 50 days (d) after 75 days (e) after 100 days (f) after 2000 days.

The exercise undertaken in this part of the study was merely a simulation; thus it is essential that the EVP model prediction be validated against experimental results upon the application and removal of vacuum. Further, in this study, vacuum intensity was kept at a reasonable level and no fluctuations in surcharge were made to avoid solution divergence. The next section uses experimental data with higher fluctuations of vacuum and surcharge to validate the EVP model predictions. The term VSR is also introduced to quantify the intensity of vacuum compared to surcharge.

6.3 Validating the EVP response on application and removal of vacuum and surcharge against experimental data

The FEA solution converged in the previous section; however, the results needed to be validated to confirm that the correct solution has been found. In the case of a vacuum intensity change or surcharge change that is close or beyond VSR = 0.5, a separate solution algorithm was used in this validation to improve the accuracy of the FEA solution. In a non-linear FEA, the main challenge may not be the solution convergence. As Zienkiewicz and Taylor (1996) stated, in a non-linear FEA, the solution achieved is not necessarily the solution sought. In this section, solution convergence and the accuracy obtained are illustrated with and without the additional steps incorporated to ensure the solution convergence and improved accuracy.

6.3.1 Correction for the EPP

An iterative process was adopted to improve the accuracy in the EPP prediction upon the removal of vacuum and surcharge. Readers might be questioning why this problem did not occur with the FEA conducted in other previous chapters (e.g. Chapter 4). To answer this question, two terms must be introduced: first is the total apparent stress, which is the

absolute sum occurred by surcharge (p_{sur}) and vacuum (p_{vac}), and second is the vacuum surcharge ratio (VSR) which can be expressed as in Eqn. (6.1).

$$VSR = \frac{\Delta P_{vac}}{P_{sur} + P_{vac}} \tag{6.1}$$

Large vacuum fluctuations (Δp_{vac}) such as the termination and re-application of vacuum (where VSR $\geq$ 0.5), can result in either divergence or converge to a wrong solution. In this section, an algorithm (see Figure 6-4) was adopted to improve the FEA results in such cases.

As Figure 6-4 shows, after a predefined time increment, a loop (i.e. the inner loop) was run to ensure the convergence before the next time increment. In this inner loop, the stiffness matrix was remade and is analogous to the Newton-Raphson iteration.

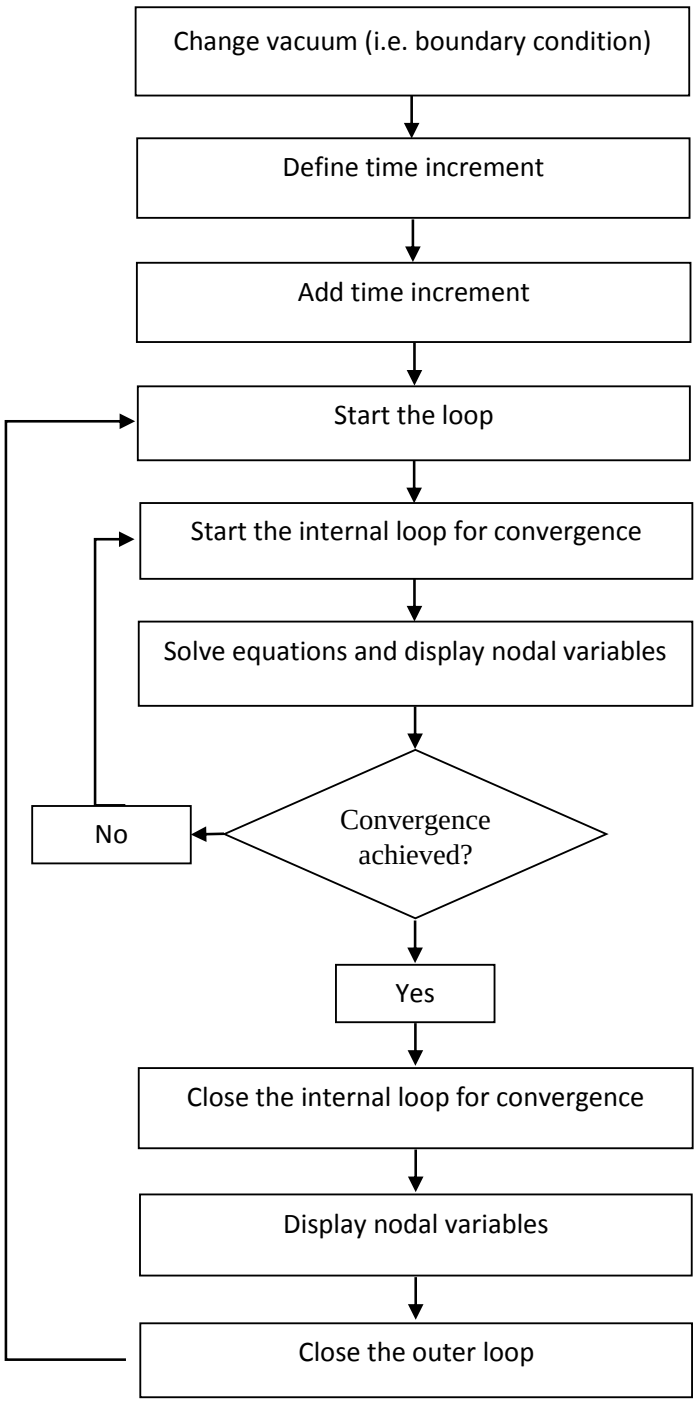

Figure 6-4: Solution algorithm to improve FEA results upon removing vacuum and surcharge.

6.3.2 Correcting volumetric strain in the swelling phase

To improve the predictions in the swelling phase, in this chapter, volumetric deformations during swelling were multiplied by a correction factor β, such that:

$$\varepsilon_v^* = \beta \times \varepsilon_v \tag{6.2}$$

where, ε_v^* is the corrected volumetric strain, ε_v is the volumetric strain during swelling and β is the correction factor during swelling.

6.3.3 Modelling the consolidation response with corrections

The consolidation response of Kaolin clay reported by Kianfar et al. (2015) was used to validate the proposed methodology. Table 6-3 sets out the properties of the clay adopted for the validation.

As Kianfar et al. (2015) reported, the apparatus was a modified Rowe cell (150 mm in diameter) and vacuum was applied through a 14.5 mm diameter drain, which was casted at the centre of the consolidation cell (see Figure 6-5).

In the FEA, the boundary of the soil-drain interface was modified to simulate vacuum suction (as discussed in Chapters 3 and 4). The mesh discretisation for the Rowe cell is presented in Figure 6-6. Only half of the cell was modelled due to symmetry. As discussed in previous chapters (e.g. Chapter 4) six-noded triangular elements were used with each node having three DOFs. Three tests were validated in this chapter, each with a surcharge and vacuum of 50 kPa and both of them were removed at different instances during the total analysis period of 144 hours.

Table 6-3: Kaolin clay properties (modified from Kianfar et al. 2013).

Property	Value
Slope of the consolidation line : λ	0.17
Slope of the swelling line : κ	0.03
e_N^1	1.85
Friction angle: φ '	27^0
Slope of the critical state line: M	1.07
Secondary compression: C_α (Assumed)[2]	0.0117

[1]Void ratio in normal consolidation line at $p' = 1$

[2]Assumed that C_α/C_c = 0.03 which represents the lowest ratio proposed by Mesri and Godlewski (1977).

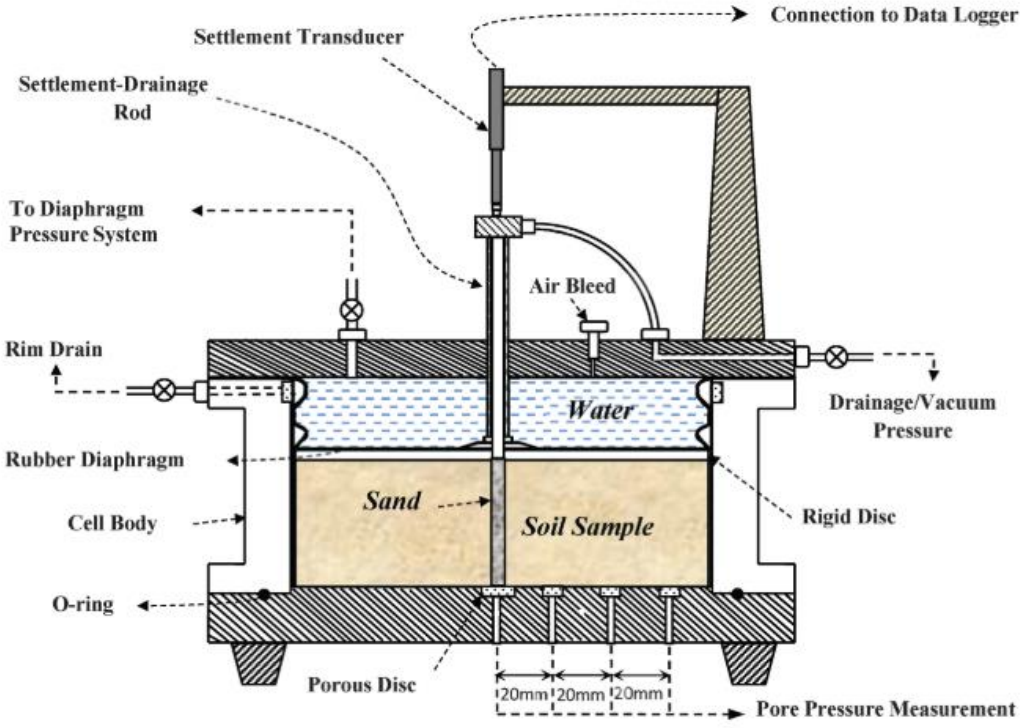

Figure 6-5: 150 mm Rowe cell (modified from Kianfar et al. 2015).

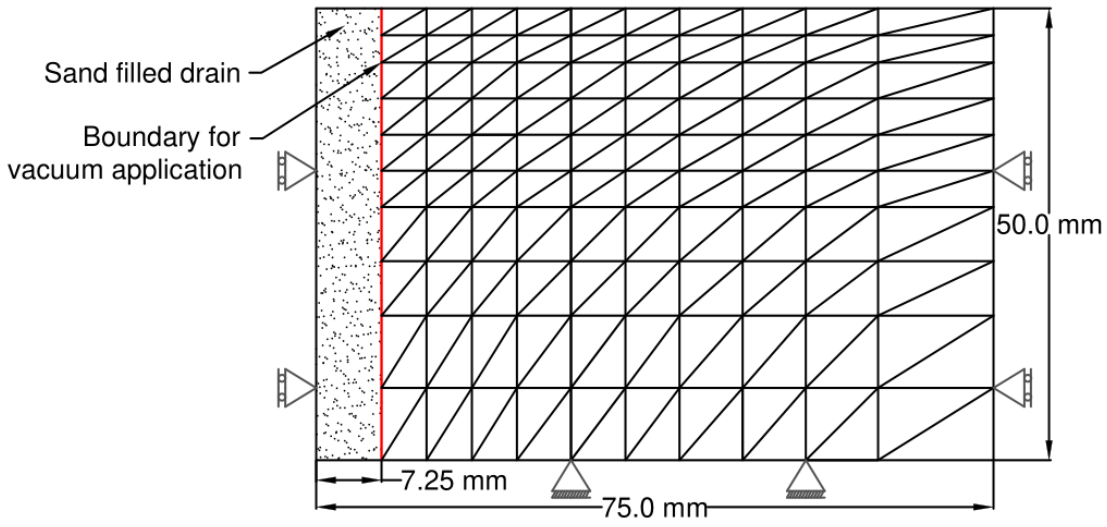

Figure 6-6: FE mesh adopted to model the Rowe cell.

Details of the tests are as follows:

- Test A: Surcharge (50 kPa) and vacuum (50 kPa) applied. Vacuum removed after 8 hours and surcharge removed after 72 hours;
- Test B: Surcharge (50 kPa) and vacuum (50 kPa) applied. Vacuum removed after 10 hours and surcharge removed after 72 hours; and
- Test C: Surcharge (50 kPa) and Vacuum (50 kPa) applied. Vacuum removed after 12 hours and surcharge removed after 72 hours.

All three tests ran up to 144 hours. Their EPP responses and strains are displayed in Figure 6-7 and Figure 6-8, respectively. EPP was monitored at the bottom of the Rowe cell at the location RR = 0.48. Where RR is defined as:

$$RR = \frac{r - r_w}{R_1 - r_w} \tag{6.3}$$

where, r is the radius from the centre for the EPP measuring location, r_w is the radius of the vertical drain and R_1 is the radius of the cell.

Given $RR = 0.48$, $r_w = 7.25$ mm and $R_1 = 75$ mm, r was calculated as $r = 39.77$ mm. Considering $r \approx 40$ mm, this corresponds to the third EPP measuring location in the experimental setup (see Figure 6-5). In the FEA, the nearest node in the FE mesh to the calculated radii (r) was selected to measure the EPP.

Figure 6-7 shows the EPP response upon removing vacuum and surcharge. Due to convergence problems, accurate predictions upon removing vacuum and surcharge were difficult to obtain. The original (unimproved) FEA results are illustrated by dashed lines in Figure 6-7(a), (b) and (c). To improve the FEA results, the solution algorithm proposed in Figure 6-4 was adopted and the improved FEA results are illustrated by the continuous line in Figure 6-7.

When vacuum was removed, an uplift of the EPP values were observed in all three tests. If the analysis is run without the improved algorithm (as mentioned above), the EVP model will fail to successfully represent the soil behaviour. However, with the improved method, such uplift is correctly represented in the FEA. A magnifier was plotted during the vacuum removal state for Test B, to make this improvement clearly visible.

The next discrepancy arose when the surcharge was removed at 72 hours. None of the three tests had any EPP present by this time. According to the experimental data, the removal of the 50 kPa surcharge resulted in an EPP of approximately –25 kPa. The EVP model grossly overestimated this value by 60%, projecting an EPP value of

approximately –40 kPa. With a time step of 0.01 hr the solution would not converge at all, thus as the first step, time-stepping was reduced to 0.001 hr per step to converge the iteration. However, as illustrated by the unimproved FEA, this resulted in a gross overestimation. To correct this, in the improved solution, surcharge removal was done within a duration of 1 hour (not instantaneously) and the algorithm presented in Figure 6-4 was applied. With the above mentioned collective numerical treatment, the solution converged accurately to match the experimental data. However, as the boundary conditions could not be changed instantaneously, a slight offset in FEA predictions against experimental data are evident as Figure 6-7(b) shows (a magnification was drawn for clarity).

As Figure 6-8 shows, a longer duration of vacuum application results in larger settlements. In each of the 8 hr, 10 hr and 12 hr vacuum applications (undertaken in Tests A, B and C respectively), it resulted in approximately 7%, 7.5% and 8% axial strain at the time of vacuum removal. FEA predictions during the vacuum application period and until the removal of surcharge were agreeable with the modified algorithm. However, vertical strain predictions of soil swelling after removing surcharge, was over-estimated approximately by 1% of the axial strain. In laboratory experiments, this could be due to the sidewall friction. However, careful investigations of this phenomenon have revealed that provided that the friction and experimental errors are small, predictions of final settlements and swelling will still be challenging in vacuum consolidation (Chai et al. 2005, Wu et al. 2016).

The correction applied in the swelling phase significantly improved the prediction as illustrated by Figure 6-8. However, as the applied vacuum duration increased, more deviations arose against the experimental data.

The correction factor β, in this case, was approximately 0.82. This had a close agreement with the minimum correction proposed by Chai et al. (2005) of 0.80 for the axisymmetric condition. As Figure 6-8 shows, deviations mainly appears during the instantaneous swelling phase. Once the swelling phase is over (e.g. after 100 hours), FEA predictions can be closely matched with the experimental data with a correction.

This validation shows that solution divergence mainly occurred due to either a sudden change in the boundary conditions (such as removal of vacuum) or rapid and significant change in stress (such as removal of the surcharge at 72 hrs). In all of the above analysis, around 10 iterations (in the inner loop of Figure 6-4) were sufficient to converge the solution accurately.

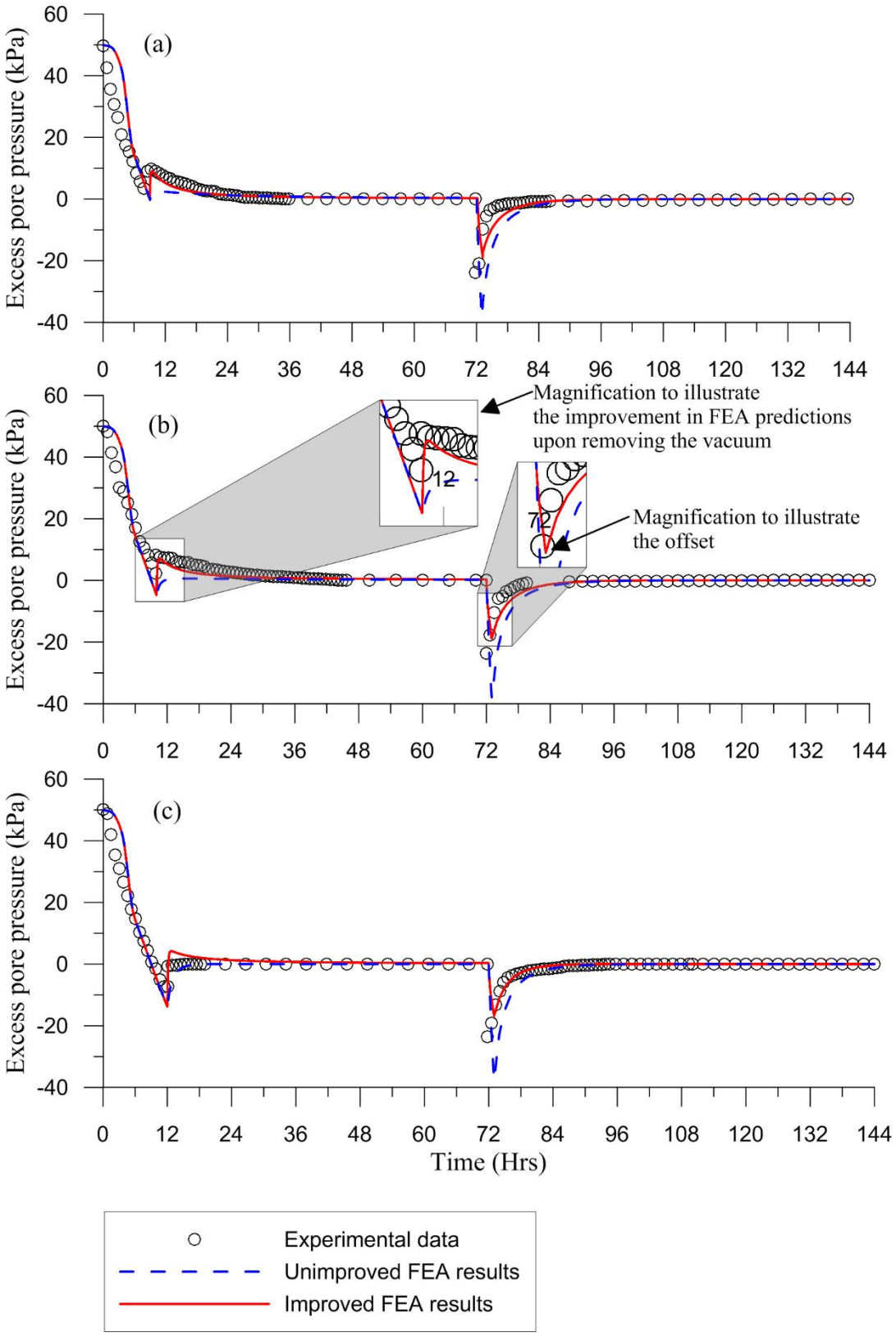

Figure 6-7: Excess pore pressure responses of the tests upon removing vacuum and surcharge (after Kumarage and Gnanendran 2018a).

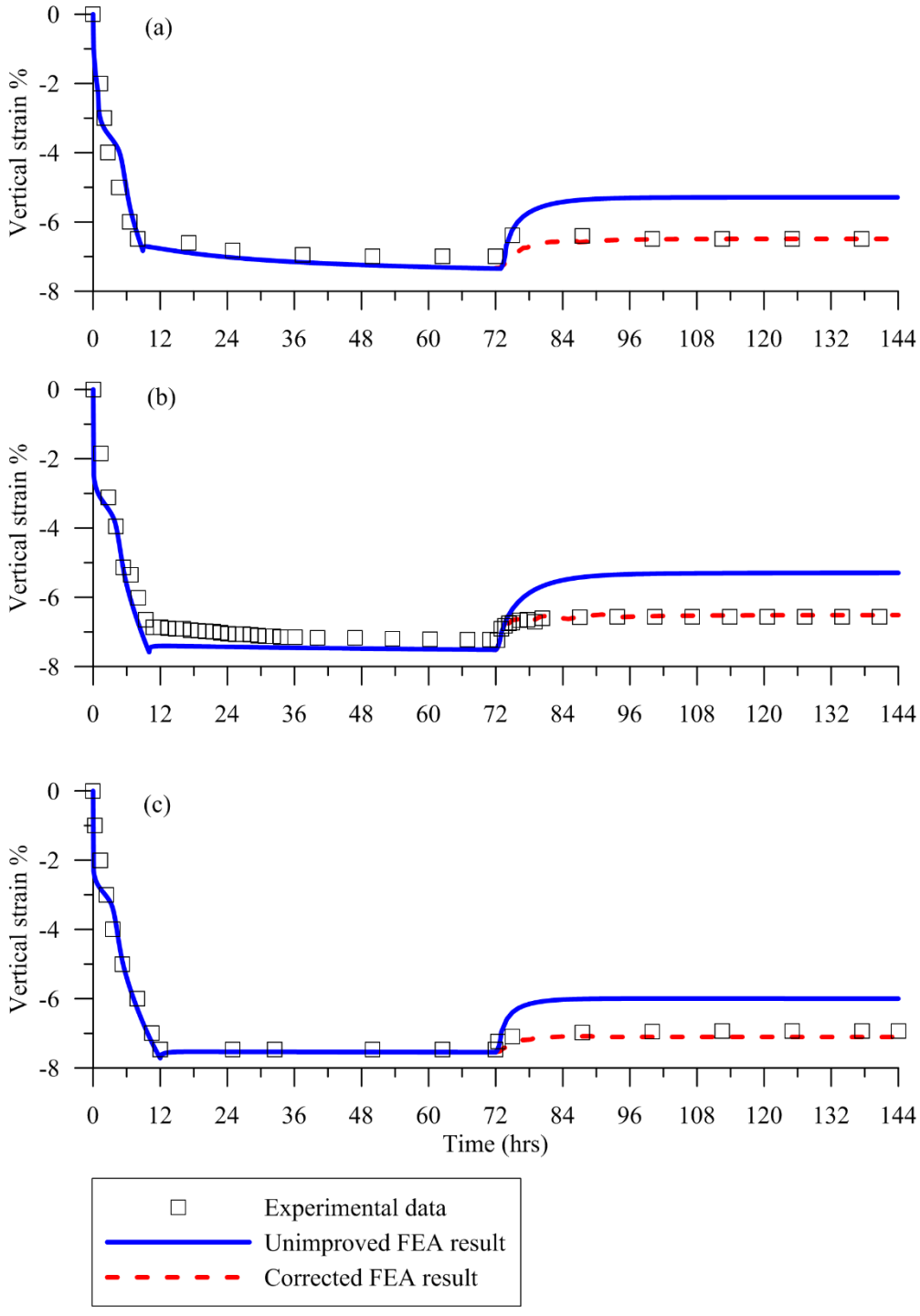

Figure 6-8: Axial strain over time with vacuum application and removal.

6.4 Field trial on reclamation site in Singapore

Singapore is a country with a very limited landmass. Land reclamation has been adopted as the key strategy of Singapore to increase its landmass since 1970s (Chu and Guo 2016, Lam et al. 2018). The main challenges in this process have been the scarcity of fill material and the movement of the reclamation works towards deeper water. In recent reclamation projects, dredged clay slurries have been used as a substitute for the granular fill materials. Improving these soft clays to increase their shear strength and to reduce the post-construction settlements presents a significant challenge. Due to near-zero shear strength at the start of the project, the use of fill surcharges with PVDs have proven difficult. Consequently, vacuum consolidation with capped PVDs (Chai et al. 2008) or membrane-less vacuum consolidation method (as it is commonly known) was selected as an economical method for ground improvement in these reclamation projects. Figure 6-9 displays a sample of the CPVD used in this project.

The reclamation site discussed in this chapter had three distinguishable soil layers (Lam et al. 2018). The soft clay layer had been sandwiched between a silty sand layer placed in 2001 at the top and a siltstone layer at the bottom. The thickness of these layers varied significantly over the treated trial area of 100 m by 50 m (see Figure 6-10[a]). Figure 6-10(b) shows the instrumentation of the reclamation site. The BH-1 location was selected for the analysis reported in this chapter since it had the highest thickness of soft clay and was in the mid-section of the treated area.

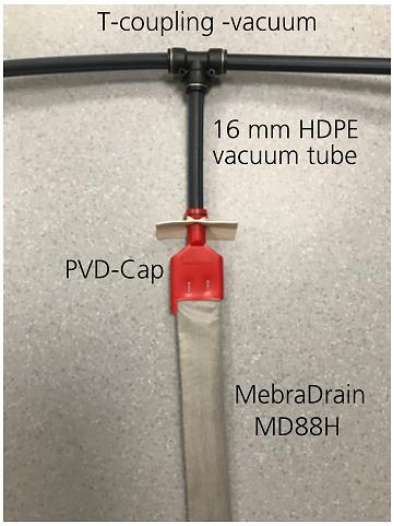

Figure 6-9: A sample CPVD used in the project (modified from Lam et al. 2018).

6.4.1 Selection of material properties

The C_α value for the soft clay layer was approximated using the ratio proposed by Mesri and Godlewski (1977) and the maximum and minimum values were calculated as 0.031 and 0.019, respectively. An average permeability of 3×10^{-10} m/s was adopted for the soft clay layer. In determining the properties of the unit cell, the procedure explained in previous chapters (e.g. Chapter 4) was adopted and has not been set out again in this chapter. Table 6-4 displays the unit cell properties adopted for the analysis. Biot type Mohr-Coulomb consolidation elements were used for the top and bottom sandy layers.

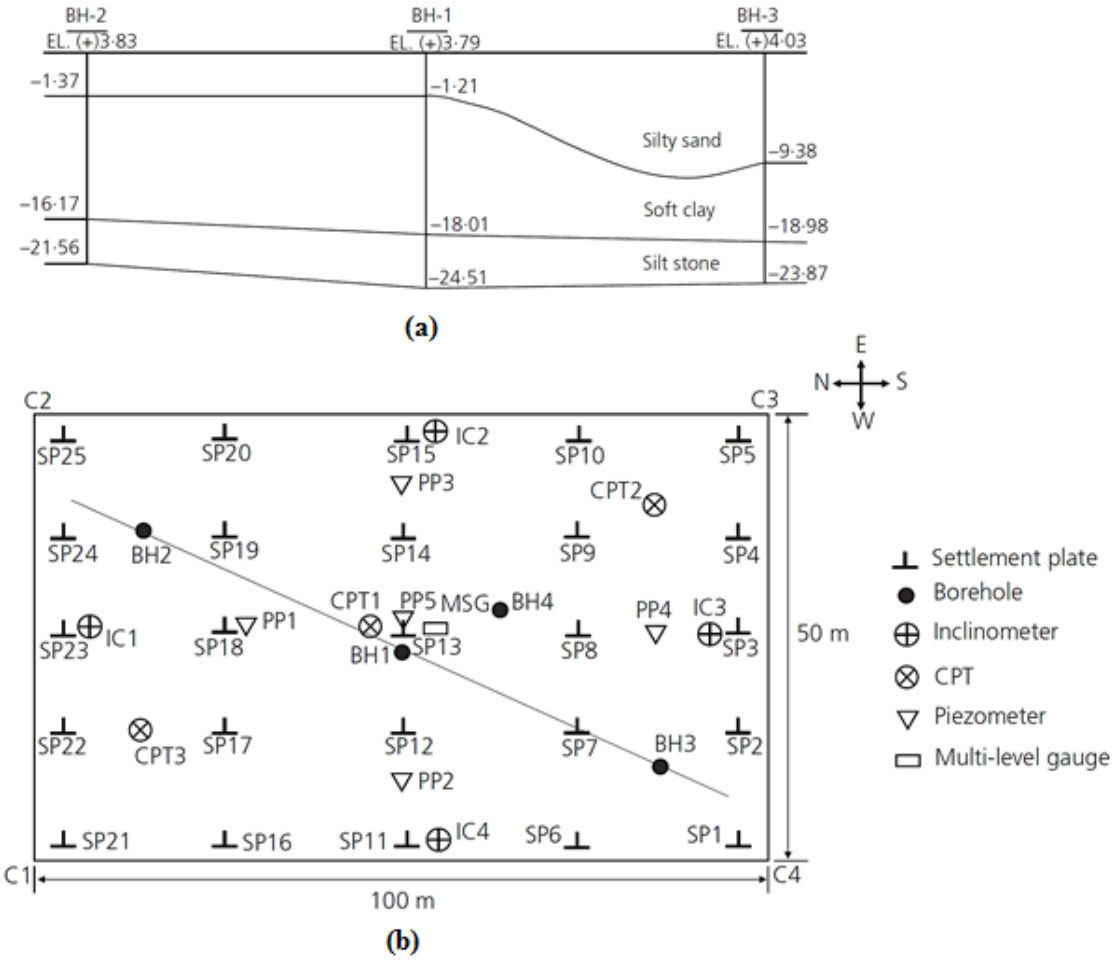

Figure 6-10: Instrumentation of the field trial site: (a) the cross-section; and (b) the plan view (modified from Lam et al. 2018).

Table 6-4: Properties of the unit cell.

Property	Value
PVD Spacing	1 m
PVD installation pattern	Triangular
r_w	0.03 m
r_s	0.12 m
r_e	0.525 m

Table 6-5: Material properties for the FEA.

Material	Depth (m)	M	κ	λ	e_0	γ_{sat}	k (m/s)	OCR
Silty Sand	0 to 5	*E=10,000 ; ν=0.3 ; φ′=32*				17.0	1.2E-08	1.0
Soft Clay	5 to 21	1.113	0.034	0.27	1.9	15.4	3.0E-10	1.0
Silt Stone	21 to 28.3	*E=10,000 ; ν=0.3 ; φ′=32*				15.8	9.3E-08	2.0

The top silty sand layer (as mentioned above) was laid in 2011; however, there was no data to confirm the degree of consolidation that the soft clay layer (lying underneath) had undergone thus far due to this layer. For convenience in modelling, it was assumed that the primary consolidation had finished and thus no EPP exists in the soft clay due to the weight of the top silty layer.

The modified version of AFENA for vacuum consolidation (see description in Chapter 3) was used in the analysis. The EVP model (described in Chapter 3) was used to model the sandwiched soft clay layer.

6.4.2 Vacuum application and embankment construction

Vacuum suction was applied four weeks prior to the commencement of embankment filling. The embankment was raised to 2.5 m in height in 25 days. The density of the filling material was 20 kN/m^3; thus the total stress acted upon the foundation soil was 50 kPa. Vacuum intensity of the same magnitude (–50 kPa) was applied. In the unit cell analysis, stress due to fill material was applied as a traction to the surface of the unit cell, and the vacuum was applied using the method introduced in Chapter 3.

The vacuum pump was not stable between 80–150 days. As mentioned above, the modified AFENA program has the capability to switch vacuum on and off and to adjust the intensity of vacuum as necessary. Thus this capability was used to call the relevant subroutine in the program to switch off (and back on) the vacuum in the respective time period.

The switching on and off of the vacuum pump creates an immediate change in the boundary condition which that can result in numerical instability. To ensure convergence, either very small time steps (0.001 days) or a few iterations using Newton-Rapson method was necessary (see description in Section 6.3).

Another important aspect of the vacuum application was that the CPVDs were installed in such a way that vacuum was applied only to the sandwiched soft clay layer. This was achieved by extending the high-density polyethylene (HDPE) tube connected to the PVD (see Figure 6-9) throughout the topmost sandy layer and stopping the bottom of the PVD at the end of the clay layer. In the FEA, careful steps were undertaken to accurately represent this condition. Simple methods proposed in the literature to model vacuum consolidation such as treating vacuum as equivalent vertical stress or modifying mass permeability of the soil could not be applied in this scenario. Figure 6-11 shows the unit cell, part of the FE mesh (only part was incorporated due to the denseness of the mesh) and its respective boundary conditions that were used to accurately represent the situation.

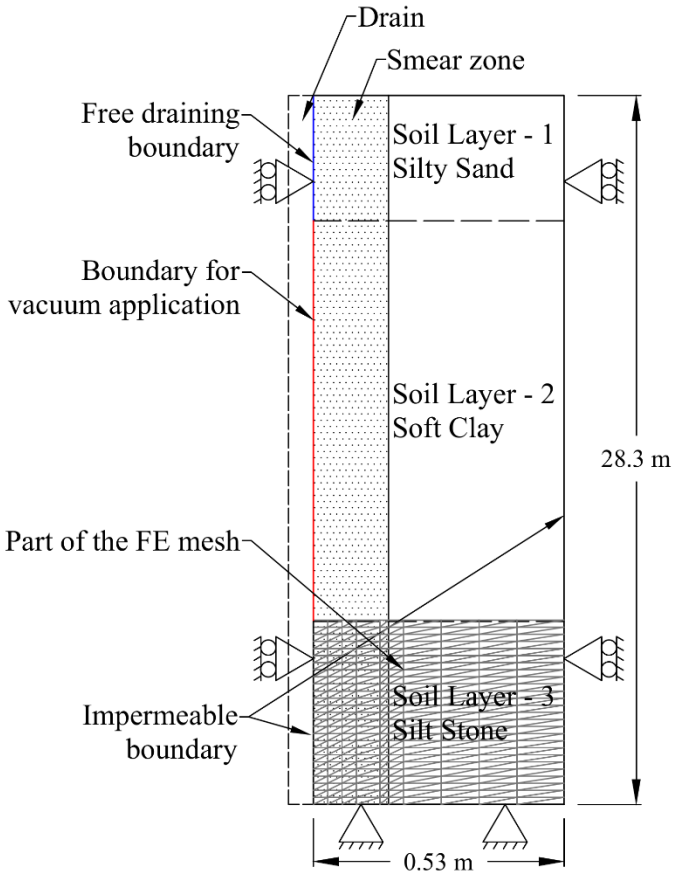

Figure 6-11: Unit cell* with boundary conditions for vacuum application (part of the FE mesh is also shown).

*Not drawn to scale.

6.4.3 Synthesis of FEA results for the case history

Figure 6-12 compares the field data to the FEA predictions of settlement and EPP. The settlement data are from the BH-1 location where the highest clay thickness was found and the EPP data came from PP5 location near the BH-1 location. As Figure 6-12(a) shows, the numerical model appears to capture the soil settlement behaviour well. Notably, the retardation of settlements can be observed from 80–150 days due to the vacuum pump failure. The settlements were accelerated once the vacuum pump is recovered. In the 200–250 days period, the FEA under-predicted the settlements. This

could be due to the unavailability of data concerning the variability of C_{α}. It appears that the C_{α} value assumed for the analysis (of C_{α} = 0.019) was an underestimation of the actual value. This value represents the maximum value of the ratio $C_{\alpha} / C_{c} = 0.04 \pm 0.01$; thus there was no reason to assume a value beyond the proposed range by Mesri and Godlewski (1977) without confirmed field data.

The EPP predictions showed some deviations from the field measurements (see Figure 6-12[b]). The increase in EPP due to embankment construction was not so obvious. This could be due to the high permeable sandy soil layers that exist above and below the soft clay layer. Additionally, there were some fluctuations in the field data around day 170. Reports showed that the area had some rainfall during the ground improvement project, however, data concerning the fluctuations in the water table were not available (Lam et al. 2018) and thus could not be incorporated in the model. This change in the water table could be another reason for the deviation. The increase in EPP due to vacuum pump failure was observed in both in the field data and FEA predictions during 80–150 days.

Given the number of uncertainties and challenges, the settlement and EPP predictions from the FEA using the EVP model appear reasonably good.

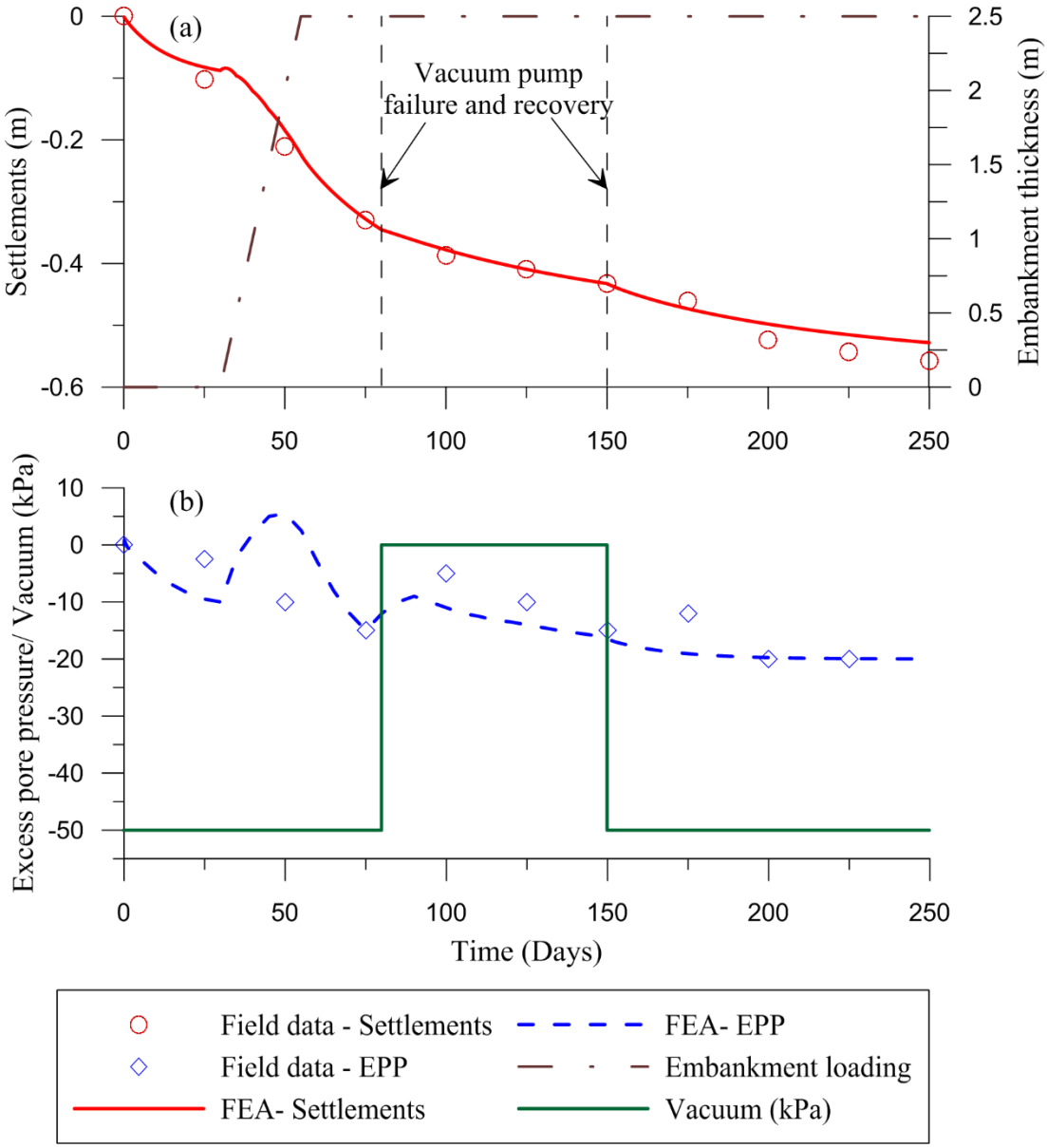

Figure 6-12: Comparison of settlements and EPP[1] with field data.

[1]EPP was measured at PP5 location at -21m depth.

6.5 Summary

In this chapter, the application and removal of vacuum and its effects were discussed. A sensitivity analysis was undertaken to illustrate the effects of vacuum removal time on soft soil deformation. The results for both sensitivity analysis and laboratory experimental data validation showed that the application of vacuum suction until EPP is negative will result in soil re-bounce. The sensitivity analysis also showed that bringing soil to an over-consolidated state drastically reduce long-term creep settlements.

The experimental results of the vacuum application and removal were also validated in this chapter. Solution divergence is a common problem in the removal and re-application of vacuum and surcharge. When the EVP model was applied without any correction, the results deviated greatly from the laboratory data. It was necessary to give careful attention to the time duration where boundary conditions are changed to achieve convergence. Even though the convergence was achieved with reduced time-stepping, it showed that the solution achieved may not necessarily be the solution sought. A solution algorithm with iterations analogous to NRM used and it was shown that the predictions in EPP values were greatly improved with the proposed algorithm. A correction factor was also proposed and validated for soil expansion upon removing surcharge.

Finally, the knowledge acquired from the sensitivity analysis and by validating the experimental laboratory data were applied to a case history. The ground improvement case from Singapore, was an interesting and practical one that included a vacuum pump failure and recovery. Additionally, the CPVDs were used and vacuum was only applied to the sandwiched clay layer. Many uncertainties arose in relation to the field data. For example, C_α was approximated; however, it appears that this value could be higher than

the range proposed by Mesri and Godlewski (1977), but there were no material data to use a higher C_{α}. Apart from disparities in data gathers beyond 200 days, the settlement predictions showed a very good agreement with FEA results. The FEA captures the elevation of EPP upon vacuum pump breakdown very well. Some discrepancies between FEA and field EPP measurements were observed due to groundwater table fluctuations related to rainfall. Overall, despite some limitations in data, a reasonable outcome through FEA was achieved.

In this chapter (and in the previous chapters) the vacuum distribution was assumed to be a constant along with the depth of the PVD; however, in certain field histories, a reduction of vacuum with depth has been reported. The next chapter (Chapter 7) discusses the reduction of vacuum with depth and its implications.

Chapter 7 : Vacuum distribution and its effects[5]

7.1 General

As described in Chapter 2, both membrane and membrane-less methods could be susceptible to air leakages. Thus, vacuum suction may not penetrate equally to the full depth of the PVD. Imperfections in the PVD, power limitations in the vacuum pump or sandwiched sand layers can be main causes for such vacuum losses. Recent developments with geosynthetic technology such as developing CPVDs (Chai 2003, Chai et al. 2008) have allowed vacuum suction to be applied to individual PVDs resulting more effective vacuum application. However, certain percentage of vacuum loss is still inevitable.

Reducing vacuum suction along the depth of PVDs both in laboratory experiments and in field cases have been reported in the literature (e.g. Chai et al. 2006, 2008; Indraratna et al. 2004). This was noted both from low strain rate at deeper depths such as that reported by Indraratna et al. (2012) and inferred from changes of soil index properties after vacuum consolidation (e.g. Chu et al. 2000). Observations such as these made the researchers to study this phenomenon further.

In membrane-less system, vacuum lines are connected to each drain with a cap. This reduces the amount of vacuum loss at the shallow level ensuring the efficiency of the method. Conversely, membrane method relies on the performance of the sealing layer

[5] Material discussed in this chapter form part of the following publications:

Kumarage, P.I., and Gnanendran, C.T. 2018b. Numerical modelling of vacuum suction distribution and its effects in ground improvement with PVD vacuum consolidation. *In* Proceedings of the 11th International Conference on Geosynthetics. Seoul, Korea.

alone to avoid leakages. Hence, apparently it can be argued that membrane method is more susceptible to leakages than the former.

Due to the vacuum loss, a plot of vacuum intensity against the depth of the PVD can have different shapes. In this chapter this shape is referred as 'the shape of the vacuum distribution' or simply 'vacuum distribution'. To date, there is no common agreement in literature to numerical model the vacuum distribution.

The main aims of this chapter are to:

(i) Illustrate different possible vacuum distributions and their implications to settlements and EPP;

(ii) propose a convenient FE implementation to model such vacuum distributions;

(iii) Validate the proposed method against laboratory and field data.

7.2 Modelling the vacuum distribution

Vacuum suction within a unit cell (Figure 7-1[e]) can be generally written as a function of time (t) and depth (z) as in Eqn. (7.1),

$$p_{vac} = p_{v-\max} f(z,t) \tag{7.1}$$

where, p_{vac} is the vacuum suction at a given time and depth, and $p_{v\text{-}max}$ is the maximum vacuum value. The function $f(z,t)$ defines the shape of the vacuum distribution such that multiplication by the $p_{v\text{-}max}$ gives the true distribution. Figure 7-1 shows other possible vacuum distributions such as no vacuum loss (Figure 7-1[c]), and distribution close to elliptical shape (Figure 7-1[a]) when CPVDs (Figure 7-1[d]) are used.

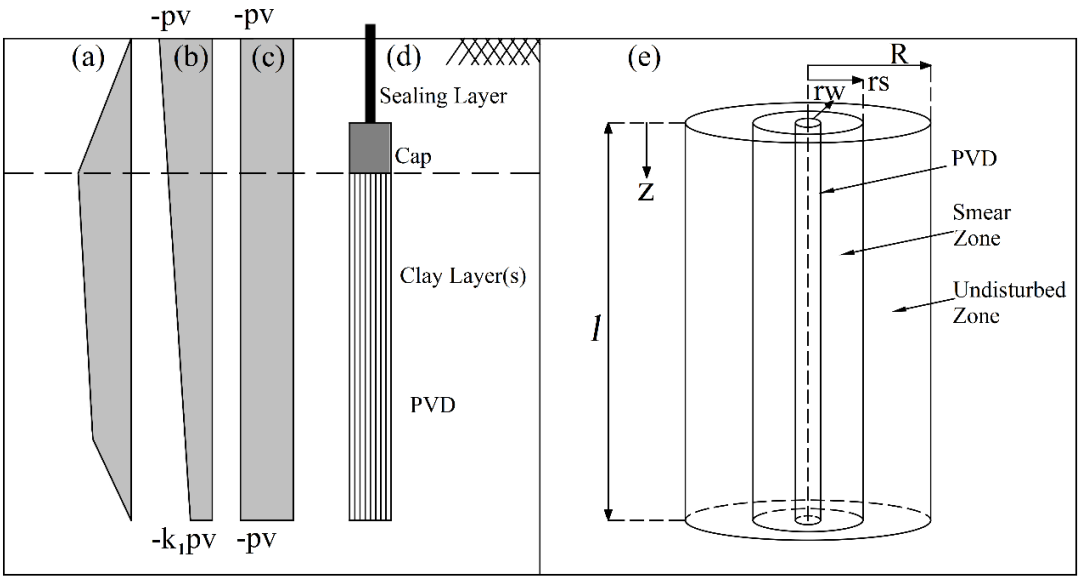

Figure 7-1: Vacuum distributions with depth (a, b, c); PVD with Cap (d); Unit cell (e).

For a liner decay of vacuum loss, at a constant rate of k_1 kPa per meter of depth, Eqn. (7.1) can be specified as in Eqn. (7.2), which is analogous to Indraratna et al. (2005) proposed method of linear decay in vacuum,

$$p_{vac} = p_{v-\max}\left[1-\left(1-k_1\right)\frac{z}{l}\right] \tag{7.2}$$

where, l is the length of the PVD and z is the depth from the ground surface (see Figure 7-1[e]). In FE implementation, the calculated negative values of vacuum suction can be fixed at the boundary of the PVD (i.e. soil PVD interface) as a negative EPP.

Liu et al. (2019) extended the above Eqn. (7.2) by introducing time variable, such that as vacuum pump starts, the intensity of vacuum increase with time as in Eqn. (7.3),

$$p_{vac} = p_{v-\max}\left[1-\left(1-k_1\right)\frac{z}{l}\right]\left(1-e^{-k_2 t}\right) \tag{7.3}$$

where, k_2 is the constant to depict the increase of vacuum with time. However, in actual field projects vacuum distribution may not be linear and the change of the vacuum intensity may not be smooth as an exponential curve, as assumed in Eqn. (7.3).

Conversely, a more practical and convenient method can be proposed as follows. First the vacuum distribution need to be determined either using the field or laboratory data (such as piezometers or pore pressure transducers). In case of a preliminary analysis (or prediction) without vacuum data, a linear, or elliptical assumption can be adopted. Then for the nodes along the PVD soil interface, a link was defined for the respective DOF as in Eqn. (7.4).

$$u_{ij} = f(z) \tag{7.4}$$

where, u_{ij} is the j^{th} DOF of the i^{th} node.

Since the 1st and 2nd DOFs are generally assigned for the horizontal and vertical deformation, 3rd DOF was used in applying Eqn. (7.4), thus j = 3 was adopted. Rather than relying on a predefined vacuum intensity over time, such as Eqn. (7.3), the proposed method can switch 'on', 'off' or vary the vacuum intensity by calling the relevant subroutine. This helps to model practical scenarios such as vacuum pump breakdowns or vacuum termination due to administration reasons. Additionally, the method could be

used either as linear nodal constrain or non-linear nodal constrain as illustrated in following sections.

Firstly, the method is validated against large-scale vacuum consolidation cell experimental results of Geng et al. (2012) performed on the clay from Moruya (300 km South to Sydney, Australia). The experimental procedure and properties of clay from Moruya area used for the experiments have been reported by Indraratna et al. (2004) and Geng et al. (2012). Secondly, a sensitivity analysis is performed with a more general type of vacuum distributions. Finally, the method is applied to a case history with non-linear vacuum distributions.

7.3 Validation against laboratory data

Data from two large-scale vacuum consolidation cell experimental results of Geng et al. (2012) are validated this section and the details of tests are displayed in Table 7-1. Both tests were continued for 40 days. Consolidation cell height was 850 mm with an internal diameter of 450 mm having a PVD installed at the centre through which vacuum was applied. Figure 7-2 illustrates the consolidation cell with the locations of EPP and vacuum measuring locations. Owing to the symmetry, only a half of the cell was modelled as an axisymmetric unit cell. The right-hand side half of the Figure 7-2 was overlapped with the adopted FE mesh. The VSR in SV1 and SV2 are 0.4 and 0.5 respectively; as such, appropriate algorithms were used to avoid numerical instabilities as discussed in Chapter 6.

Table 7-1: Details of experiments.

Test Number	Applied Vacuum suction (kPa)	Applied Surcharge pressure (kPa)	Preconsolidation Pressure (kPa)
SV1	20	30	20
SV2	40	30	20

The vacuum distributions measured in two tests are illustrated in Figure 7-3. This distribution was approximated by a third order polynomial function as in Eqn. (7.5),

$$p_{vac} = a_1 + a_2 h + a_3 h^2 + a_4 h^3 \tag{7.5}$$

where, h is the height of the PVD, a_i are respective constants. In FE implementation, u_{ij} was defined to satisfy the above polynomial function. Dimensions of the FE mesh adopted are R = 225 mm, r_s = 100 mm and l = 850 mm to match the experimental setup (Figure 7-2).

Properties of Moruya clay used for the analysis are displayed in Table 7-2. Basic Cam-clay parameters were adopted from (Indraratna et al. 2005a, Geng et al. 2012) reported values. C_α was assumed as per the ratio C_α/C_c = 0.03.

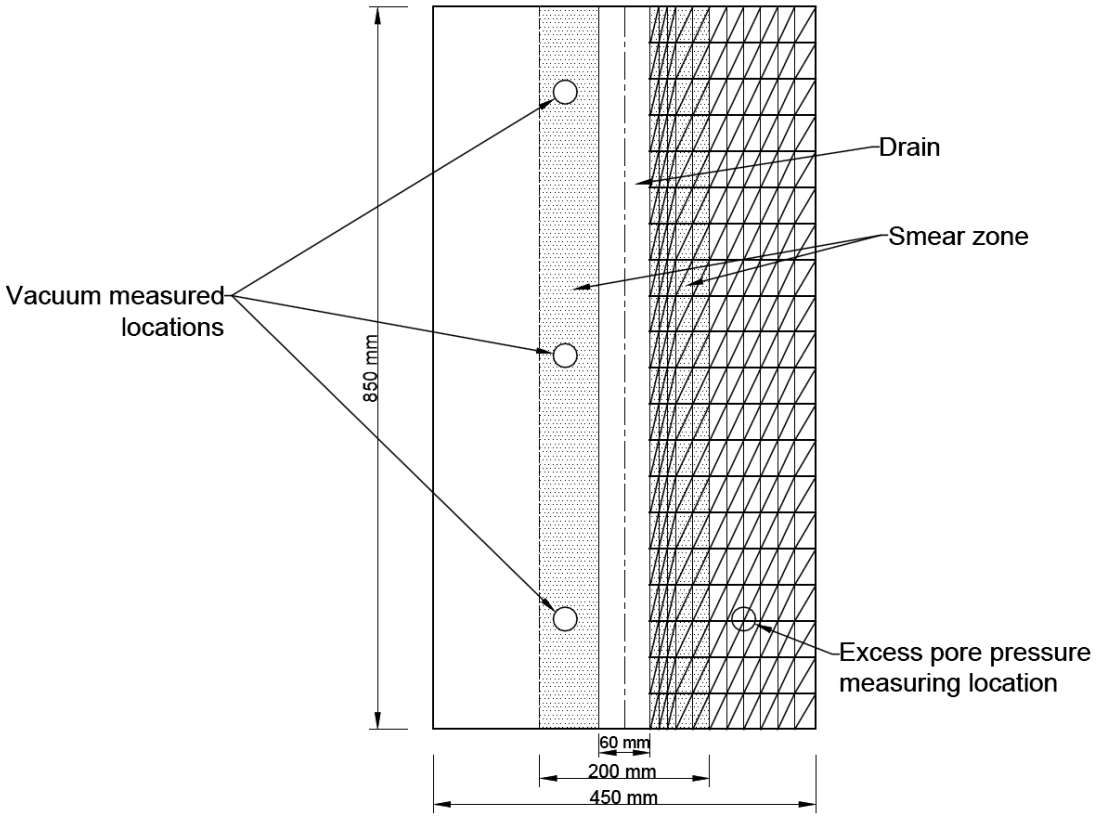

Figure 7-2: Consolidation cell and adopted FE mesh with EPP and vacuum measuring locations (modified from Geng et al. 2012).

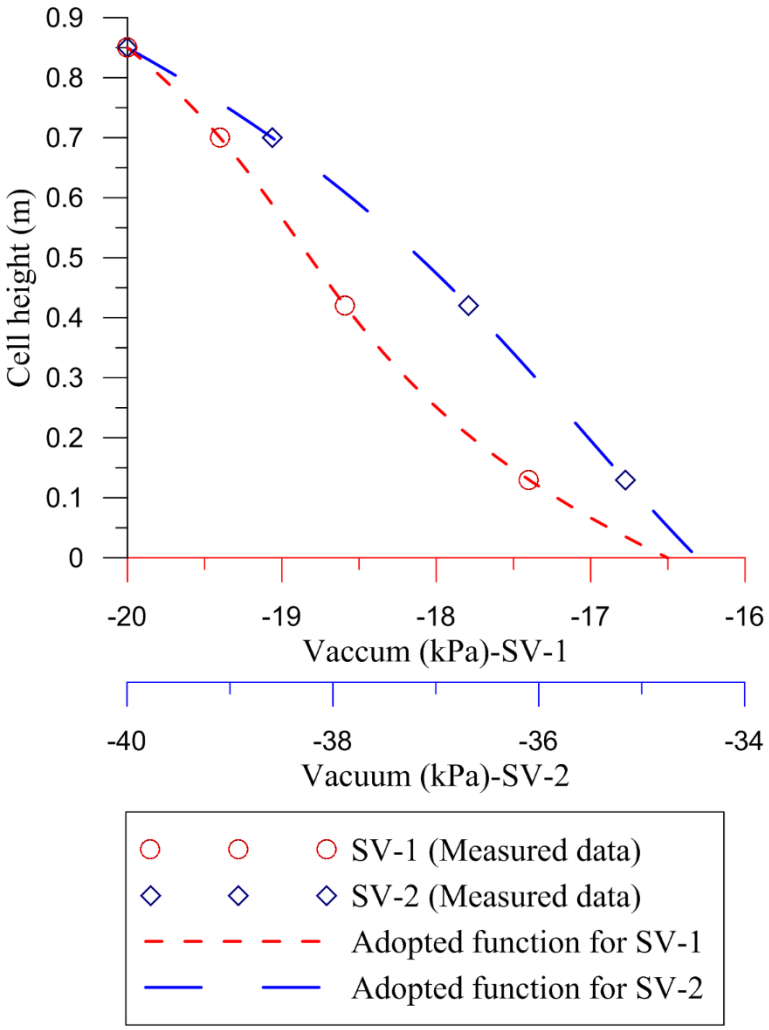

Figure 7-3: Measured (by Geng et al. 2012) and adopted functions (in this study) for vacuum distribution.

Figure 7-4(a) presents the EPP results of the FEA with different vacuum distributions, and Figure 7-4(b) presents the settlement results. The continuous lines corresponds to the actual non-linear vacuum distributions in each SV1 and SV2 tests. Short and long dash lines correspond to the constant maximum and minimum vacuum intensities reported (i.e. –20 kPa and –16.5 kPa for SV1; –40 kPa and –34.5 kPa for SV2). As shown from both Figure 7-4 (a) and (b), for both SV1 and SV2 cases, the FEA model with the actual vacuum distribution has results best match for the experimental data. Constant vacuum with depth, representing higher and lower vacuum intensities have over predicted and under predicted EPP values respectively in both SV1 and SV2 tests.

Table 7-2: Properties of Moruya clay adopted for the FEA.

Parameter	Value
M	1.0358
λ	0.236
κ	0.023
γ_{sat} (kN/m^3)	18.1
e_0	4.0
C_α	0.0163
K_h (m/s)	15.72E-05
p_c' (kPa)	20

It is worth to re-emphasize the importance of time stepping in application of vacuum, for example without vacuum a time step of 0.01 days enough to converge the solution, but in activating vacuum suction this time step will diverge the solution. A time step of 0.001 days was used for convergence.

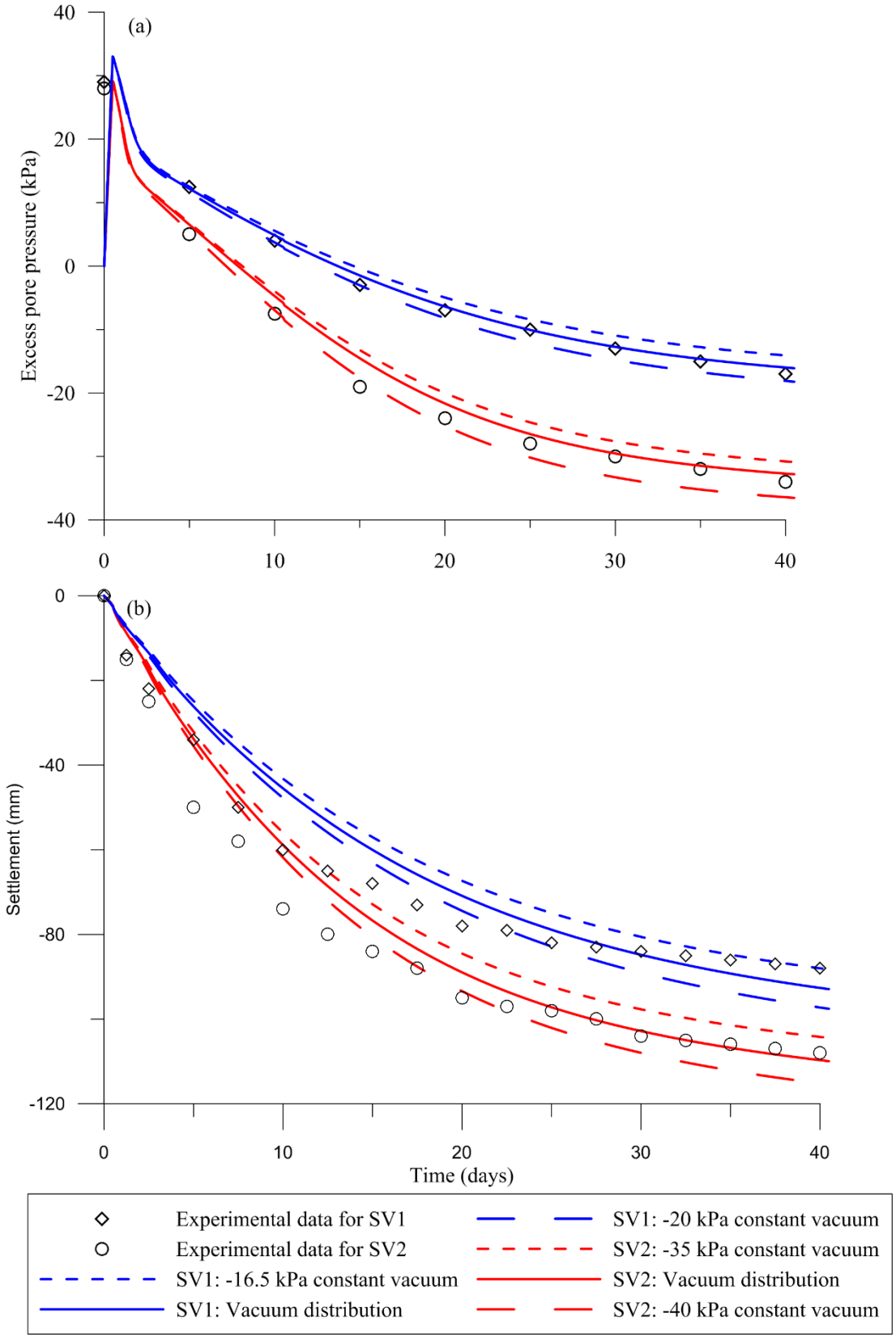

Figure 7-4: Comparison of EPP values from FEA against laboratory data[1].

[1]Laboratory data are from Geng et al. (2012).

7.4 Sensitivity Analysis on vacuum distribution

The effect of the vacuum distribution with depth can be illustrated using a sensitivity analysis. The dimensions of the unit cell was changed to $R = 0.5$ m and $l = 10$ m for convenience (Figure 7-5). Soil parameters adopted are displayed in the Table 7-3. These parameters attribute to the soft soil in Ballina area reported by Pineda et al. (2016).

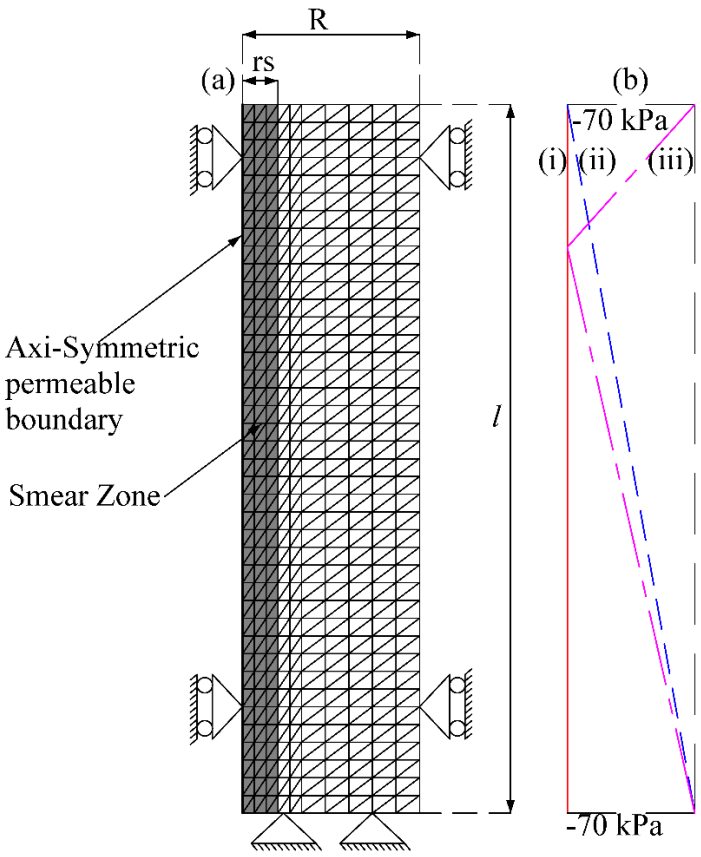

Figure 7-5: (a) The unit cell and (b) different vacuum distributions for the sensitivity analysis.

Table 7-3: Properties of clay adopted for the sensitivity analysis.

Parameter	Value
M	1.515
λ	0.525
κ	0.053
e_0	2.80
C_α	0.057
K_h (m/s)*10^{-10}	9.38
p_c' (kPa)	60

The maximum vacuum applied was –70 kPa and the surcharge applied was 70 kPa. The distributions of applied vacuum in each case are illustrated in Figure 7-5(b) (i), (ii) and (iii). The analysis was carried out for a period of 1,000 days. Apparently, vacuum distribution (i) imposes twice higher vacuum than distribution (ii), which intern results in larger settlement (In this case the ultimate settlement may not be obvious since Ballina clay shows very high compression and creep). However, when comparing the distributions (ii) and (iii), it may not be intuitive to infer which distribution imposes higher vacuum at the soil-PVD interface. In this case, it is more appropriate to integrate the vacuum distribution over the full depth for comparison.

Figure 7-6 shows the settlement response (as strain %) for each vacuum distribution. After 1000 days, distributions (i), (ii) and (iii) have resulted in overall surface strain of 20%, 17.2% and 18.2% respectively. Vacuum distributions (ii) and (iii) have only 1% difference in the surface strain. Whether this is significant or not depends on the total thickness of the clay deposit. Since vacuum assisted PVDs are often used for the stabilisation of thick clay deposits (>10m), this strain can be significant. When comparing

the settlements for the non-vacuum case with the full vacuum (distribution-i) case, the time duration to complete 90% of the primary consolidation with vacuum takes one third of the time of conventional method. This observation agrees with the results of other researchers (e.g. Lam et al. 2015; Saowapakpiboon et al. 2010). However, when long-term effects are considered, the effectiveness of vacuum consolidation is much higher. The reason for the continuous settlements after ~500 days is due to the creep based viscoplastic model used for the sensitivity analysis and the validity of the creep model was discussed in Chapters 3, 4 and 5.

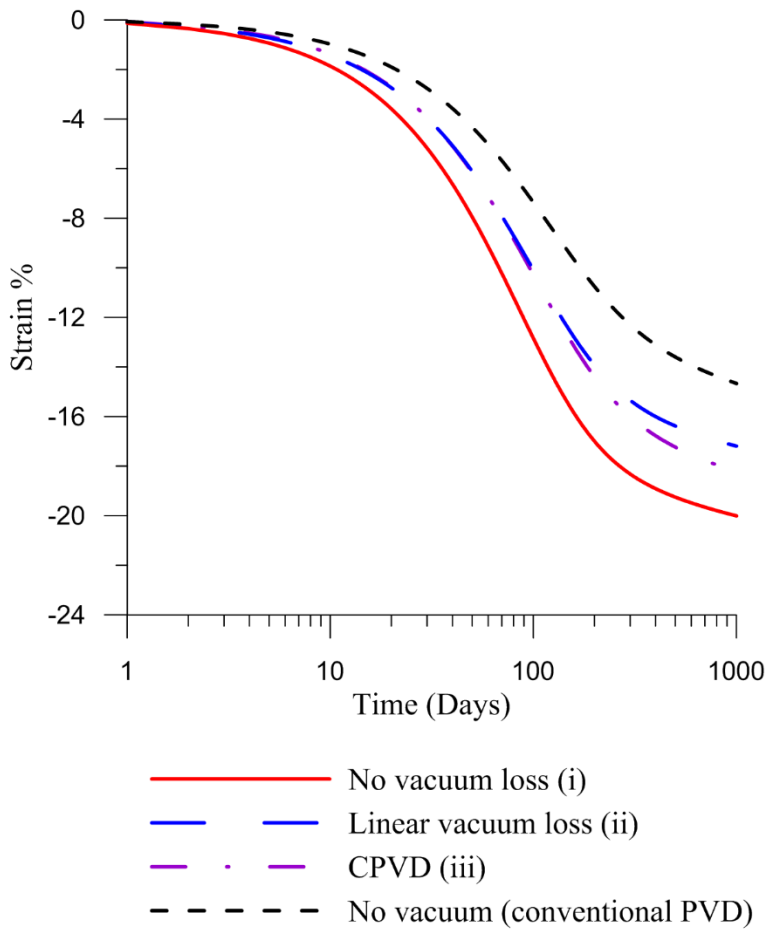

Figure 7-6: Strain percentage with different vacuum distributions (modified from Kumarage and Gnanendran 2018b).

7.5 Analysis of a case history

A vacuum-applied test section of the reclamation project in Tokyo Bay in Japan (Chai et al. 2010) is analysed in this section with the proposed method. A plan view of the area is illustrated in the Figure 7-7. Since both Section A and B are almost identical, only one section (Section A) was studied.

The area has three distinguishable soil layers. The top layer consists of reclaimed clayey silt, with a thickness of 12 m approximately. The second layer is soft clay of about 29 m thickness, which is underlain by a sand layer. Due to the presence of the bottom most sand layer, CPVDs are partially penetrated as shown in the sandwiched clay layer up to 30m depth as shown in Figure 7-7. In the Section A, CPVDs had a cross-section of 150 mm × 3 mm. They had been installed with a spacing of 2.0 m in a square pattern. As such, CPVD properties adopted for the analysis are set out in Table 7-4. Cam-clay equivalent soil parameters were available in literature (Chai et al. 2010). However, to apply the EVP model, C_α had to be assumed as shown in Table 7-5. Permeability values were set by back analysing the period before the vacuum application. These back analysed values were then used for the remaining period with vacuum application.

The analysis was carried out for 400 days. There was a partial self-weight consolidation period of 165 days before vacuum application. During this period, the PVD-soil interface was treated as a simple drained boundary. A vacuum of 80–90 kPa was then applied and kept for 204 days.

7.5.1 Vacuum distribution and boundary conditions

As Figure 7-8 shows, this case history has a unique setup from other cases analysed in this thesis. This uniqueness is brought with a CPVD installed in a two-way drainage system which creates the vacuum distribution and associated boundary conditions complex and interesting.

The ground surface is a drained boundary, thus there exists no EPP or vacuum on the ground surface. Maximum vacuum can be expected at the cap location (where vacuum tube connects) of the PVD. Thereafter, vacuum may reduce with depth depending on the soil strata. Soft clay layer is under laid with a sand layer and this clay-sand interface acts as a drained boundary. Due to the same reason CPVD is partially penetrated to the clay layer to avoid vacuum loss.

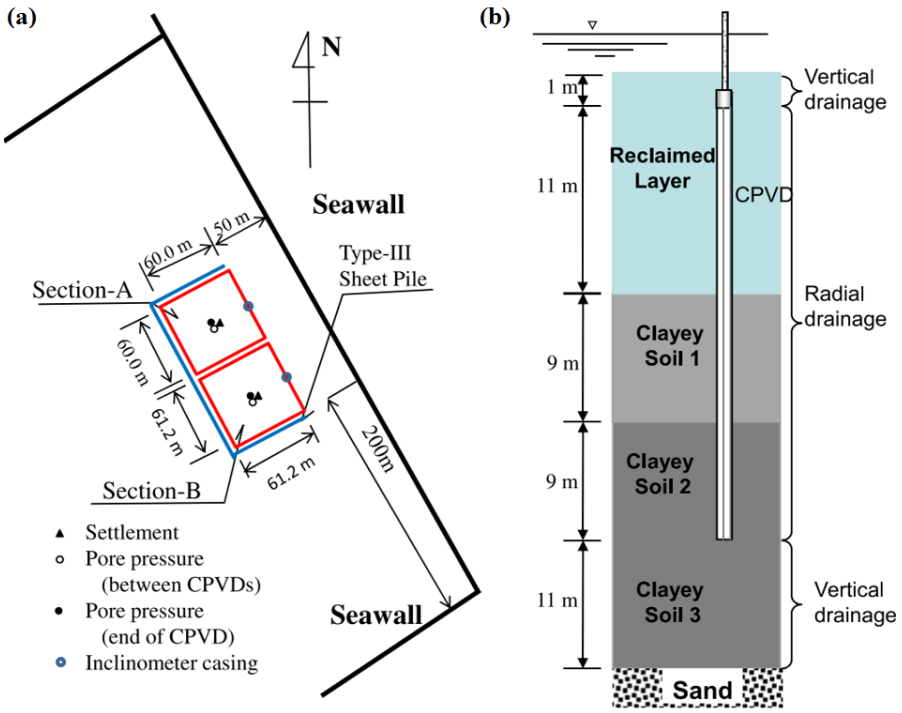

Figure 7-7: (a) Plan view of the site; (b) Soil strata and the CPVD (modified from Chai et al. 2010).

Table 7-4: PVD properties adopted for the case study.

Parameter	Value
r_e (m)	1.13
r_w (m)	0.0375
r_s/r_w	4
k_h/k_s	2

Table 7-5: EVP material parameters adopted for the FE analysis.

Depth (m)	λ	κ	e_0	k_v (m/s)×10^{-9}	[1]C_α
0-12 m	0.382	0.038	2.41	9.48	0.0352
12–21 m	0.477	0.048	3.28	4.56	0.0440
21–41 m	0.651	0.065	3.28	4.56	0.0600

[1]Asssumed based on C_α/C_c = 0.04

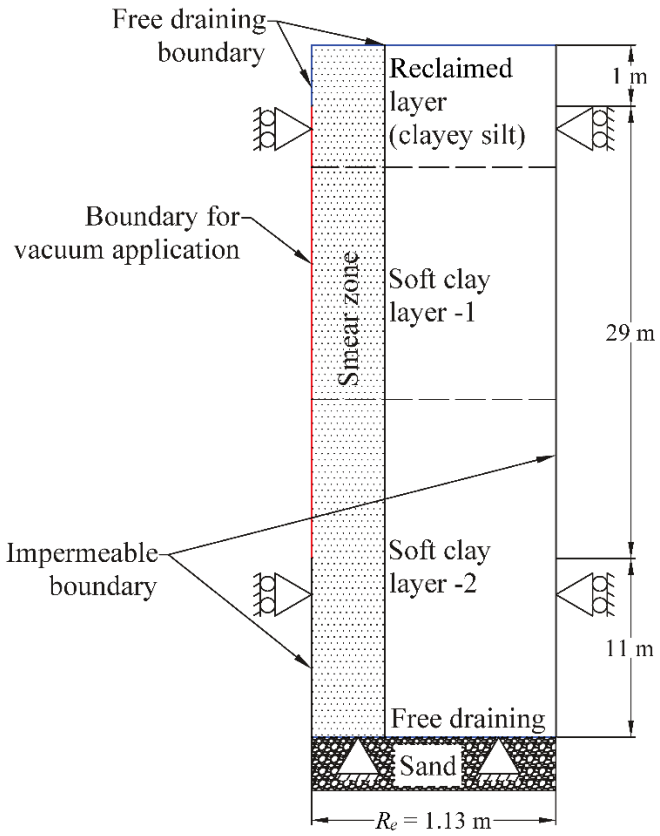

Figure 7-8: CPVD-unit cell with boundary conditions for the case study.

As such, with this setup three scenarios can be adopted to model the vacuum distribution. Firstly, a constant vacuum throughout the length of the PVD would be the simplest approach; secondly, a linear vacuum loss which fully diminishes at the end of the PVD can be assumed. Firstly, a constant vacuum throughout the length of the PVD would be the simplest approach (Case–i); secondly, a linear vacuum loss which fully diminishes at the end of the PVD can be assumed (Case–ii). These two scenarios represent the two extreme ends of the spectrum as maximum and minimum vacuum distributions respectively.

The actual vacuum distribution in a CPVD lies somewhere in between these two extreme cases. A non-linear vacuum distribution can be assumed and such cases are

evident as reviewed in Chapter 2 (Case–iii). Illustration of these three cases are shown in Figure 7-9.

In the Figure 7-9, the maximum vacuum intensity of Case-(iii), reaches not at the PVD cap location, but Δh depth below. To quantify Δh the empirical Eqn. (7.6) proposed by Chai et al. (2010) was used.

$$\Delta h = 1.0\left(\frac{D_e}{1.36}\right)^{1.7}\left(\frac{k_h/k_v}{1.5}\right)^{-0.65}\left(\frac{k_h}{k_s}\right)^{0.45} \tag{7.6}$$

According to the information in Table 7-4, Δh was calculated as 2.69.

7.5.2 Settlement responses of different vacuum distributions

FEA was carried out with each case (Cases–i, ii and iii) and was compared against field data. Firstly, Cases–(i) and (ii) were considered. As shown in Figure 7-10 Case–(i) and (ii) overestimate and underestimate settlements respectively. This suggest that actual vacuum distribution lies somewhere in between these cases. Case – (iii) is a more realistic vacuum distribution when CPVDs are involved. As shown in FEA results this case gave better match for the field data.

However, some over prediction can be observed as the analysis time elapses. This could be due to vacuum loss from the pump to the PVD location. To confirm this, $p_{v\text{-}max}$ at the PVD cap location was reduced to –70 kPa and same pattern for vacuum was adopted

(Case – iv in Figure 7-9). Consequently, Case–(iv) resulted the best match for reported settlement data.

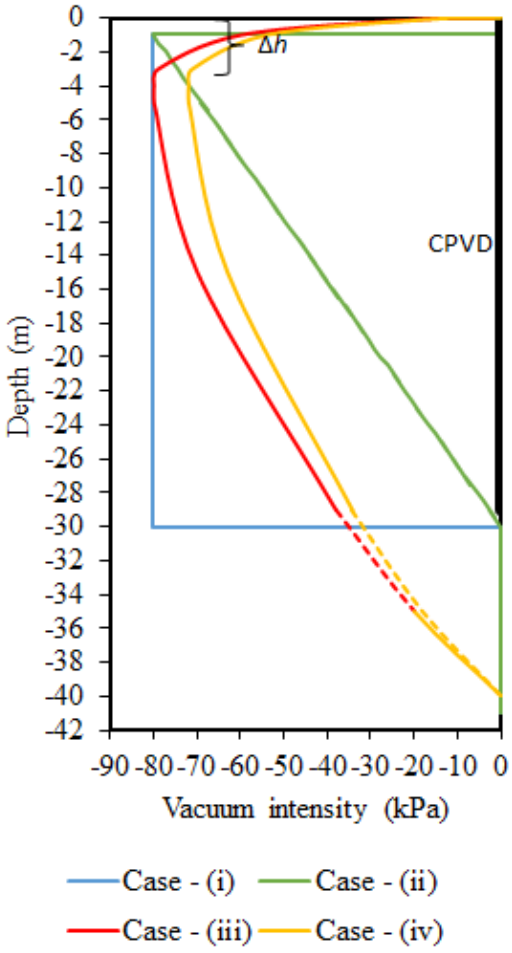

Figure 7-9: Different possible vacuum distributions.

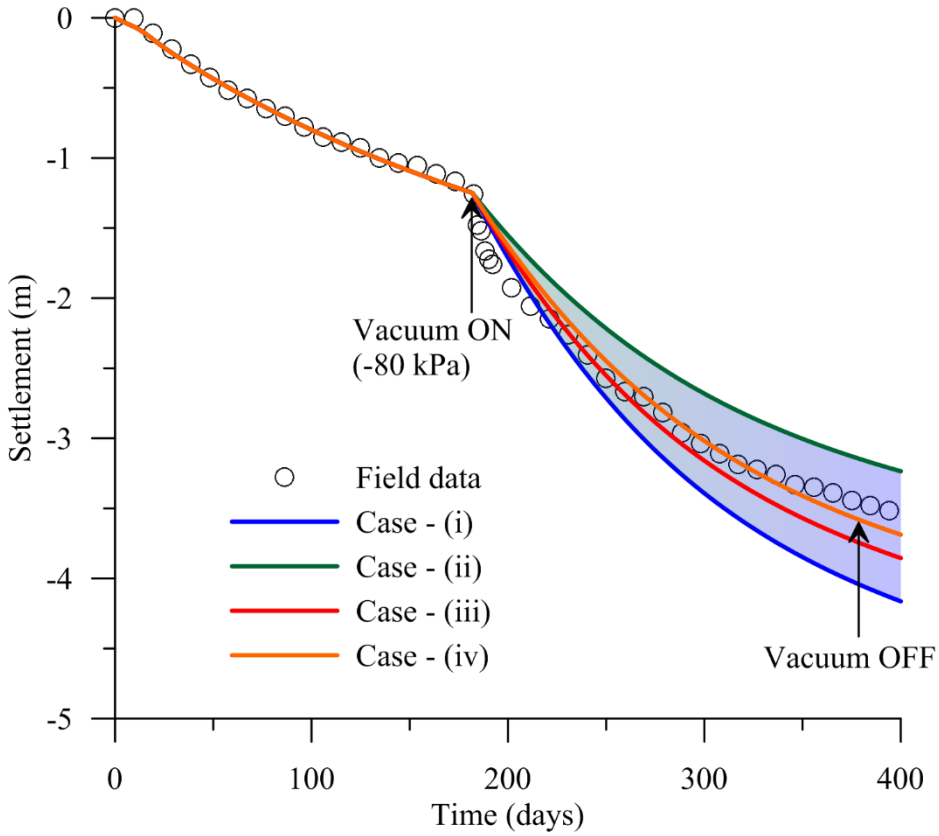

Figure 7-10: Settlement with time from FEA results.

7.6 Summary

Patterns of vacuum suction distribution and their implications on deformational and EPP behaviour (where applicable) were investigated using unit cell analyses in this chapter. It was shown that vacuum suction can be practically of a complex shape than a constant value or a linear reduction. FE modelling of such distributions can be challenging and the methods to perform the same is not consistent in literature. Consequently, the nodal constrain method was proposed in this chapter as a systematic and convenient method to model any complex vacuum distribution. Firstly, FEA was validated using the laboratory experiment data of Geng et al. (2012). Secondly, a sensitivity analysis was carried out with the properties of Ballina clay and the implications on vertical strain of different

assumed (yet realistic) vacuum distributions were illustrated. Finally, the proposed method was applied to a case history to predict the settlements with different vacuum distributions.

In overall, by matching the actual vacuum distribution, the accuracy of FEA predictions can be improved. This was illustrated both in laboratory scale and in the field case as well. However, in the field case, the effect is significant than the former. In the sensitivity analysis, the effect of different vacuum distributions was discussed. When the surface settlement predictions of different vacuum distributions are compared, a maximum of 3% difference in overall strain was observed. In a thick clay deposit, this can be significant. However, the method of modelling vacuum reduction as a constant decay is still acceptable at least for preliminary investigation since the method is very easy to implement and only 1% different in strain was observed, which may not be significant for a shallow deposit or laboratory experiments.

Chapter 8: Summary, conclusions and recommendations

8.1 Summary

This research introduced an EVP model with time-dependent boundary conditions to numerically simulate vacuum-assisted PVDs. As highlighted, vacuum application can be idealised as a boundary value modification, which however may change with time and depth. Since vacuum assisted PVDs are used to improve foundation soils with thick soft clays, a numerical model which account for creep deformations is essential.

First, Chapter 2 presented a comprehensive literature review that identified a clear research gap in the use of EVP models to numerically simulate ground improvements with vacuum-assisted PVDs, despite the rationality behind their use. Although some analytical models are available, their usage is strictly limited to straightforward scenarios, such as those involving a fixed vacuum for the total duration of the analysis. This can be for either constant or linear decay of vacuum distribution and have been developed based on elastic or elasto-plastic models. That said, numerical modelling of most practical possibilities such as variable vacuum intensities over time, vacuum distributions along the depth close to elliptical distributions were not suffitiently explored in the research.

To address the aforementioned research gaps, the time-dependent boundary conditions were introduced to an EVP model in Chapter 3. A non-linear creep function was also used, and its behaviour was illustrated. Biot-type coupled model was implemented in the AFENA (Carter and Balaam 1995) numerical algorithm with a newly written subroutine that can be called to switch ‘on’ and ‘off’ or to change the vacuum intensity. EPP response with time-dependent vacuum applications was also illustrated using the properties of

HKMD clay. Further, the soil responses reported by Saowapakpiboon et al. (2011) were validated using the model and the developed methodology.

In Chapter 4 an axisymmetric unit cell analysis of the Ballina test embankment was performed. FEA results were compared against the reported field data and alongside some previously published results, with the improvements duly highlighted. This chapter specifically addressed the research gaps pointed out by Kelly et al. (2018) on modelling the said embankment behaviour. The 3D creep surface (Chapter 3, Figure 3-2) was reduced to a non-linear creep function by calibrating according to the properties of Ballina clay and its effects within the context of vacuum consolidation were illustrated. The effect of vacuum intensity for this ground-improvement project was also discussed.

PS FEA was subsequently carried out for the Ballina test embankment in Chapter 5. Settlements and EPP were compared with the axisymmetric solution obtained from FEA in Chapter 4. Lateral displacements were evaluated and compared against field data and the effect of unit cell width towards the settlements, EPP and lateral displacements were examined within the context of vacuum consolidation. Furthermore, simple methods to approximately estimate maximum lateral displacements and embankment stability were also carried out and evaluated.

Vacuum application and removal remains an important area of research, with only a few attempts made to gain insight (e.g. Bamunawita 2004, Kianfar et al. 2015). As such, numerical modelling of vacuum application and its removal represent a clear gap in the research and it is filled with the work in this thesis. Laboratory experimental data by Kianfar et al. (2015) was used and FEA carried out. Numerical errors in convergence was

shown. Then, a simple yet effective algorithm was proposed and applied to converge the iteration process to the correct solution. A land reclamation case history in Singapore (Lam et al. 2018) which had a vacuum pump breakdown and recovery was modelled and ground response was validated.

The effects of vacuum distribution were discussed in Chapter 7. Implications of the vacuum distribution were illustrated using a sensitivity analysis. It was also illustrated with published data that vacuum distribution can have complex shapes than a constant value or a linear reduction. Simple but effective FE method was proposed to model the variation of vacuum pressure with depth and validated against previously published laboratory and field data.

8.2 Conclusions

The adopted EVP model combined with time-dependent boundary conditions approach developed in this thesis can successfully model vacuum consolidation and, in particular, lead to better long-term EPP predictions than the FEA results previously reported (e.g. Parsa-Pajouh et al. 2014).

C_α has a significant influence on settlement and EPP predictions even when the vacuum suction prevails. With the work carried out in Chapter 4, it can be concluded that for numerical simulations of long-term analysis (i.e. several years) creep function provides better results than a constant C_α. Although creep models were pointed out as a better option by several previous researchers (e.g. Parsa-Pajouh et al. 2014, Kelly et al. 2018) in modelling vacuum-assisted PVDs, long-term FEA was a research gap exited which has been filled with the research work of this thesis.

A vacuum intensity of |-70 kPa| appears to be the optimum value for the Ballina embankment project. It was identified that increasing the vacuum further has less effects (provided an upper bound of |-90 kPa| for practical reasons) and reducing the value less than |-70 kPa| significantly retard the consolidation process.

In PS conditions with vacuum-assisted PVDs, increasing the unit cell width has almost no influence on settlements. However, EPP and lateral displacements are affected. With regard to vacuum assisted PVDs, very limited reporting has been made on the influence of PS unit cell width. With conventional PVDs (i.e. without vacuum) Karim (2011) has reported some trial and error was necessary to select appropriate PS unit cell width, but did not mention what these trials are for (i.e. whether to match settlements, EPP or lateral displacements), and any rational way of determining the same has not been made clear. As the selected unit cell width is increased in the PS analysis, predicted lateral displacements get reduced and EPP dissipation gets faster.

Removing and reapplication of vacuum had not been adequately understood and modelled previously and this can prove both numerically challenging and often result in convergence issues. It can be concluded that, since vacuum and surcharge are commonly applied together, numerical instability occurs when the fluctuated vacuum intensity is comparatively significant to the latter. This significance can be quantified with the VSR ratio. Vacuum fluctuations with $VSR \geq 0.5$ can lead to numerical instabilities. Several steps were taken to converge the solution to the correct answer, such as reducing the time stepping, introducing iterations (analogous to NRM by regenerating the stiffness matrix) in each time and carrying out boundary modification over a short period than an instant

change. These steps must be carried out in a logical order and such simple yet effective algorithm can solve the convergence issues and significantly increase the accuracy of the FEA predictions.

Constraining the respective DOF of nodes along the boundary, through which vacuum suction is applied can serve as a simple but effective method to model vacuum distribution. Almost all the previous research has limited the modelling of vacuum distribution either to a constant vacuum or a linear reduction along the PVD. With the method illustrated in Chapter 7, any complex vacuum distribution, such as that in Chai et al. (2010) and Chen et al. (2019), can be conveniently modelled. When surface settlements are compared with different vacuum distributions, maximum difference of 3% in vertical strain can result. Hence, whether the effect of vacuum distribution is significant or not largely depends on the total thickness of the soil being treated. For example, considering a 20 m thick foundation, a 3% strain would result up to 0.6 m difference in prediction.

Although it was not the primary objective of this research to delve into optimising time stepping in FEA solution algorithms, it was repeatedly noted that large time steps often diverge the solution in modelling vacuum consolidation (e.g. see Chapters 5, 6 and 7). Since vacuum was modelled as a time-dependent boundary condition in this thesis, proper use of time stepping is essential. Even if a researcher models vacuum as a constant boundary condition, relatively small time steps should be used. It is understood that such words as ‘large’ and ‘small’ are not quantitative but relative. Hence, to ensure the convergence, a good rule of thumb to start with, would be to reduce the time stepping by

10-fold that would be used for a conventional consolidation analysis (i.e. without vacuum) when boundary conditions or vacuum intensities are changed.

8.3 Recommendations for future research

As this thesis covered only a creep-based EVP model, it is recommended that future research carries out numerical analysis with a rate-based EVP model as well. It may be useful to simulate the short-term rate effects of soft clay, even though the long-term would not be very accurate. Certainly, time-dependent boundary conditions must be introduced, and the model should be implemented in a FE program.

As reviewed in Chapter 2, experiments have revealed that C_h in the presence of vacuum is higher than consolidation with PVD alone. Further, upon removal of the vacuum, materials experience a higher OCR than when an equivalent surcharge is solely used. That said, only limited research has been carried out in this regard (e.g. Kianfar et al. 2015), hence more laboratory experiments are recommended to better understand and quantify the effects of OCR with vacuum consolidation.

The duration of most laboratory experiments are limited to the apparent EOP consolidation. In addition, most of them have been carryout with remoulded clay. Thus, vacuum consolidation experiments using undisturbed soil samples beyond the EOP consolidation is necessary to further improve the accuracy of long-term numerical simulations.

Appendices

Appendix–A: Summary of k_h/k_s and r_s/r_w ratios reported in literature

Table A- 1: Summary of k_h/k_s and r_s/r_w ratios reported in literature.

Reference	Reported k_h/k_s ratio
Barron (1948)	3
Hansbo (1981)	3
Hansbo et al. (1981)	2
Bergado et al. (1993)	2 to 10
Hansbo (1997)	4
Chai and Miura (1999)	9 to 10
Sharma and Xiao (2000)	1.3
Hird and Moseley (2000b)	3
Indraratna et al. (2005b)	10
Sathananthan et al. (2008)	1.1 to 1.6
Eriksson et al. (2009)	3
Indraratna et al. (2012a)	2

Table A- 2: Summary of r_s/r_w ratio reported in literature.

Reference	Reported r_s/r_w ratio
Barron (1948)	1.5
Hansbo (1981)	1.5
Hansbo et al. (1981)	2
Bergado et al. (1993)	2
Hansbo (1997)	2
Chai and Miura (1999)	2 to 4
Sharma and Xiao (2000)	4
Hird and Moseley (2000b)	1.5
Indraratna et al. (2005b)	2
Walker and Indraratna (2006)	8.4
Sathananthan et al. (2008)	4 to 6
Eriksson et al. (2009)	2
Indraratna et al. (2012a)	2

Appendix–B: A summary some of the recent vacuum consolidation projects with their salient properties

Table B- 1: A summary some of the recent vacuum consolidation projects with their salient properties.

Title	Location	PVD installation pattern	Drain spacing (m)	Vacuum intensity (kPa)	Reference
Tianjin Port	China	Square	1.0	80	Chu and Yan (Chu and Yan 2005b)
Ballina bypass	Australia	Square	1.2	70	Kelly et al. (2008)
Southern expressway project	Sri Lanka	Square	1.0	50	Karunawardena & Nithiwana (2009)
Suvarnabhumi Airport	Thailand	Triangular	0.85	60	Saowapakpiboon et al. (2010)
Tokyo Bay	Japan	Square	2.0	80–90	Chai et al. (2010)
Port of Brisbane	Australia	Square	1.2	60–75	Indraratna et al. (2011)
Land reclamation site in Tianjin	China	Square	0.8	85–90	Sun et al. (2018)

Land reclamation site in Singapore	Singapore	Triangular	1.0	50	Lam et al. (2018)
The new Mexico International Airport	Mexico	Triangular	1.2	70	López-Acosta et al. (2019)

Appendix–C: Elastic moduli tensor

Elastic moduli tensor

$$C_{ijkl} = \begin{bmatrix} 1/E & -\nu/E & -\nu/E & 0 & 0 & 0 \\ -\nu/E & 1/E & -\nu/E & 0 & 0 & 0 \\ -\nu/E & -\nu/E & 1/E & 0 & 0 & 0 \\ 0 & 0 & 0 & G & 0 & 0 \\ 0 & 0 & 0 & 0 & G & 0 \\ 0 & 0 & 0 & 0 & 0 & G \end{bmatrix}$$

where,

$$E = \frac{3(1-2\nu)(1+e_0)\,p'}{\kappa} \text{ and } G = \frac{E}{2(1+\nu)}$$

References

Abuel-Naga, H., and Bouazza, A. 2009. Equivalent diameter of a prefabricated vertical drain. Geotextiles and Geomembranes, **27**(3): 227–231. doi:10.1016/j.geotexmem.2008.11.006.

Alonso, E.E., Gens, A., and Lloret, A. 2000. Precompression design for secondary settlement reduction. Géotechnique, **50**(6): 645–656. doi:10.1680/geot.2000.50.6.645.

Amavasai, A., Sivasithamparam, N., Dijkstra, J., and Karstunen, M. 2018. Consistent Class A & C predictions of the Ballina test embankment. Computers and Geotechnics, **93**: 75–86. Elsevier Ltd. doi:10.1016/j.compgeo.2017.05.025.

Australian Bureau of Statistics. 2001. Regional Population Growth, Australia and New Zealand, 2001-02, cat. no. 3218.0. Available from https://www.abs.gov.au/Ausstats/abs@.nsf/Previousproducts/1301.0Feature Article32004.

Bamunawita, C. 2004. Soft clay foundation improvement via prefabricated vertical drains and vacuum preloading. University of Wollongong.

Barron, R.A. 1948. Consolidation of fine-grained soils by drain wells. Trans. Am. Soc. Civ. Eng., **113**: 718–742.

Barron, R.A. 1952. Consolidation of clay soil by means of atmospheric pressure. *In* Soil Stabilization Conference. Boston, MA, USA. pp. 258–263.

Bergado, D.., Mukherjee, K., Alfaro, M.., and Balasubramaniam, A.. 1993. Prediction of vertical-band-drain performance by the finite-element method. Geotextiles and Geomembranes, **12**(6): 567–586. doi:10.1016/0266-1144(93)90044-O.

Bjerrum, L. 1967. Engineering Geology of Norwegian Normally-Consolidated Marine

Clays as Related to Settlements of Buildings. Géotechnique, **17**(2): 83–118. Thomas Telford Ltd. doi:10.1680/geot.1967.17.2.83.

Booker, J.R., and Small, J.C. 1975. An investigation of the stability of numerical solutions of Biot's equations of consolidation. International Journal of Solids and Structures, **11**(7–8): 907–917. Pergamon Press. doi:10.1016/0020-7683(75)90013-X.

Britto, A.M., and Gunn, M.J. 1987. Critical State Soil Mechanics via Finite Elements. Ellis Horwood Ltd.

Carter, J.P., and Balaam, N.P. 1995. AFENA User Manual. Version 6.0. Centre for Geotechnical Research University of Sydney,Sydney 2006, Australia.

Chai, J.-C. 2003. Vacuum consolidation of soft clayey subsoil using cap-drain. *In* Proceedings of 18th geosynthetics symposium, vol. 18, Japan Branch. International Geosynthetics Society. pp. 231–236.

Chai, J.-C., Carter, J.P., and Hayashi, S. 2005a. Ground Deformation Induced by Vacuum Consolidation. Journal of Geotechnical and Geoenvironmental Engineering, **131**(12): 1552–1561. doi:10.1061/(ASCE)1090-0241(2005)131:12(1552).

Chai, J.-C., Carter, J.P., and Hayashi, S. 2006. Vacuum consolidation and its combination with embankment loading. Canadian Geotechnical Journal, **43**(10): 985–996. doi:10.1139/t06-056.

Chai, J.-C., Hayashi, S., and Carter, J.P. 2005b. Characteristics of vacumm consolidation. *In* Proceedings of the 16th International Conference on Soil Mechanics and Geotechnical Engineering. Millpress, Osaka, Japan. pp. 1167–1170. doi:10.3233/978-1-61499-656-9-1167.

Chai, J.-C., Hong, Z., and Shen, S. 2010. Vacuum-drain consolidation induced pressure distribution and ground deformation. Geotextiles and Geomembranes, **28**(6): 525–535. Elsevier Ltd. doi:10.1016/j.geotexmem.2010.01.003.

Chai, J.-C., and Miura, N. 1999. Investigation of Factors Affecting Vertical Drain Behavior. Journal of Geotechnical and Geoenvironmental Engineering, **125**(3): 216–226. doi:10.1061/(ASCE)1090-0241(1999)125:3(216).

Chai, J.-C., Miura, N., and Bergado, D.T. 2008. Preloading clayey deposit by vacuum pressure with cap-drain: Analyses versus performance. Geotextiles and Geomembranes, **26**(3): 220–230. doi:10.1016/j.geotexmem.2007.10.004.

Chai, J.-C., Ong, C.Y., Carter, J.P., and Bergado, D.T. 2013. Lateral displacement under combined vacuum pressure and embankment loading. Géotechnique, **63**(10): 842–856. doi:10.1680/geot.12.P.060.

Chai, J.-C., Shen, J.S.-L., Liu, M.D., and Yuan, D.-J. 2018. Predicting the performance of embankments on PVD-improved subsoils. Computers and Geotechnics, **93**: 222–231. Elsevier Ltd. doi:10.1016/j.compgeo.2017.05.018.

Chai, J.-C., Shen, S.-L., Miura, N., and Bergado, D.T. 2001. Simple Method of Modeling PVD-Improved Subsoil. Journal of Geotechnical and Geoenvironmental Engineering, **127**(11): 965–972. doi:10.1061/(ASCE)1090-0241(2001)127:11(965).

Chan, K.F., Poon, B.M., and Perera, D. 2018. Prediction of embankment performance using numerical analyses – Practitioner's approach. Computers and Geotechnics, **93**: 163–177. Elsevier Ltd. doi:10.1016/j.compgeo.2017.07.012.

Chen, L., Gao, Y., Elsayed, A., and Yang, X. 2019. Soil Consolidation and Vacuum Pressure Distribution Under Prefabricated Vertical Drains. Geotechnical and Geological Engineering, **3**. Springer International Publishing. doi:10.1007/s10706-019-00822-3.

Chu, J., and Guo, W. 2016. Land reclamation using clay slurry or in deep water: challenges and solutions. Japanese Geotechnical Society Special Publication, **2**(51): 1790–1793. doi:10.3208/jgssp.TC217-02.

Chu, J., and Yan, S.W. 2005a. Chapter 3 Application of the vacuum preloading method in soil improvement projects. *In* Ground Improvement — Case Histories. pp. 91–117. doi:10.1016/S1571-9960(05)80006-0.

Chu, J., and Yan, S.W. 2005b. Estimation of Degree of Consolidation for Vacuum Preloading Projects. International Journal of Geomechanics, **5**(2): 158–165. doi:10.1061/(ASCE)1532-3641(2005)5:2(158).

Chu, J., Yan, S.W., and Yang, H. 2000. Soil improvement by the vacuum preloading method for an oil storage station. Géotechnique, **50**(6): 625–632. doi:10.1680/geot.2000.50.6.625.

Cognon, J.M., Juran, I., and Thevanayagam, S. 1994. Vacuum consolidation technology - principles and field experience. *In* Geotechnical Special Publication, 40th edition. *Edited by* A.T. Yeung and G.Y. Felio. Publ by ASCE. pp. 1237–1248.

Dafalias, Y.F., and Herrmann, L.R. 1986. Bounding Surface Plasticity. II: Application to Isotropic Cohesive Soils. Journal of Engineering Mechanics, **112**(12): 1263–1291. American Society of Civil Engineers. doi:10.1061/(ASCE)0733-9399(1986)112:12(1263).

Deng, Y., Kan, M.E., Indraratna, B., and Zhong, R. 2017. Finite Element Analysis of Vacuum Consolidation With Modified Compressibility and Permeability Parameters. International Journal of Geosynthetics and Ground Engineering, **3**(2): 15. doi:10.1007/s40891-017-0092-8.

Eriksson, U., Hansbo, S., and Torstensson, B.-A. 2009. Soil improvement at Stockholm-Arlanda Airport. Proceedings of the Institution of Civil Engineers - Ground Improvement, **4**(2): 73–80. doi:10.1680/grim.2000.4.2.73.

Fellenius, B.H., and Castonguay, N.G. 1985. The Efficiency of Band Shaped Drains: a Full Scale Laboratory Study. Report to National Research Council and the Industrial

Research Assistance Programme.

Flodin, N., and Broms, B. 1981. Historical Development of Civil Engineering in Soft Clay. *In* Soft Clay Engineering, Volume 20. *Edited by* E.W. Brand and R.P. Brenner. Elsevier Science. pp. 25–156. doi:10.1016/B978-0-444-41784-8.50004-6.

Fukazawa, E., Yamada, K., and Kurihara, H. 1994. Predicting Long-Term Settlement of Highly Organic Soil Ground Improved by Preloading. Doboku Gakkai Ronbunshu, **493**(493): 59–68. doi:10.2208/jscej.1994.493_59.

Gao, Y., Zhu, H., and Yang, X. 2006. Application of a Relationship between C a and OCR* in 1-D Compression Analysis for Clays. *In* Soil and Rock Behavior and Modeling. American Society of Civil Engineers, Reston, VA. pp. 42–47. doi:10.1061/40862(194)4.

Geng, X., Indraratna, B., and Rujikiatkamjorn, C. 2012. Analytical Solutions for a Single Vertical Drain with Vacuum and Time-Dependent Surcharge Preloading in Membrane and Membraneless Systems. International Journal of Geomechanics, **12**(1): 27–42. doi:10.1061/(ASCE)GM.1943-5622.0000106.

Gnanendran, C.T., Manivannan, G., and Lo, S.-C. 2006. Influence of using a creep, rate, or an elastoplastic model for predicting the behaviour of embankments on soft soils. Canadian Geotechnical Journal, **43**(2): 134–154. doi:10.1139/t05-090.

Gong, Y., and Chok, Y.H. 2018. Predicted and measured behaviour of a test embankment on Ballina clay. Computers and Geotechnics, **93**: 178–190. Elsevier Ltd. doi:10.1016/j.compgeo.2017.06.003.

Hansbo, S. 1979. Consolidation of clay by band-shaped prefabricated drains. Ground Engineering, **12**(5): 16–25.

Hansbo, S. 1981. Consolidation of Fine-grained Soils by Prefabricated Drains. *In* Proceedings of the International Conference on Soil Mechanics and Foundation

Engineering. Stockholm.

Hansbo, S. 1997. Practical aspects of vertical drain design. *In* 14th international conference on soil mechanics and foundation engineering. Hamburg. pp. 1749–1752.

Hansbo, S., Jamiolkowski, M., and Kok, L. 1981. Consolidation by vertical drains. Geotechnique, **31**(1): 45–66.

Higgins, B. 2016. History along the Pacific Highway and decision making. *In* Embankment Prediction Symposium. Newcastle.

Hird, C.C., and Moseley, V.J. 2000a. Model study of seepage in smear zones around vertical drains in layered soil. Géotechnique, **50**(1): 89–97. doi:10.1680/geot.2000.50.1.89.

Hird, C.C., and Moseley, V.J. 2000b. Model study of seepage in smear zones around vertical drains in layered soil. Géotechnique, **50**(1): 89–97. doi:10.1680/geot.2000.50.1.89.

Hird, C.C., Pyrah, I.C., and Russel, D. 1992. Finite element modelling of vertical drains beneath embankments on soft ground. Géotechnique, **42**(3): 499–511. doi:10.1680/geot.1992.42.3.499.

Holtz, R.D., Jamiolkowski, M.B., Lancellotta, R., and Pedroni, R. 1991. Prefabricated vertical drains: design and performance.

Hu, Y.-Y., Zhou, W.-H., and Cai, Y.-Q. 2014. Large-strain elastic viscoplastic consolidation analysis of very soft clay layers with vertical drains under preloading. Canadian Geotechnical Journal, **51**(2): 144–157. doi:10.1139/cgj-2013-0200.

Huang, C., Deng, Y., and Chen, F. 2016. Consolidation theory for prefabricated vertical drains with elliptic cylindrical assumption. Computers and Geotechnics, **77**: 156–166. Elsevier Ltd. doi:10.1016/j.compgeo.2016.04.015.

Indraratna, B., Bamunawita, C., and Khabbaz, H. 2004. Numerical modeling of vacuum preloading and field applications. Canadian Geotechnical Journal, **41**(6): 1098–1110. doi:10.1139/t04-054.

Indraratna, B., Baral, P., Rujikiatkamjorn, C., and Perera, D. 2018a. Class A and C predictions for Ballina trial embankment with vertical drains using standard test data from industry and large diameter test specimens. Computers and Geotechnics, **93**: 232–246. Elsevier Ltd. doi:10.1016/j.compgeo.2017.06.013.

Indraratna, B., Baral, P., Rujikiatkamjorn, C., and Perera, D. 2018b. Class A and C predictions for Ballina trial embankment with vertical drains using standard test data from industry and large diameter test specimens. Computers and Geotechnics, **93**: 232–246. Elsevier Ltd. doi:10.1016/j.compgeo.2017.06.013.

Indraratna, B., Kianfar, K., and Rujikiatkamjorn, C. 2013. Laboratory Evaluation of Coefficient of Radial Consolidation Based on Pore-Water-Pressure Dissipation and Settlement. Geotechnical Testing Journal, **36**(1): 20120032. doi:10.1520/GTJ20120032.

Indraratna, B., and Redana, I.W. 2000. Numerical modeling of vertical drains with smear and well resistance installed in soft clay. Canadian Geotechnical Journal, **37**(1): 132–145. doi:10.1139/t99-115.

Indraratna, B., Rujikiatkamjorn, C., Ameratunga, J., and Boyle, P. 2011. Performance and Prediction of Vacuum Combined Surcharge Consolidation at Port of Brisbane. Journal of Geotechnical and Geoenvironmental Engineering, **137**(11): 1009–1018. doi:10.1061/(ASCE)GT.1943-5606.0000519.

Indraratna, B., Rujikiatkamjorn, C., Balasubramaniam, A.S., and McIntosh, G. 2012a. Soft ground improvement via vertical drains and vacuum assisted preloading. Geotextiles and Geomembranes, **30**: 16–23. Elsevier Ltd.

doi:10.1016/j.geotexmem.2011.01.004.

Indraratna, B., Rujikiatkamjorn, C., Kelly, R., and Buys, H. 2012b. Soft soil foundation improved by vacuum and surcharge loading. Proceedings of the Institution of Civil Engineers - Ground Improvement, **165**(2): 87–96. doi:10.1680/grim.10.00032.

Indraratna, B., Rujikiatkamjorn, C., and Sathananthan, I. 2005a. Analytical and numerical solutions for a single vertical drain including the effects of vacuum preloading. Canadian Geotechnical Journal, **42**(4): 994–1014. doi:10.1139/t05-029.

Indraratna, B., Sathananthan, I., Rujikiatkamjorn, C., and Balasubramaniam, A.S. 2005b. Analytical and Numerical Modeling of Soft Soil Stabilized by Prefabricated Vertical Drains Incorporating Vacuum Preloading. International Journal of Geomechanics, **5**(2): 114–124. doi:10.1061/(ASCE)1532-3641(2005)5:2(114).

Islam, M.N. 2014. Associated and non-associated flow rule based elastic-viscoplastic models for soft clays. UNSW Canberra.

Islam, M.N., and Gnanendran, C.T. 2017. Elastic-Viscoplastic Model for Clays: Development, Validation, and Application. Journal of Engineering Mechanics, **143**(10): 04017121. doi:10.1061/(ASCE)EM.1943-7889.0001345.

Janbu, N. 1963. Soil Compressibility as Determined by Oedometer and Triaxial Tests. European Conference on Soil Mechanics & Foundation Engineering, **1**: 19–25.

Kabbaj, M., Tavenas, F., and Leroueil, S. 1988. In situ and laboratory stress–strain relationships. Géotechnique, **38**(1): 83–100. doi:10.1680/geot.1988.38.1.83.

Karim, M.R. 2011. Modeling the long term behaviour of soft soils. The University of New South Wales.

Karim, M.R., Gnanendran, C.T., Lo, S.-C.R., and Mak, J. 2010. Predicting the long-term performance of a wide embankment on soft soil using an elastic–viscoplastic model. Canadian Geotechnical Journal, **47**(2): 244–257. doi:10.1139/T09-087.

Karim, M.R., Manivannan, G., Gnanendran, C.T., and Lo, S.-C.R. 2011. Predicting the long-term performance of a geogrid-reinforced embankment on soft soil using two-dimensional finite element analysis. Canadian Geotechnical Journal, **48**(5): 741–753. doi:10.1139/t10-104.

Karunawardena, A., and Nithiwana, W. 2009. Construction of a trial emnbankment on peaty ground using vacuum consolidation method for a highway construction project in Sri Lanka. *In* Proceedings of the 17th International Conference on Soil Mechanics and Geotechnical Engineering. pp. 2200–2203.

Kelly, R., Small, J., and Wong, P. 2008. Construction of an Embankment Using Vacuum Consolidation and Surcharge Fill. *In* GeoCongress 2008. American Society of Civil Engineers, Reston, VA. pp. 578–585. doi:10.1061/40971(310)72.

Kelly, R.B., Sloan, S.W., Pineda, J.A., Kouretzis, G., and Huang, J. 2018. Outcomes of the Newcastle symposium for the prediction of embankment behaviour on soft soil. Computers and Geotechnics, **93**: 9–41. Elsevier Ltd. doi:10.1016/j.compgeo.2017.08.005.

Kelly, R.B., and Wong, P.K. 2009. An embankment constructed using vacuum consolidation. Australian Geomechanics, **44**(2): 55–64.

Khan, A.Q. 2010. Ground improvement using vacuum preloading together with prefabricated vertical drains. University of Illinois at Urbana-Champaign, IL, USA.

Kianfar, K. 2013. Implications of PVD and vacuum preloading on viscoplastic behaviour of soft soils. University of Wollongong.

Kianfar, K., Indraratna, B., and Rujikiatkamjorn, C. 2013. Radial consolidation model incorporating the effects of vacuum preloading and non-Darcian flow. Géotechnique, **63**(12): 1060–1073. doi:10.1680/geot.12.P.163.

Kianfar, K., Indraratna, B., Rujikiatkamjorn, C., and Leroueil, S. 2015. Radial

consolidation response upon the application and removal of vacuum and fill loading. Canadian Geotechnical Journal, **52**(12): 2156–2162. doi:10.1139/cgj-2014-0511.

Kjellman, W. 1952. Consolidation of Clayey Soils by Atmospheric Pressure. *In* Proceedings of a Conference on Soil Stabilization. Massachusetts Institute of Technology, Boston. pp. 258–263.

Kosaka, T., Hayashi, H., Kawaida, M., and Teerachaikulpanich, N. 2016. Performance of vacuum consolidation for reducing a long-term settlement. Japanese Geotechnical Society Special Publication, **2**(59): 2015–2020. doi:10.3208/jgssp.JPN-068.

Kumarage, P.I., and Gnanendran, C.T. 2017. Viscoplastic behaviour of soft soil in vacuum consolidation. *In* Proceedings of the 70th Canadian Geotechnical Conference. Canadian Geotechnical Society (CGS), Ottawa, Canada.

Kumarage, P.I., and Gnanendran, C.T. 2018a. Creep based viscoplastic numerical modelling of soil deformations in vacuum application and removal. *In* Proceedings of the 71st Canadian Geotechnical Conference. Edmonton, AB, Canada.

Kumarage, P.I., and Gnanendran, C.T. 2018b. Numerical modelling of vacuum suction distribution and its effects in ground improvement with PVD vacuum consolidation. *In* Proceedings of the 11th International Conference on Geosynthetics. Seoul, Korea.

Kumarage, P.I., and Gnanendran, C.T. 2019a. Plane strain viscoplastic modelling in vacuum consolidation. *In* Proceedings of the 17th African Regional Conference on Soil Mechanics and Geotechnical Engineering. Cape Town, South Africa.

Kumarage, P.I., and Gnanendran, C.T. 2019b. Long-term performance predictions in ground improvements with vacuum assisted Prefabricated Vertical Drains. Geotextiles and Geomembranes, **47**(2): 95–103. Elsevier. doi:10.1016/j.geotexmem.2018.11.002.

Kutter, B.L., and Sathialingam, N. 1992. Elastic-viscoplastic modelling of the rate-

dependent behaviour of clays. Géotechnique, **42**(3): 427–441. doi:10.1680/geot.1992.42.3.427.

Ladd, C.C. 1991. Stability Evaluation during Staged Construction. Journal of Geotechnical Engineering, **117**(4): 540–615. doi:10.1061/(ASCE)0733-9410(1991)117:4(540).

Lam, K.P., Wu, S., and Chu, J. 2018. Field trial of a membraneless vacuum preloading system for soft soil improvement. Proceedings of the Institution of Civil Engineers - Ground Improvement, (2012): 1–11. doi:10.1680/jgrim.17.00081.

Lam, L.G., Bergado, D.T., and Hino, T. 2015. PVD improvement of soft Bangkok clay with and without vacuum preloading using analytical and numerical analyses. Geotextiles and Geomembranes, **43**(6): 547–557. Elsevier Ltd. doi:10.1016/j.geotexmem.2015.07.013.

Leong, E.C., Soemitro, R. a. a., and Rahardjo, H. 2000. Soil improvement by surcharge and vacuum preloadings. Géotechnique, **50**(5): 601–605. doi:10.1680/geot.2000.50.5.601.

Lin, D.G., Kim, H.K., and Balasubramaniam, A.S. 2000. Numerical modeling of prefabricated vertical drain. Geotechnical Engineering, **31**(2): 109–125. School of Civil Engineering, Asian Institute of Tech., P.O. Box 4, Klong Luang, Pathumthani 12120, Thailand. Available from https://www.scopus.com/inward/record.uri?eid=2-s2.0-7044286544&partnerID=40&md5=bf8a21bc2654b4d788a3858f5d3f139a.

Liu, S., Geng, X., Sun, H., Cai, Y., Pan, X., and Shi, L. 2019. Nonlinear consolidation of vertical drains with coupled radial-vertical flow considering time and depth dependent vacuum pressure. International Journal for Numerical and Analytical Methods in Geomechanics, **43**(4): 767–780. doi:10.1002/nag.2888.

Long, R.P., and Covo, A. 1994. Equivalent Diameter of Vertical Drains with an Oblong

Cross Section. Journal of Geotechnical Engineering, **120**(9): 1625–1630. Univ. of Connecticut, Storrs, CT, 06269-3037, United States. doi:10.1061/(ASCE)0733-9410(1994)120:9(1625).

López-Acosta, N.P., Espinosa-Santiago, A.L., Pineda-Núñez, V.M., Ossa, A., Mendoza, M.J., Ovando-Shelley, E., and Botero, E. 2019. Performance of a test embankment on very soft clayey soil improved with drain-to-drain vacuum preloading technology. Geotextiles and Geomembranes, (xxxx): 103459. Elsevier. doi:10.1016/j.geotexmem.2019.103459.

Mesri, G., and Godlewski, P.M. 1977. Time and stress compressibility interrelationship. Journal of the Geotechnical Engineering Division, ASCE, **103**(5): 417–430.

Mesri, G., and Khan, A.Q. 2012. Ground Improvement Using Vacuum Loading Together with Vertical Drains. Journal of Geotechnical and Geoenvironmental Engineering, **138**(6): 680–689. doi:10.1061/(ASCE)GT.1943-5606.0000640.

Mesri, G., Stark, T.D., Ajlouni, M.A., and Chen, C.S. 1997. Secondary compression of peat with or without surcharging. Journal of Geotechnical and Geoenvironmental Engineering, **123**(5): 411–421.

Mohamedelhassan, E., and Shang, J.Q. 2002. Vacuum and surcharge combined one-dimensional consolidation of clay soils. Canadian Geotechnical Journal, **39**(5): 1126–1138. doi:10.1139/t02-052.

Müthing, N., Zhao, C., Hölter, R., and Schanz, T. 2018. Settlement prediction for an embankment on soft clay. Computers and Geotechnics, **93**: 87–103. doi:10.1016/j.compgeo.2017.06.002.

Nash, D.F.T. 2001. Discussion: Precompression design for secondary settlement reduction. Géotechnique, **51**(9): 822–826. doi:10.1680/geot.2001.51.9.822.

Nguyen, M.D., Van Le, D., and Pham, B.T. 2017. Prediction of lateral displacement of

ground improved by mernard vacuum consolidation method based on characteristics of soft soil and settlement observation results. International Journal of Civil Engineering and Technology, **8**(11): 526–535.

Parsa-Pajouh, A., Fatahi, B., Vincent, P., and Khabbaz, H. 2014. Trial Embankment Analysis to Predict Smear Zone Characteristics Induced by Prefabricated Vertical Drain Installation. Geotechnical and Geological Engineering, **32**(5): 1187–1210. doi:10.1007/s10706-014-9789-9.

Perzyna, P. 1963. Constitutive equations for rate-sensitive plastic materials. Quarterly of Applied Mathematics, **20**: 321–331.

Pineda, J.A., Suwal, L.P., Kelly, R.B., Bates, L., and Sloan, S.W. 2016. Characterisation of Ballina clay. Géotechnique, **66**(7): 556–577. doi:10.1680/jgeot.15.P.181.

PLAXIS. 2016. Modelling technique: Vacuum consolidation. Available from https://www.plaxis.com/support/tips-and-tricks/modelling-technique-vacuum-consolidation/.

Poulos, H.G., and Davis, E.H. 1974. Elastic Solutions for Soil and Rock Mechanics. Centre for geotechnical research University of Sydney.

Pradhan, T.B.S., Imal, G., Murata, T., Kamon, M., and Suwa, S. 1993. Experiment study on the equivalent diameter of a prefabricated band-shaped drain. *In* Proceedings of the 11th Southeast Asian Geotechnical Conference. pp. 391–396.

Rezania, M., Bagheri, M., Mousavi Nezhad, M., and Sivasithamparam, N. 2017. Creep analysis of an earth embankment on soft soil deposit with and without PVD improvement. Geotextiles and Geomembranes, **45**(5): 537–547. Elsevier Ltd. doi:10.1016/j.geotexmem.2017.07.004.

Rixner, J.J., Kraemer, S.R., and Smith, A.D. 1986. Prefabricated vertical drains. Vol. II: Summary of research effort — final report. *Edited By*H.& Aldrich. Available from

https://rosap.ntl.bts.gov/view/dot/25323.

Robinson, R.G., Indraratna, B., and Rujikiatkamjorn, C. 2012. Final state of soils under vacuum preloading. Canadian Geotechnical Journal, **49**(6): 729–739. doi:10.1139/t2012-024.

Roscoe, K.H., and Burland, J.B. 1968. On the generalized stress-strain behaviour of 'wet' clay. *In* Engineering Plasticity. *Edited by* J. Heyman and F.. Leckie. Cambridge University Press, Cambridge. pp. 535–609.

Roscoe, K.H., and Schofield, A.N. 1963. Mechanical behavior of an idealised 'wet clay.' *In* European Conference of Soil Mechanics and Foundation Engineering. Wiesbaden. pp. 47–54.

Rowe, R.K., and Li, a. L. 2002. Behaviour of reinforced embankments on soft rate-sensitive soils. Géotechnique, **52**(1): 29–40. doi:10.1680/geot.2002.52.1.29.

Saowapakpiboon, J., Bergado, D.T., Voottipruex, P., Lam, L.G., and Nakakuma, K. 2011. PVD improvement combined with surcharge and vacuum preloading including simulations. Geotextiles and Geomembranes, **29**(1): 74–82. Elsevier Ltd. doi:10.1016/j.geotexmem.2010.06.008.

Saowapakpiboon, J., Bergado, D.T., Youwai, S., Chai, J.-C., Wanthong, P., and Voottipruex, P. 2010. Measured and predicted performance of prefabricated vertical drains (PVDs) with and without vacuum preloading. Geotextiles and Geomembranes, **28**(1): 1–11. Elsevier Ltd. doi:10.1016/j.geotexmem.2009.08.002.

Sathananthan, I., Indraratna, B., and Rujikiatkamjorn, C. 2008. Evaluation of Smear Zone Extent Surrounding Mandrel. Intenational Journal of Geomechnics, **8**(December): 355–365.

Sharma, J.S., and Xiao, D. 2000. Characterization of a smear zone around vertical drains by large-scale laboratory tests. Canadian Geotechnical Journal, **37**(6): 1265–1271.

doi:10.1139/t00-050.

Sun, L., Gao, X., Zhuang, D., Guo, W., Hou, J., and Liu, X. 2018. Pilot tests on vacuum preloading method combined with short and long PVDs. Geotextiles and Geomembranes, **46**(2): 243–250. Elsevier. doi:10.1016/j.geotexmem.2017.11.010.

Sun, L., Guo, W., Chu, J., Nie, W., Ren, Y., Yan, S., and Hou, J. 2017. A pilot test on a membraneless vacuum preloading method. Geotextiles and Geomembranes, **45**(3): 142–148. Elsevier Ltd. doi:10.1016/j.geotexmem.2017.01.005.

Tang, M., and Shang, J.Q. 2000. Vacuum preloading consolidation of Yaoqiang Airport runway. Géotechnique, **50**(6): 613–623. doi:10.1680/geot.2000.50.6.613.

Tavenas, F., Jean, P., Leblond, P., and Leroueil, S. 1983. The permeability of natural soft clays. Part II: Permeability characteristics. Canadian Geotechnical Journal, **20**(4): 645–660. doi:10.1139/t83-073.

Tavenas, F., and Leroueil, S. 1980. The behaviour of embankments on clay foundations. Canadian Geotechnical Journal, **17**(2): 236–260. doi:10.1139/t80-025.

Tschuchnigg, F., and Schweiger, H.F. 2018. Embankment prediction and back analysis by means of 2D and 3D finite element analyses. Computers and Geotechnics, **93**: 104–114. Elsevier Ltd. doi:10.1016/j.compgeo.2017.05.012.

UN. 2017. Factsheet: People and Oceans: The United Nations Ocean Conference. New York. Available from https://www.un.org/sustainabledevelopment/wp-content/uploads/2017/05/Ocean-fact-sheet-package.pdf.

Walker, R., and Indraratna, B. 2006. Vertical Drain Consolidation with Parabolic Distribution of Permeability in Smear Zone. Journal of Geotechnical and Geoenvironmental Engineering, **132**(7): 937–941. doi:10.1061/(ASCE)1090-0241(2006)132:7(937).

Wu, Z.-X., Jin, Y.-F., and Yin, Z.-Y. 2013. Nonlinear Creep Behavior of Normally

Consolidated Soft Clay. *In* Constitutive Modeling of Geomaterials. *Edited by* Q. Yang, J.-M. Zhang, H. Zheng, and Y. Yao. Beijin. pp. 145–148. doi:10.1007/978-3-642-32814-5_16.

Yin, J.-H. 1999. Non-linear creep of soils in oedometer tests. Géotechnique, **49**(5): 699–707. doi:10.1680/geot.1999.49.5.699.

Yin, J.-H. 2015. Fundamental Issues of Elastic Viscoplastic Modeling of the Time-Dependent Stress – Strain Behavior of Geomaterials. International Journal of Geomechanics, **15**(5): 1–9. doi:10.1061/(ASCE)GM.1943-5622.0000485.

Yin, J.-H., and Graham, J. 1989. Viscous-elastic-plastic modelling of one-dimensional time-dependent behaviour of clays. Canadian Geotechnical Journal, **26**: 199–209.

Yin, J.-H., and Graham, J. 1994. Equivalent times and one-dimensional elastic visco-plastic modelling of time-dependent stress–strain behaviour of clays. Canadian Geotechnical Journal, **31**: 42–52.

Yin, J.-H., and Graham, J. 1999. Elastic viscoplastic modelling of the time-dependent stress-strain behaviour of soils. Canadian Geotechnical Journal, **36**(4): 736–745. doi:10.1139/t99-042.

Yin, J.-H., and Zhu, J.-G. 1999. Measured and predicted time-dependent stress-strain behaviour of Hong Kong marine deposits. Canadian Geotechnical Journal, **36**(4): 760–766. doi:10.1139/t99-043.

Yin, J.-H., Zhu, J.-G., and Graham, J. 2002. A new elastic viscoplastic model for time-dependent behaviour of normally and overconsolidated clays: theory and verification. Canadian Geotechnical Journal, **39**(1): 157–173. NRC Research Press Ottawa, Canada. doi:10.1139/t01-074.

Zhou, W.-H., Lok, T.M.-H., Zhao, L.-S., Mei, G., and Li, X.-B. 2017. Analytical solutions to the axisymmetric consolidation of a multi-layer soil system under surcharge

combined with vacuum preloading. Geotextiles and Geomembranes, **45**(5): 487–498. Elsevier Ltd. doi:10.1016/j.geotexmem.2017.06.003.

Zienkiewicz, O.C., and Taylor, R.L. 1996. The Finite Element method Volume 2.